

**CHARACTERIZATION OF THE UBC13-MMS2
LYSINE-63-LINKED UBIQUITIN CONJUGATING COMPLEX**

A Thesis Submitted to the College of
Graduate Studies and Research
In Partial Fulfillment of the Requirements
For the Degree of Doctor of Philosophy
In the Department of Microbiology and Immunology
University of Saskatchewan
Saskatoon

By

LANDON PASTUSHOK

PERMISSION TO USE

In presenting this thesis in partial fulfillment of the requirements for a Postgraduate degree from the University of Saskatchewan, I agree that the Libraries of this University may make it freely available for inspection. I further agree that permission for copying of this thesis in any manner, in whole or in part, for scholarly purposes may be granted by the professor or professors who supervised my thesis work or, in their absence, by the Head of the Department or the Dean of the College in which my thesis work was done. It is understood that any copying or publication or use of this thesis or parts thereof for financial gain shall not be allowed without my written permission. It is also understood that due recognition shall be given to me and to the University of Saskatchewan in any scholarly use which may be made of any material in my thesis. Requests for permission to copy or to make other use of material in this thesis in whole or part should be addressed to:

Head of the department of Microbiology and Immunology

University of Saskatchewan

Saskatoon, SK, S7N 5E5

ABSTRACT

Ubiquitylation is an indispensable post-translational modification system in eukaryotic cells that leads to the covalent attachment of a small ubiquitin (Ub) protein onto a target. The traditional and best-characterized role for ubiquitylation is a fundamental regulatory mechanism whereby target proteins are tagged with a characteristic Lys48-linked Ub chain that signals for their elimination through proteasomal degradation. Challenging this conventional wisdom is the finding that some ubiquitylated proteins are modified by Ub chains linked through Lys63, providing a molecular signal that is thought to be structurally and functionally distinct from Lys48-linked Ub chains. Of further interest and significance is that the Lys63-linked Ub chains are apparently synthesized through a novel biochemical mechanism employing a unique complex formed between a true Ub conjugating enzyme (E2), Ubc13, and an E2-variant (Uev), Mms2 (or Uev1A). The goal of this thesis was to employ structural and functional approaches in order to better characterize the Ubc13-Mms2 Lys63-linked Ub conjugation complex.

Error-free DNA damage tolerance (DDT) in the budding yeast is dependent on Lys63-linked Ub chains synthesized by Ubc13-Mms2 and thus provided the opportunity to experimentally test the function of the human *UBC13* and *MMS2* genes in a simple model organism. Human *UBC13* and *MMS2* were each shown to function in place of their yeast counterparts and in accordance, human Ubc13 was shown to physically interact with yeast Mms2, and *vice versa*. Two human *MMS2* homologs were also tested and it was determined that *UEV1A* but not *UEV1B* can function in place of *mms2* in yeast DDT. Physical interactions were observed between Ubc13 and Uev1A, but not between

Ubc13 and Uev1B, suggesting that Ubc13-Uev complex formation is required for function.

In collaboration with a research group at the University of Alberta, crystal structure and NMR data were used to develop a mechanistic model for the conjugation of Lys63-linked Ub chains by the Ubc13-Mms2 heterodimer, whereby the special orientation of two Ub molecules facilitates a specific Ub-Ub linkage via Lys63. In order to help support the *in vitro* model and to determine how the Ubc13-Mms2 structure relates to biological function, I used a structure-based approach to direct the creation of point mutations within four key regions of the Ubc13-Mms2 heterodimer; the Ubc13 active-site, the Ubc13-E3 (Ub ligating enzyme) interface, the Mms2-Ub interface, and the Ubc13-Mms2 interface.

Underscoring the importance of the Ub conjugation by Ubc13-Mms2, a Ubc13-C87S active-site mutation was created that could bind to Mms2 but was unable to function in DDT. Regarding the Ubc13-E3 interface, a single Ubc13-M64A point mutation had a potent effect on disrupting Ubc13 function in DDT, as well as its physical interaction with Rad5, TRAF6, and CHFR. The results suggest that different RING finger E3s use the same Ubc13 surface to sequester the Ub conjugation activity of Ubc13-Mms2. Two human Mms2 mutations at Ser32 and Ile62, which are contained within the Mms2-Ub interface, were found to reduce the ability of Mms2 to bind Ub. When the corresponding yeast mutations are combined, a synergistic loss in DDT function is observed. The relative orientation of Ser32 and Ile62 suggests that the Mms2 and Tsg101 Uev families use different Uev surfaces to physically interact with Ub. A 200 μ M dissociation constant for the wild-type Mms2-Ub interaction was also

determined. The systematic mutagenesis and testing of 14 Ubc13-Mms2 interface residues led to mutants with partial or complete disruption of binding and function. Using this data, a model involving the insertion of a specific Mms2-Phe residue into a unique Ubc13 hydrophobic pocket was created to explain the specificity of Mms2 for Ubc13, and not other E2s. In addition, the dissociation constant for the wild-type Ubc13-Mms2 heterodimer was determined to be approximately 50 nM.

The structural and functional studies strongly support the notion that Ubc13-Mms2 complex has the unique ability to conjugate Lys63-linked Ub chains. However, several reported instances of Lys63-linked Ub chains *in vivo* have not yet been attributed to Ubc13 or Mms2. To address the disparity I was able to demonstrate and map a physical interaction between Mms2 and Rsp5, an E3 implicated in Lys63-linked Ub conjugation. Surprisingly, it was found that *MMS2* is not responsible for the *RSP5*-dependent Lys63-linked Ub conjugation of a plasma membrane protein. A possible explanation for the apparent paradox is presented.

ACKNOWLEDGEMENTS

I would first like to acknowledge three important people who, in my mind, have had the greatest influence on my budding scientific career. Thank you Dr. Sean Hemmingsen for helping me to realize that the minute details which can consume some scientists must ultimately fit within a grander scheme. You have taught me to think differently, and more effectively, about scientific problems. Parker Andersen, I sincerely thank you for the countless enthusiastic scientific arguments over the years. You have taught me that criticism should not be met with offense, but embraced as a privilege that encourages better science. Most importantly, thank you Dr. Wei Xiao for providing supervision that strikes a perfect balance between scientific direction and scientific freedom. I appreciate the many opportunities and challenges that you bestow upon your students in order to help them reach their potential; our ability to grow and improve as scientists truly rests on us alone. Finally, your mastery of scientific execution is to be idolized, and I will be forever conscious of your example.

I want to thank my advisory committee; Dr. Hughes Goldie, Dr. Troy Harkness, Dr. Dwayne Hegedus, Dr. Lambert Loh, and Dr. Peter Howard, for their selfless acts of guidance. I am impressed by and grateful for the time and energy you sacrificed to ensure my success.

I sincerely thank my fellow lab-mates, past and present, for creating a most pleasant and productive work environment. A special thank you is reserved for the brilliant Michelle Hanna, who in addition to fulfilling an outlet for interesting intellectual discussion, has also provided me with unconditional scientific assistance and support.

Thank you also to the support staff in the department, especially Mary Woodsworth, Sherry Olauson, and Shirley Cooke.

I thank my Uncle Rick Holwinko, Grandfather John Holwinko, and Mother-in-law Colleen Teague for their unconditional love and support, and the lowest monthly rent in Saskatoon. Thank you to my Mom and Dad for instilling in me the desire to achieve, and my sister for her undying praise and encouragement. Last, I am eternally thankful to my lovely wife Danielle, who was a necessary and fulfilling distraction from my studies. Thank you for keeping my eyes open to the “real world” while I was focused on science.

Funding was provided by: John Larson Cancer Research Trust Fund; College of Medicine Graduate Teaching Fellowship; Natural Sciences and Engineering Research Council Scholarship; Arthur Smyth Graduate Scholarship; University of Saskatchewan Graduate Scholarship.

TABLE OF CONTENTS

	<u>page</u>
PERMISSION TO USE.....	i
ABSTRACT.....	ii
ACKNOWLEDGMENTS	v
LIST OF TABLES	x
LIST OF FIGURES	xi
LIST OF ABBREVIATIONS	xiv
CHAPTER ONE - LYS63-LINKED UBIQUITYLATION	1
1.1 Ubiquitylation and ubiquitylation enzymology	2
1.2 The ubiquitin-proteasome system	6
1.3 Mono-ubiquitylation	8
1.4 Alternative ubiquitin linkages.....	10
1.5 Discovery of Lys63-linked ubiquitin chains <i>in vivo</i>	11
1.6 DNA damage tolerance in <i>Saccharomyces cerevisiae</i>	14
1.7 Lys63-linked ubiquitin chains signal for error-free DNA damage tolerance ..	20
1.8 Structure and proposed mechanism of Ubc13-Mms2 ubiquitin conjugation ..	22
1.9 Structure of Lys63-linked ubiquitin chains.....	31
1.10 Cellular roles for Lys63-linked ubiquitin chains	33
1.10.1 Cellular roles for Lys63-linked ubiquitin chains generated by Ubc13- Uev	33
1.10.2 Cellular roles implicated with Lys63-linked ubiquitin chains.....	37
1.11 Summary and significance.....	39
CHAPTER TWO - MATERIALS AND METHODS	41
2.1 Strains, cell culture, transformation, and storage.....	41
2.1.1 Yeast	41
2.1.2 Bacteria	41
2.2 Plasmids and DNA.....	45
2.2.1 <i>UBC13</i> and <i>MMS2</i>	45
2.2.2 <i>UEV1A</i> and <i>UEV1B</i>	47
2.2.3 <i>RSP5</i>	47
2.2.4 <i>CHFR</i> , <i>TRAF6</i> , and <i>FUR4</i>	48
2.2.5 DNA cloning and analysis	49
2.3 Polymerase chain reaction	50
2.4 Site-directed mutagenesis	50
2.5 Recombinant protein expression and purification	54
2.6 Protein analysis	55

2.7	GST pull-down assays	56
2.8	Co-immunoprecipitation	58
2.9	Yeast two-hybrid assay	58
2.10	Functional complementation assays	59
2.11	Yeast membrane protein enrichment	60
2.12	Antibody generation and antibodies used	61
2.13	Ubiquitylation assays	62
2.14	Surface plasmon resonance	63
 CHAPTER THREE - FUNCTION OF HUMAN UBC13-UEV COMPLEXES IN YEAST DNA DAMAGE TOLERANCE		67
3.1	Rationale	67
3.2	Results	72
3.2.1	Human <i>UBC13</i> and <i>MMS2</i> are able to function in <i>Saccharomyces cerevisiae</i>	72
3.2.2	Human <i>UBC13</i> and <i>MMS2</i> complement their corresponding genes in <i>S. cerevisiae</i>	74
3.2.3	Functional complementation by human <i>MMS2</i> homologs in <i>S. cerevisiae</i>	77
3.2.4	Physical interactions between Ubc13-Uev proteins	80
3.3	Discussion	85
 CHAPTER FOUR - STRUCTURAL AND FUNCTIONAL CHARACTERIZATION OF UBC13-MMS2		91
4.1	Introduction	91
4.2	Ubc13 active-site results	93
4.2.1	The Ubc13 active-site is required for its function in DDT	95
4.3	Ubc13-E3 interface results	97
4.3.1	Design of a Ubc13-M64A mutant	98
4.3.2	The <i>UBC13-M64A</i> mutant does not function in DDT	101
4.3.3	Ubc13-M64A disrupts a physical interaction with RING finger E3s	103
4.3.4	Discussion of the Ubc13-E3 interface	109
4.4	Mms2-Ub interface results	111
4.4.1	NMR-directed design of Mms2 surface mutations	111
4.4.2	Mutagenesis of a putative Mms2 phosphorylation site	113
4.4.3	Identification of Mms2 surface mutants defective in binding Ub <i>in vitro</i>	115
4.4.4	Functional complementation in DDT is impaired by Mms2-Ub interface mutations	119
4.4.5	Discussion of the Mms2-Ub interface	122
4.5	Ubc13-Mms2 interface results	129
4.5.1	Structure of the Ubc13-Mms2 interface	129
4.5.2	Design of Ubc13 mutants and their interaction in the yeast two-hybrid assay	134

4.5.3	Design of Mms2 Mutants and their interaction in the yeast two-hybrid assay.....	138
4.5.4	The <i>in vivo</i> function of MMS2 and UBC13 mutants correlates with their <i>in vivo</i> interaction.....	139
4.5.5	Binding ability of interface mutants by <i>in vitro</i> pull-down	142
4.5.6	Binding ability of interface mutants by surface plasmon resonance	145
4.5.7	Catalytic activity of interface mutants in ubiquitylation assays	150
4.5.8	Interactions between Ubc13-Arg70 and Mms2-Phe13.....	152
4.5.9	Discussion of the Ubc13-Mms2 interface.....	156
CHAPTER FIVE - A PHYSICAL RELATIONSHIP BETWEEN MMS2 AND RSP5		
5.1	Rationale	162
5.2	Results.....	165
5.2.1	Stable physical interactions are observed for Mms2 and Rsp5	165
5.2.2	A physical interaction is observed for Mms2 and Rsp5 in the yeast two-hybrid assay	168
5.2.3	A physical interaction between Ubc13 and Rsp5 is not observed.....	170
5.2.4	Deletion mapping of the Mms2-Rsp5 physical interaction	172
5.2.5	Rsp5 does not likely function in error-free DDT.....	176
5.2.6	Rsp5 is involved in the Lys63-dependent Ub conjugation of plasma membrane permeases.....	177
5.2.7	<i>MMS2</i> is not required for the Lys63-dependent Ub conjugation of the uracil permease	179
5.3	Discussion.....	182
CHAPTER SIX - CONCLUSIONS AND FUTURE DIRECTIONS187		
6.1	Conclusions.....	187
6.1.1	Major conclusions from chapter three	187
6.1.2	Major conclusions from chapter four.....	187
6.1.3	Major conclusions from chapter five.....	188
6.2	Future directions	189
6.2.1	Can an E2 be engineered to create a new physical interaction with Mms2?	189
6.2.2	What is the mechanism of Lys63-linked Ub conjugation <i>in vivo</i> ?	190
6.2.3	Possible misinterpretation of Lys63-dependent Ub conjugation <i>in vivo</i>	192
REFERENCES.....195		

LIST OF TABLES

<u>Table</u>	<u>page</u>
2-1. Oligonucleotides used for site-directed mutagenesis and PCR amplification.....	53
3-1. Sequence conservation of eukaryotic DDT proteins	71
4-1. SPR binding data of Ubc13-Mms2 and their mutants.....	149

LIST OF FIGURES

<u>Figure</u>	<u>page</u>
1-1. Overview of DNA damage tolerance genes.	15
1-2. Overall structure of the human Ubc13-Mms2 heterodimer.....	25
1-3. Channels created by the Ubc13-Mms2 heterodimer provide the framework for Lys63-linked Ub conjugation.	27
1-4. Model for the mechanism of Lys63-linked Ub conjugation by Ubc13-Mms2	29
2-1. Site-directed mutagenesis strategy	52
2-2. Example of binding curves used for computer-generated binding constant determination	65
2-3. Example of plots used in the manual calculation of dissociation constants.....	66
3-1. Functional complementation of yeast <i>ubc13 mms2</i> double deletions by their corresponding human genes.....	73
3-2. Functional complementation of yeast <i>ubc13</i> and <i>mms2</i> single deletions by their corresponding human genes.....	75
3-3. Dilution plate analysis of the functional complementation of yeast <i>ubc13</i> and <i>mms2</i> single deletions by their corresponding human genes	76
3-4. Heterologous functional complementation of human UEV genes in yeast.....	79
3-5. Ubc13–Uev physical interactions.....	81-82
3-6. Heterologous Ubc13–Mms2 complex formation	84
4-1. Residues mutated in Ubc13-Mms2 structure-function studies.....	92
4-2. Protein sequence alignment of the E2 homologs in <i>S. cerevisiae</i> and human Ubc13 ...	94
4-3. The Ubc13-C87S substitution abrogates its function in yeast DDT but not its physical interaction with Mms2.....	96
4-4. Identification of a Ubc13 residue of putative importance in binding RING finger domains	100
4-5. The Ubc13-M64A substitution abrogates its function in yeast DDT but not its physical interaction with Mms2.....	102

4-6. The Ubc13-M64A substitution abolishes its physical interaction with Rad5	104
4-7. The Ubc13-M64A substitution abolishes its physical interaction with TRAF6	106
4-8. The Ubc13-M64A substitution abolishes its physical interaction with CHFR	108
4-9. The mutation of the Mms2-Ub interface disrupts its binding with Ub <i>in vitro</i>	118
4-10. The mutation of the Mms2-Ub interface disrupts the <i>in vivo</i> function of <i>MMS2</i>	120
4-11. The <i>MMS2-S27A/I57A</i> double-mutant causes an additive MMS sensitive phenotype.....	121
4-12. The Uev domains of human Mms2 and Tsg101 use different surfaces to physically interact with Ub.....	127
4-13. Protein sequence alignment of Mms2 proteins from various model organisms.....	128
4-14. Secondary and tertiary structures of Ubc13 and Mms2	131-133
4-15. <i>In vivo</i> interaction of mutated Ubc13 and Mms2 with wild-type partners by a yeast two-hybrid assay	137
4-16. Functional complementation of yeast <i>ubc13</i> and <i>mms2</i> mutants by corresponding human genes and their derivatives.....	141
4-17. Binding of Ubc13 and Mms2 mutants <i>in vitro</i>	144
4-18. Relative <i>in vitro</i> binding of Ubc13 and Mms2 mutants measured by surface plasmon resonance.....	148
4-19. Catalytic activity of Ubc13 and Mms2 mutants <i>in vitro</i>	151
4-20. Physical and functional relationships between Ubc13-Arg70 and Mms2-Phe13	154-155
4-21. The Mms2-Phe insertion into a Ubc13 hydrophobic pocket is important for Ubc13-Mms2 affinity.....	160
4-22. A hydrophobic pocket is conserved in Ubc13 but not other Ubcs	161
5-1. An Mms2-Rsp5 physical interaction is detected <i>in vitro</i>	167
5-2. An Mms2-Rsp5 physical interaction is detected in the yeast two-hybrid assay	169
5-3. A Ubc13-Rsp5 physical interaction is not observed	171
5-4. Mapping the Mms2-Rsp5 physical interaction.....	174-175
5-5. <i>MMS2</i> is not required for the polyubiquitylation of the uracil permease.....	181

6-1. Proposed mechanisms for the Lys63-linked Ub conjugation of a target <i>in vivo</i>	191
6-2. Possibilities for Ub ₄ chain formation involving Ub-Lys48 and -Lys63	194

LIST OF ABBREVIATIONS

3-AT	3-aminotriazole
A	alanine
Ala	alanine
AD	activation domain
Ade	adenine
amp	ampicillin
Arg	arginine
Asp	aspartate
β -gal	β -galactosidase
BD	binding domain
BLAST	basic local alignment search tool
bp	base pair
C	cysteine, carboxy
CDART	conserved domain architecture research tool
Cys	cysteine
D	aspartate
Da	Dalton
dd	double-distilled
DDT	DNA damage tolerance
DMSO	dimethyl sulfoxide
E	glutamate
E1	ubiquitin activating enzyme
E2	ubiquitin conjugating enzyme
E3	ubiquitin ligating enzyme
E-tube	Eppendorf-tube
F	phenylalanine
Gln	glutamine
Glu	glutamate
Gly	glycine
GST	glutathione-S-transferase
h	human
HECT	homology to the E6-AP carboxyl terminus
His	histidine
I	isoleucine
Ile	isoleucine
IPTG	isopropyl- β -D-thiogalactopyranoside
K	lysine
K_d	dissociation constant
L	leucine
LB	Luria broth
Leu	leucine
M	methionine
Met	methionine

MMS	methylmethane sulfonate
N	amino, asparagine
NMR	nuclear magnetic resonance
nt	nucleotide
OD	optical density
ORF	open reading frame
P	proline
PBS	phosphate-buffered saline
PCNA	proliferating cell nuclear antigen
PCR	polymerase chain reaction
Phe	phenylalanine
Pro	proline
PRR	postreplication repair
Q	glutamine
R	arginine
RING	really interesting new gene
rpm	revolutions per minute
RU	response units
S	serine
SD	synthetic dextrose
SDS-PAGE	sodium dodecyl sulfate-polyacrylamide gel electrophoresis
Ser	serine
SPR	surface plasmon resonance
ss	single strand
TLS	translesion synthesis
Trp	tryptophan
ts	temperature sensitive
Tyr	tyrosine
Ub, Ub ₂ , Ub ₄	ubiquitin, di-ubiquitin, tetra-ubiquitin
Uev	ubiquitin conjugating enzyme variant
UPS	ubiquitin proteasome system
UV	ultraviolet
Wt	wild-type
X-Gal	5-bromo-4-chloro-3-indolyl- β -D-galactoside
y	yeast (budding)
Y	tyrosine
YPD	yeast extract-peptone-dextrose

CHAPTER ONE

LYS63-LINKED UBIQUITYLATION

Originating from the discovery of Ubiquitin (Ub) (Schlesinger et al., 1975) over 30 years ago, ubiquitylation (Hershko et al., 1983) has become one of the cornerstones of covalent protein modification in eukaryotic cells. For perspective, an incredible surge in Ub-related research in the last decade has revealed an astonishing number of ubiquitylation targets with a breadth and diversity that may very well rival phosphorylation. Underscoring this significance, the scientists who pioneered the ubiquitylation field were awarded the 2004 Nobel Prize in Chemistry. The traditional and best characterized role for ubiquitylation is targeted protein turnover through proteasome-dependent degradation. The targeted removal of proteins is a simple yet powerful strategy that can be envisioned to influence essentially any given cellular pathway. However, drawing some of the great interest in the field are recent discoveries that have revealed unexpected complexity and versatility regarding ubiquitylation. The findings have challenged our way of thinking about the biochemical mechanisms and cellular roles traditionally attributed to this important type of covalent modification. In the best and arguably most intriguing example to date, a unique Ub conjugating enzyme heterodimer comprised of Ubc13 and Mms2 generates atypical Ub linkages. Most interestingly, these specialized Ub chains seem to provide a molecular signal that is distinct from proteasome-dependent degradation. During my graduate studies, I have thus undertaken a research program to determine how the novel molecular structure of

the Ubc13-Mms2 complex relates to its biological function. Through the effective use of genetic and biochemical approaches, I was able to substantiate, challenge, and provide greater insight into the conventional wisdom regarding the molecular mechanisms and cellular roles of Ubc13-Mms2. This introductory chapter aims to provide a sufficient overview of ubiquitylation in general, with particular emphasis on Ubc13-Mms2 and Lys63-linked Ub chains.

1.1 Ubiquitylation and ubiquitylation enzymology

In the simplest sense, ubiquitylation is a three-step biochemical reaction that uses ubiquitin, a small globular 76 amino acid protein, to covalently modify target proteins. As the name implies, Ub is found throughout eukaryotic cells. With a mere three amino acid sequence difference between lower and higher eukaryotes, it is one of the most conserved proteins in nature (Ozkaynak et al., 1984). The biochemical reaction is initiated when an ATP-dependent ubiquitin-activating enzyme (Uba or E1) forms a high-energy thioester bond between the carboxy-terminal (C-terminal) Gly76 residue of Ub, and an internal Cys residue of the E1. Ub is next transferred from the E1 to form another thioester bond, this time with the active-site Cys residue of a ubiquitin-conjugating enzyme (Ubc or E2). The final step in the covalent modification links the C-terminal residue of Ub to a Lys ϵ -amino group on the target, forming an isopeptide bond in a process that usually requires a ubiquitin-ligating enzyme (Ubl or E3). For review, please see (Hershko and Ciechanover, 1998; Hochstrasser, 1996; Jentsch, 1992; Pickart, 2001).

Whereas the E1 is encoded by a single or very few genes in the cell and performs a general role in activating the Ub molecule, E2s and E3s are responsible for the versatility and target specificity of ubiquitylation. E2s comprise a family of proteins with

a highly conserved core domain of approximately 150 amino acids. Based on 3-dimensional structure comparisons, the core domain forms a globular α/β fold with a central β -sheet and surrounding α -helices (Moraes et al., 2001; Pickart, 2001). Within this region lies an active-site with the aforementioned Cys residue that is absolutely conserved among all E2s, and is housed in a shallow cleft in the center of the protein (VanDemark and Hill, 2002). Based on data generated from multiple E2 crystal structures (for example see Cook et al., 1993; Moraes et al., 2001; Worthylake et al., 1998) this characteristic 3-dimensional organization has been termed the Ubc- or E2-fold. Although confined to these general similarities, E2 enzymes are found to participate in very different and numerous cellular roles. Because *S. cerevisiae* contains only eleven E2s that can covalently attach Ub to various target proteins, it is at first surprising that they can specifically select between hundreds (if not thousands) of potential ubiquitylation targets. This diversity and specificity is achieved in several ways. First, many E2s are longer than the ~150 amino-acid core domain itself, and instead contain non-conserved carboxy- or amino-terminal extensions, leading them to be characterized as Class II and Class III E2s, respectively (Jentsch, 1992). It is believed that such extensions impart additional functions on the particular E2s, such as the mediation of specific downstream interactions with E3(s) or the eventual ubiquitylation target itself (Pickart, 2001). Second, at least one E2, Ubc13, requires a specialized accessory factor protein in order to carry out ubiquitylation. The requirement of an E2-variant in this case is a large focus of this thesis. Last, a single E2 may independently associate with multiple E3s. Because the E3s represent the most abundant family of ubiquitylation proteins, the E2-E3 affiliation is likely the most significant factor in creating target

diversity for the E2s. The E3s are thus often responsible for specifying the biological process or cellular role in which a particular ubiquitylation event is performed.

The remarkable variability of the E3 family of proteins is attributed to several factors. First, they are generally very large and contain multiple different protein domains, many of which do not function in the ubiquitylation process itself. This leads to large structural diversity, with inter-domain regions that often bear no significant homology to other proteins. Another level of complexity is added because E3s may act independently with the cognate E2 or with other proteins as a part of a multi-subunit E3 complex. Furthermore, from a mechanistic standpoint, E3s may actively participate in ubiquitylation reactions (by forming covalent bonds with Ub) or act as passive adapters that physically bridge a given E2 to its target.

Aside from a small variable subset, E3s normally contain one of two well-defined and characteristic domains. One of these is the HECT (homology to the E6-AP carboxyl terminus) domain which can bind Ub in a thioester-dependent manner, similar to E1 and E2 enzymes (Scheffner et al., 1995). Several documented examples suggest that the covalent bonds generated between the HECT domain E3s and Ub are absolutely required for their role in the ubiquitylation process. The HECT domain normally binds directly to the E2, as seen in an E2-E3 crystal structure (Huang et al., 1999), while other regions or domains are available to bind the target.

The other predominant E3 domain is signified by the RING (really interesting new gene) finger motif (Freemont, 1993). The RING finger generally does not participate in Ub conjugation reactions directly, but instead acts as physical adaptor between E2s and their substrates (reviewed in Joazeiro and Weissman, 2000). The

discovery of the RING finger was based on its similarity to the DNA-binding zinc finger motif (Freemont et al., 1991; Lovering et al., 1993). Like the zinc finger, the RING finger requires a Zn^{2+} ion to stabilize and create a scaffold for an otherwise unstructured loop region. Compared to the well-known zinc finger motif, the RING finger has a long consensus sequence designated Cys- X_2 -Cys₍₉₋₃₉₎-Cys- $X_{(1-3)}$ -His- $X_{(2-3)}$ -Cys/His- X_2 -Cys- $X_{(4-48)}$ -Cys- X_2 -Cys, where X is any amino acid (Saurin et al., 1996). The flexibility of the consensus sequence is likely one of the complicating factors in identifying novel RING finger E3s based on sequence alignments. Unlike the zinc finger, the RING finger motif binds other proteins, especially E2s, instead of DNA. Several crystal structures of proteins containing RING finger motifs have been solved, the most significant of which is the structure of the E2-RING finger heterodimer formed by UbcH7 and c-Cbl (Zheng et al., 2000). The structure reveals that the E2-E3 physical interaction is directly mediated by the RING finger motif. The functional importance of this specific interaction is evidenced by point mutations that prevent the formation of the Zn^{2+} cross-bridge or in deletions that remove the RING finger all-together. The E2-E3 physical interaction is thus destroyed and the ubiquitylation of the target is prevented.

In the last few years, a third family of E3s has emerged with a characteristic U-box domain that is highly similar to the RING finger (Aravind and Koonin, 2000; Hatakeyama and Nakayama, 2003). Based on sequence analysis and structural data, the position of key residues and the 3-dimensional conformation adopted is remarkably similar to the RING finger (Ohi et al., 2003). The distinction is that the stabilization of the U-box domain is achieved through a cross-bridge comprised of intra-peptide hydrogen bonds and salt-bridges, instead of the metal chelation necessary for the RING

finger domain. In accordance, the mutation of key residues in the U-box domain leads to the severe destabilization of the U-box tertiary structure (Ohi et al., 2003). Like the HECT and RING finger E3s, proteins containing a U-box work with E1 and E2 enzymes in order to promote ubiquitylation (Hatakeyama et al., 2001). However, with the small number of U-box E3s identified to date, including only two in *S. cerevisiae*, it is suggested that they may not ubiquitylate a range of targets as substantial as the HECT and RING finger E3s.

1.2 The Ubiquitin-Proteasome System

From a biochemical standpoint, a single round of ubiquitylation causes the conjugation of a single Ub (mono-Ub) moiety onto the target. In some cases, this is the desired end product. Alternatively, poly-Ub chains can be formed if, through mostly unknown mechanisms, successive conjugation reactions take place and a lysine residue of another Ub molecule is used as the subsequent site of attachment. Poly-Ub chains linked through Lys48 participate in the Ub-proteasome system (UPS; also called the Ub-proteasome pathway), which is the best understood cellular role for ubiquitylation. Lys48 Ub-conjugates of at least four Ub molecules in length act as characteristic molecular signals that allow the proteasome to specifically recognize the conjugated target (Thrower et al., 2000). The proteasome is a large, barrel-like multi-subunit complex (~2.1 MDa) with ATP-dependent protein unfolding and cleavage activity. The successful passage of the target protein through the lumen of the proteasome causes its irreversible cleavage into short polypeptides. The Ub chain itself is also cleaved during

proteasome-mediated degradation, but is done so by Ub-specific proteases in a particular manner that allows the eventual generation of re-usable Ub molecules.

Because the targeted degradation of proteins is a straightforward means for their regulation, it is reasonable to imagine that the UPS is likely to exert its effects on essentially any cellular pathway or function. The type of proteins targeted by the UPS run the gamut of possibilities, from transcription activators, DNA binding proteins, signal transducers, and structural proteins, to name but a few. There are generally no spatial or temporal limitations for the UPS, as it occurs throughout the cell and over the various cell-cycle stages. For example, the UPS is responsible for terminating the activity of cytosolic signaling pathways (Chen et al., 1995; Tanaka et al., 2001) and degrading nuclear transcription factors (Salghetti et al., 2001). Also, the UPS has an integral role in regulating cell-cycle control through the timely degradation of key regulatory proteins such as cyclins, which govern the transition from one cell cycle stage to another (Glotzer et al., 1991). Several large review articles have done well to address many of the major roles of the UPS (Devoy et al., 2005; Hershko and Ciechanover, 1998; Hochstrasser, 1996; Smith et al., 1996; Ulrich, 2002)

The cell's devotion to the UPS is also observed from the standpoint of the Ub-conjugating enzymes themselves. The budding yeast dedicates almost all of its 11 E2s to the UPS. Given the ability of multiple E2-E3 combinations and the potential for multi-subunit E3s, it is apparent that the cell contributes a large arsenal toward protein degradation. Furthermore, in higher eukaryotes, the encoding of the same E2 by several different genes helps to ensure the availability of particular E2s involved in the UPS. In some cases, the functional complementation of completely different E2s provides yet

another level of safeguarding. For example, Ubc4 and Ubc5 in *S. cerevisiae* are both involved in the response to various cellular stresses and in many cases have been shown to functionally complement for one another. An even more striking example is seen in cases where *ubc4ubc5* double-knockout strains are complemented by a divergent E2, *UBC1* (Seufert and Jentsch, 1990). The redundancy and interchangeability of E2s likely provides a necessary backup for important cellular functions that require the UPS. From another perspective, these properties can complicate experimental testing and make it difficult to attribute particular functions to specific E2s.

1.3 Mono-ubiquitylation

The conjugation of a single Ub moiety to the target is a necessary step toward poly-Ub chains, and in some cases is the desired modification. In other words, what may be considered as an intermediate en route to the poly-Ub chain is actually a *bona fide* modification with a possibly distinct purpose and function. It could be suggested that cellular roles involving mono-ubiquitylation may have very well preceded those for poly-ubiquitylation. The conjugation of mono-Ub to target proteins was observed more than 20 years ago (Busch and Goldknopf, 1981). The nucleosome histone proteins were the first discovered to be mono-ubiquitylated, but it was not until quite recently that a function for the modification was attributed. Yeast cells that are unable to conjugate mono-Ub to the histones H2A and H2B because of mutations in the E2 Rad6 (Ubc2) exhibit a slow-growth phenotype and are defective in sporulation (Robzyk et al., 2000). This apparent defect in meiosis extends to higher eukaryotic systems because *rad6* knockout mice (*mHR6B^{-/-}*) have a defect in spermatogenesis leading to male sterility

(Roest et al., 1996). Other predominant roles involving the mono-ubiquitylation of target proteins are in viral budding (Morita and Sundquist, 2004; Patnaik et al., 2000), the endocytosis and transport of membrane permeases (Shih et al., 2003; Urbe, 2005), and translesion DNA synthesis (Hoegel et al., 2002; Kannouche et al., 2004).

In contrast to the numerous E2s used for the UPS, only a small subset has been implicated in mono-ubiquitylation to date. Interestingly, two of these E2s, Rad6 and Ubc5, are also involved in the poly-ubiquitylation of target proteins. It is presumably the association with a particular E3 or substrate that specifies the nature of the Ub conjugation to be performed in each case. For example, the association of Rad6 with the E3 Ubr1 leads to Lys48-linked Ub conjugation for N-end rule protein degradation by the 26S proteasome (Sung et al., 1991a). On the other hand, complexes formed by Rad6 and the RING finger E3s Rad18 and Bre1 lead to the mono-ubiquitylation of PCNA (Hoegel et al., 2002) and histone proteins (Hwang et al., 2003; Wood et al., 2003), respectively. The physical association of Ubc5 and the HECT domain E3s Nedd4 and Rsp5 lead to the mono-ubiquitylation of the viral Gag protein (Ott et al., 1998; Strack et al., 2000) and several yeast plasma-membrane proteins (Rotin et al., 2000), respectively.

Regardless of the specific ubiquitylation proteins or particular cellular pathway, the common factor in all cases of mono-ubiquitylation described so far is that the modification does not lead to proteasome-mediated degradation. Physical studies of Ub recognition support such findings, because mono-Ub is an insufficient modification to be effectively recognized by the proteasome (Thrower et al., 2000). At least one particular fate of mono-ubiquitylated proteins does in fact lead to degradation; however, the notable difference is that the protein degradation is unrelated to the UPS. The covalent

modification by mono-Ub in these cases directs protein traffic into and through the multivesicular sorting pathway, which often leads to proteasome-independent protein degradation within the lysosome.

Because mono-ubiquitylation is a functional molecular signal as well as an unavoidable step in building poly-Ub chains, an interesting regulatory opportunity is inherently possible during the process of poly-ubiquitylation. In a hypothetical scenario, the linkage of a single Ub could turn on a particular protein function and subsequently, the simple addition of Ub molecules linked through Lys48 would turn off the function by causing the degradation of the modified target. Exciting possibilities for this kind of dynamic regulatory mechanism through Ub chain building are beginning to emerge (Hoege et al., 2002; Li et al., 2003).

1.4 Alternative ubiquitin linkages

The sections above outline some of the ways that ubiquitylation exerts its versatility and variability. On one level, the various E2s offer a number of conjugation factors that can act upon many different, albeit generalized cellular roles throughout the cell. Then, a given E2 may often separately associate with many different E3s to impinge on a specific biological target. Because the E3s are such a plentiful group of proteins, the sheer number of possible E2-E3 combinations is immense. Another level of complexity in ubiquitylation is added because targets may be modified by mono-Ub or poly-Ub chains. Furthermore, while the prototypical Ub chain is synthesized via Lys48 linkages, poly-Ub chains can be linked through other Lys residues as well. In this way,

ubiquitylation proves to be an even more functionally powerful and versatile signal than was first imagined.

There are a total of seven surface-exposed Lys residues on Ub which allow the possibility that Ub can be conjugated through many different non-Lys48 linkages. Indeed, poly-Ub chains made via Lys63 (Arnason and Ellison, 1994; Spence et al., 1995), Lys-11 (Baboshina and Haas, 1996), Lys29 (Arnason and Ellison, 1994; Johnson et al., 1995), and Lys6 (Baboshina and Haas, 1996; Wu-Baer et al., 2003) have been demonstrated *in vitro* or *in vivo* (Peng et al., 2003). Because the lysines are well dispersed on the Ub surface, it is expected that the linkage specificity may be governed by different Ub conjugation mechanisms. Thus, given the high degree of structural conservation between all E2s, the ability to conjugate different Ub chains is an important mechanistic question in the field. Distinct Ub conjugation activities presumably arise from intrinsic E2 differences, such as small sequence variations that may alter the linkage specificity, or through the association with specialized accessory factor(s). An intriguing case for the latter was recently discovered through studies of a very unique Ub conjugating complex comprised of Ubc13 and Mms2 (Hofmann and Pickart, 1999; McKenna et al., 2001).

1.5 Discovery of Lys63-linked ubiquitin chains *in vivo*

While a few earlier studies suggested that Ub conjugation may occur via non-Lys48 linkages (Haas et al., 1991; Hochstrasser et al., 1991; Johnson, 1992; Johnson et al., 1995), a systematic approach in budding yeast was the first to clearly demonstrate the existence of atypical Ub conjugates *in vivo* (Arnason and Ellison, 1994). The authors of

the landmark study created a complete panel of Myc-Ub constructs (seven in total) that were each mutated Lys to Arg at all but a single Lys residue. Western Blots against the myc epitope of total-cell lysates then revealed whether poly-ubiquitylation was dependent on any of the seven lysine residues (Lys6, Lys11, Lys27, Lys29, Lys33, Lys48, or Lys63). The results showed that Ub conjugates are formed *in vivo* via Lys29, Lys48, and Lys63. The authors also observed an increase in Lys63-dependent ubiquitylation under stress-inducing conditions. Ubiquitylation through Lys63 was required for cell survival after canavanine treatment and heat stress (Arnason and Ellison, 1994). The finding was the first evidence that Lys63-linked Ub conjugates are physiologically relevant. Due to the nature of the Myc-Ub fusions used, they were not able to address the possible substrate(s) of the atypical Ub modifications. Only “free” poly-Ub conjugates were monitored.

Shortly after these findings, a similar approach in yeast was undertaken by a separate research group in order to shed more light on Lys63 Ub chains *in vivo* (Spence et al., 1995). A yeast strain was generated with all of its four Ub-encoding genes deleted from the genome, with viability maintained by the introduction of single Ub gene of choice, ensuring it as the only source of Ub in the cell. This approach circumvented the need for tagging Ub with an epitope in order to keep track of the Ub derivative of choice. As analysed by 2-D polyacrylamide gel electrophoresis, several protein spots were shifted in the *ub-K63R* mutant strain, indicating the dependence upon Ub conjugation via Lys63. Although their identities were not determined, at least three different proteins were found to be conjugated in a Lys63-dependent manner. Expanding on the affiliation between stress conditions and Lys63 Ub chains, the authors attributed the *ub-K63R*

mutant phenotype to the *RAD6* DNA damage tolerance pathway (also called postreplication repair) (Spence et al., 1995).

Taken together, these studies provided the foundation for a novel field of ubiquitylation research that deals with atypical poly-Ub chains. Perhaps as exciting as the discovery of the novel chains themselves, these studies opened the door to several questions that are still of great significance in the ubiquitylation field today. From a biological standpoint, the identification of the particular targets modified by the variant chains and their eventual fate within the cell became central questions. From a biochemical standpoint, research was spurred to determine the precise E2(s) responsible and to decipher the molecular mechanisms that could lead to the conjugation of such atypical Ub chains.

A greater emphasis was placed upon the Ub linkages made via Ub Lys63 in the landmark studies above. This was likely due in part to the abundance of Lys63-linked Ub conjugates observed in the experiments and the fact that Lys63-linked Ub conjugates were not previously demonstrated. On the other hand, Ub-Lys29 chains had been shown in an artificial Ub-fusion degradation system (Johnson et al., 1995). More significantly, however, each study demonstrated that the *ub-K63R* mutation causes a detectible phenotype after stress treatments such as DNA damage. This phenotype was linked many years later to the budding yeast *UBC13* and *MMS2* genes of the DNA damage tolerance (DDT) pathway (Hofmann and Pickart, 1999). Subsequent studies showed that Ubc13 and Mms2 form a specific E2 complex that generates atypical poly-Ub chains linked through Lys63. Furthermore, these Lys63 Ub conjugates were found to be absolutely required for error-free DDT (Hofmann and Pickart, 1999). Since that time,

several breakthroughs in the field (several involving this thesis work) have revealed detailed insight into the molecular underpinnings and cellular function of Ubc13-Mms2 (or Ubc13-Uev1A) and their unique Lys63 poly-Ub chains.

1.6 DNA damage tolerance in *Saccharomyces cerevisiae*

My work involving Ubc13 and Mms2 began from genetics-based approaches that led to the discovery of the *MMS2* gene in *Saccharomyces cerevisiae*. Our subsequent studies led to the characterization of a novel error-free pathway of DNA postreplication repair (PRR) (Broomfield et al., 1998). It is notable that the term “postreplication repair” is mainly used in a historical sense based upon the early methods used to characterize it in *S. cerevisiae*. I currently favour the use of a more technically accurate term, replication-associated DNA damage tolerance (DDT). DDT in this sense is a eukaryotic process that allows cells to evade replication-blocking DNA damage that would otherwise lead to cell death. Because the replicative polymerases rely on a pristine DNA template, the DDT pathway is triggered by a wide range of DNA lesions that can be caused by various DNA damaging agents.

Classical genetic analyses has led to the convention that DDT consists of a branched pathway that includes at least one error-free and one translesion synthesis (mostly error-prone) pathway (Figure 1-1 and reviewed in (Broomfield et al., 2001). The *RAD6* and *RAD18* genes are required for both sub-pathways and mutations that disrupt either gene result in the most severe DNA damage sensitivities of all DDT

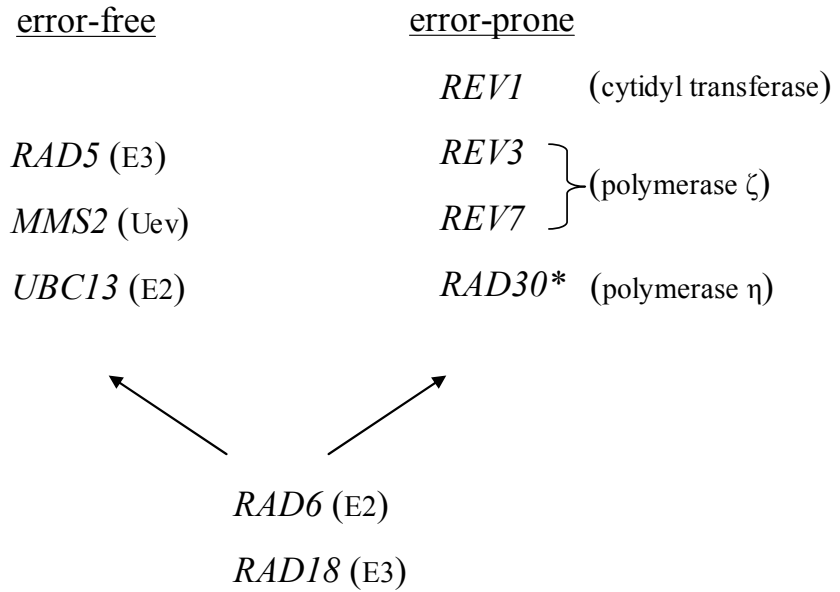


Figure 1-1. Overview of DNA damage tolerance genes in *S. cerevisiae*. Epistatic analysis has outlined a branched pathway for DDT originating from *RAD6* and *RAD18* and leading to at least one error-free and error-prone component as indicated. Brackets indicate gene product function: E2 (Ub conjugating enzyme); E3 (Ub ligating enzyme); Uev (E2-variant). For clarity, the genes for polymerase δ and its subunits are not shown. **RAD30* is conditionally error-prone.

genes. Yeast *RAD6* encodes a multi-functional E2 (Jentsch et al., 1987) that in addition to DNA repair, functions in histone modification (Sung et al., 1988; Haas et al., 1991) and “N-end rule” protein degradation (Bachmair et al., 1986; Dohmen et al., 1991). Because the Ub-conjugating activity of Rad6 is required for all its known biological roles (Sung et al., 1991a; Sung et al., 1990), it stands to reason that Rad6 fulfills its distinct functions through interactions with different E3s or via different Ub conjugations, or both. Indeed, Rad6 is able to form exclusive complexes with Ubr1 or Rad18 (Bailly et al., 1994) for N-end rule protein degradation and DDT (Bailly et al., 1997b), respectively.

RAD18 encodes a RING finger E3 with ATPase and ssDNA-binding activities (Bailly et al., 1997a). The *rad18* mutant is completely defective in DDT and does not influence the other functions associated with *RAD6*. The affinity of Rad18 for both ssDNA and Rad6 (and proliferating-cell nuclear antigen as will be discussed later) fits well with a working model whereby Rad18 brings Rad6 into close proximity with ssDNA gaps left by a stalled polymerase, so that the ubiquitylation of a target protein can initiate the DDT pathway. The ssDNA-binding activity of Rad18 is consistent with observations that DDT mutants are sensitive to killing by a broad range of DNA damaging agents that may all potentially lead to a common replication-blocking end-product (Broomfield et al., 2001; Prakash et al., 1993).

The translesion synthesis (TLS) branch of DDT consists of *REV3* and *REV7* (encoding subunits of Pol ζ), *RAD30* (Pol η), and *REV1*. These genes encode non-essential DNA polymerases with very low processivity that are involved in translesion synthesis that is for the most part mutagenic (Prakash et al., 2005). The majority of spontaneous and DNA-damage-induced mutagenesis in *S. cerevisiae* is attributed to the

predominant TLS polymerase, Pol ζ . Several properties lead to the mutagenic designation of the TLS polymerases. First, they do not have the proofreading subunits or editing activity of the high-fidelity replicative polymerases. Second, the active-site through which the DNA template passes is larger and less stringent and thus leads to “sloppy” nucleotide additions. Last, some TLS polymerases have a bias for inserting particular nucleotides, which can be mutagenic when placed across an incorrect template nucleotide. For example, Pol η inserts adenine nucleotides that are appropriate when placed across thymine dimers, but are otherwise potentially mutagenic. Mutants of the TLS pathway lead to relatively moderate DNA-damage sensitivities that vary somewhat with the particular DNA lesion encountered.

In a slight simplification, the error-free component of DDT consists of the *RAD5*, *UBC13*, and *MMS2* genes, and an unknown mechanism for circumventing DNA damage. The *MMS2* gene was isolated by functional complementation of an *mms2-1* allele that is sensitive to the DNA damaging agent methylmethane sulfonate (MMS). Subsequent genetic analysis revealed that *MMS2* belongs to the *RAD6* epistasis pathway (Broomfield et al., 1998). However, unlike the *rad6* and *rad18* mutants which are severely sensitive to DNA damaging agents, the *mms2* mutant displays only moderate DNA damage sensitivity, but significantly increased mutation rates. The dramatic increase in mutation rates is attributed to the redirection of the pathway to the TLS side, because mutagenesis is abolished through the inactivation of *REV3*. Another significant genetic relationship is that *mms2* and *rev3* mutations exhibit a remarkable synergism with respect to killing by DNA damaging agents. Taken together, these observations placed *MMS2* in an error-free

branch of DDT that is parallel to the Pol ζ -mediated mutagenesis pathway (Broomfield et al., 1998; Xiao et al., 1999).

The first study to isolate the *MMS2* gene also reported that it encodes an E2-like or Ubc-variant (Uev) domain (Broomfield et al., 1998). The Uev domain shares a high degree of protein sequence and tertiary structure similarity to the Ubc domain, but lacks the obligatory active-site Cys residue required for Ub conjugation. Due to this fact, it was originally hypothesized that UeVs would function as dominant-negative regulators of Ub conjugation (Koonin and Abagyan, 1997). Homologs containing Uev domains have been found in all eukaryotic organisms examined to date, including humans (Sancho et al., 1998; Xiao et al., 1998). Phylogenetic analysis indicates that UeVs evolved from Ubcs as a distinct class of proteins, early on in eukaryotic evolution (Villalobo et al., 2002). There are two Uev-containing proteins in the budding yeast, Mms2 and Vps23, and they are representative of the two predominant Uev-containing protein families. The Mms2/Uev1 family is marked by proteins that contain the Uev domain alone and are occasionally accompanied by short variable N- or C-terminal extensions. The Vps23/Tsg101 family contains proteins with a Uev domain as one of several identifiable protein domains. The Uev domain in the Vps23/Tsg101 proteins functions as a Ub-interacting module for protein-protein interactions, whereas the Mms2/Uev1 family of proteins function to promote Ub conjugation.

Given the epistatic relationship between *rad6* and *mms2* in DNA repair, it was originally suggested that Mms2 functions as an accessory protein that positively regulates the ubiquitylation activity of Rad6 (Broomfield et al., 1998). However, rigorous *in vivo* and *in vitro* studies failed to demonstrate a physical link between Mms2 and Rad6 (Xiao

et al., unpublished observations) and it turned out that Mms2 forms a stable complex with a different and novel E2 in DNA repair, named Ubc13.

In contrast to the genetic approaches that placed many of the players within the DDT pathway, a relatively indirect biochemical approach led to the involvement of Ubc13 in DDT. In the landmark study, a special Ub derivative was used to test the ability of seven partially purified E2s from mammalian cell extracts for the formation of Lys63 poly-Ub chains *in vitro* (Hofmann and Pickart, 1999). Based on previous studies that found DNA damage sensitivity in *ub-K63R* mutant strains (Arnason and Ellison, 1994; Spence et al., 1995), the experiment had some immediate relevance to DDT. Of all the E2s tested, only Ubc13 was able to form Lys63-linked Ub conjugates; however, the conjugation activity could not be reproduced with purified Ubc13 from bacterial sources. The failure was due to a surprising dependence on a protein cofactor, Mms2 (Uev1), which was present in the original eukaryotic extracts. The requirement for Mms2 was specifically demonstrated through a restoration-of-activity experiment using mammalian cell extract fractions. Using a co-purification approach, they went on to demonstrate a physical interaction between the yeast Ubc13 and Mms2 proteins (Hofmann and Pickart, 1999). A preliminary genetic experiment was used to demonstrate an equivalent sensitivity to ultraviolet (UV) radiation in *ubc13*, *mms2*, and *ub-K63R* mutant yeast strains. The definitive placement of *UBC13* in the error-free branch of *S. cerevisiae* DDT was done in our laboratory. We found that *ubc13* exhibits the characteristic phenotypes of error-free DDT genes (Brusky et al., 2000). With respect to DNA damage sensitivity, *rad6* is epistatic to *ubc13* and *ubc13* is synergistic with *rev3*. In addition, as with *mms2Δ*,

a mostly *REV3*-dependent increase in mutagenesis is seen in a *ubc13Δ* strain (Brusky et al., 2000).

RAD5 was genetically placed within the DDT pathway with the epistatic grouping of radiation sensitive yeast mutants. *RAD5* was also isolated as *rev2* in an early study due to a reversion (mutator) phenotype that is characteristic of error-prone DDT genes (Lawrence, 1982). More recent studies have resolved the role of *RAD5* within the error-free DDT pathway (Johnson et al., 1992; Ulrich and Jentsch, 2000; Xiao et al., 2000). The Rad5 protein is a RING finger E3 with a ssDNA-dependent ATPase domain (Johnson et al., 1992) and Swi2/Snf2-like domains that are suggested for roles in chromatin remodeling (Richmond and Peterson, 1996). The Swi2/Snf2-like and ATPase domains have not been linked to DDT to date, but the Rad5 RING finger binds to Ubc13 in yeast two-hybrid and *in vitro* co-immunoprecipitation experiments (Ulrich and Jentsch, 2000). The functional significance of this interaction is a DNA-damage-dependent nuclear localization of Ubc13-Mms2, and the co-localization of Ubc13-Rad5 to chromatin (Ulrich and Jentsch, 2000). It was also found that Rad5 physically interacts with Rad18 through a region that is independent of the RING finger that is responsible for binding to Ubc13.

1.7 Lys63-linked ubiquitin chains signal for error-free DDT

The description of DDT above paints a picture of an interesting branched pathway with two distinct ways of dealing with DNA damage through error-free and TLS (error-prone) processes. In addition to the mystery surrounding the role of Lys63-linked Ub chains in DDT, a central question in the field is thus how the choice is made between the

error-free and TLS pathways. Perhaps not surprisingly, some answers came through studies that identified the proliferating-cell nuclear antigen (PCNA) as the target of ubiquitylation in DDT (Hoege et al., 2002). Homotrimers of PCNA encircle DNA to function as the essential sliding-clamp subunits that garner processivity for the replicative polymerases (Waga and Stillman, 1998). In addition, PCNA is involved in other forms of DNA metabolism such as nucleotide excision repair, base excision repair, mismatch repair, chromatin assembly, and post-replicative processing (Kelman and Hurwitz, 1998; Paunesku et al., 2001; Zhang et al., 2000). The involvement of PCNA in DDT was originally implicated through the characterization of the gene encoding PCNA in *S. cerevisiae*, *POL30*. The mutant allele *pol30-46* conferred UV sensitivity (Ayyagari et al., 1995) and genetic analysis of *pol30-46* placed *POL30* within the *RAD6* epistasis pathway (Torres-Ramos et al., 1996). In addition, *pol30-46* appeared to be defective in the error-free branch of DDT (Xiao et al., 2000).

Given that PCNA was genetically linked to DDT (Torres-Ramos et al., 1996), the poly-ubiquitylation of PCNA after DNA damaging treatment (Hoege et al., 2002) suggested that one of the E2 complexes of the DDT pathway was responsible. Indeed, the DNA-damage-induced ubiquitylation of PCNA was completely abolished in *rad6Δ* mutant strains. Furthermore, mutants in the error-free genes *ubc13*, *mms2*, and *rad5* also led to the disappearance of poly-Ub conjugates, however, a mono-ubiquitylated PCNA species was still present. It was deduced that mono-ubiquitylation of PCNA is performed by the Rad6-Rad18 complex, while Ubc13-Mms2-Rad5 is responsible for the poly-ubiquitylation of PCNA (Hoege et al., 2002). Providing a further connection between Ubc13-Mms2 and the ubiquitylation of PCNA was the finding that the poly-Ub

conjugates of PCNA were absent in yeast cells solely expressing Lys63-mutated Ub. The poly-Ub conjugates were thus attributed to the Lys63-linked Ub conjugation activity of Ubc13-Mms2 (Hoege et al., 2002).

Another striking finding in the pivotal DDT study by Hoege et al. was that PCNA is predominantly ubiquitylated, by both mono- and poly-Ub, at a single Lys residue that is invariant among PCNA proteins throughout eukaryotes (Pastushok and Xiao, 2004). The single site for Ub conjugation enabled the creation of a regulatory model for DDT whereby the sequential addition of mono-Ub and Lys63-linked poly-Ub chains onto PCNA leads to the TLS and error-free DDT processes, respectively. Indeed, the model is in accordance with various genetic data (Brusky et al., 2000; Hofmann and Pickart, 1999; Stelter and Ulrich, 2003).

To further describe the mechanisms behind PCNA modification by Ub, Hoege *et al.* (2002) demonstrated a physical molecular framework for the relevant DDT proteins. The authors identified novel interactions between PCNA and the two RING finger proteins, Rad18 and Rad5. Considering their ssDNA-binding affinities, the interactions involving Rad18 and Rad5 can be seen as physical connections between the substrate (ssDNA), conjugation machinery (Rad6 and Ubc13-Mms2), and ubiquitylation target (PCNA) of the DDT pathway. Taking into account the earlier report that Rad5 binds to Ubc13 and Rad18 (Ulrich and Jentsch, 2000), a large multi-subunit conjugation complex and its biological effects through the Ub modification of PCNA can be envisioned.

1.8 3-dimensional structure and proposed mechanism of Ubc13-Mms2 Ub conjugation

Shortly after the discovery which found that Ubc13 and Mms2 co-purify and generate Lys63-linked Ub chains, studies with the corresponding human Ubc13 and Mms2 proteins provided greater detail into their biochemical properties. Using highly purified Ubc13 and Mms2 proteins, a 1:1 Ubc13:Mms2 heterodimer with an approximate $K_d = 2 \mu\text{M}$ was demonstrated (McKenna et al., 2001; Moraes et al., 2001). Performing ubiquitylation reactions *in vitro* with a reconstitution approach, it was revealed that the Ubc13-Ub thioester targets a free “acceptor” Ub for conjugation. The thioester can be formed with or without Mms2; however, the Ubc13-Mms2 heterodimer thioester is more stable. In light of more recent *in vivo* findings it is expected that heterodimer formation precedes thioester generation because the Ubc13-Mms2 complex is recruited to the site of DNA damage where it subsequently ubiquitylates PCNA (Hoegge et al., 2002; Ulrich, 2003). The most groundbreaking finding from the *in vitro* studies came from nuclear magnetic resonance (NMR) data which helped to propose a mechanistic basis for Ubc13-Mms2-mediated Ub conjugation through Ub-Lys63. Two dimensional ^1H - ^{15}N heteronuclear single nuclear quantum coherence was used in chemical-shift perturbation experiments to show that Mms2 binds to Ub in a non-covalent manner *in vitro*. Furthermore, the detailed data generated in the experiment allowed the creation of an elegant model to explain the Ub conjugation by Ubc13-Mms2. It was suggested that Mms2 is responsible for the proper orientation of the acceptor Ub, such that Ub-Lys63 is made available to the donor Ub of the Ubc13 active-site thioester (McKenna et al., 2001). Shortly thereafter, the solving of the yeast (VanDemark et al., 2001) and human (Moraes et al., 2001) Ubc13-Mms2 heterodimer crystal structures provided a visual basis to support the model. Additional NMR data generated through the careful analysis of each

component (Ubc13, Mms2, donor Ub, acceptor Ub) involved in the Lys63 Ub-conjugation reaction provided further refinement of the model (McKenna et al., 2003b).

The overall structure of the human Ubc13-Mms2 heterodimer is shown in Figure 1-2 and is highly super-imposable with the corresponding *S. cerevisiae* structure. Owing to the high degree of protein sequence similarity in the core regions of the E2 and Uev protein families, it was not surprising that each molecule adopts the characteristic globular α/β E2 fold (for example see Cook et al., 1993; Worthylake et al., 1998). The main exception is that Mms2 lacks two carboxy-terminal α -helices. The most striking and exciting feature of the heterodimer is that it is asymmetrical, with Mms2 binding Ubc13 in an “end-on” or “T-shaped” manner. Because the crystal structures of Ubc13 and Mms2 were also solved on their own, it was observed that neither protein undergoes a large overall structural change upon heterodimer formation, except for a localized displacement of the most N-terminal residues of Mms2 up to its first α -helix (Moraes et al., 2001). Further inspection reveals that the Mms2 N-terminus, $\alpha 1$ helix, and Loop 1 portions apparently pack against Ubc13 to form the unique E2-Uev structure. This physical interaction creates a long channel which buries ~ 1500 Å² of solvent-accessible surface area (Moraes et al., 2001; VanDemark et al., 2001).

Perhaps the greatest contribution of the Ubc13-Mms2 crystal structures is the insight they gave into the possible mechanistic basis behind Lys63-mediated poly-Ub chain formation. Visual inspection of the 3-dimensional structures reveals three predominant channels through which Ub could be envisioned to bind or pass along.

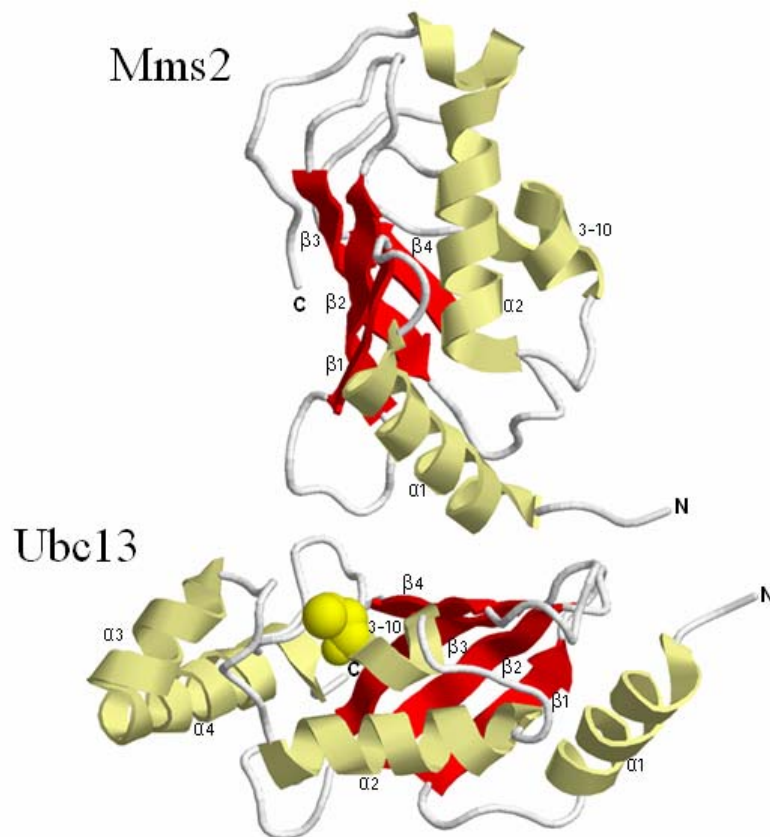
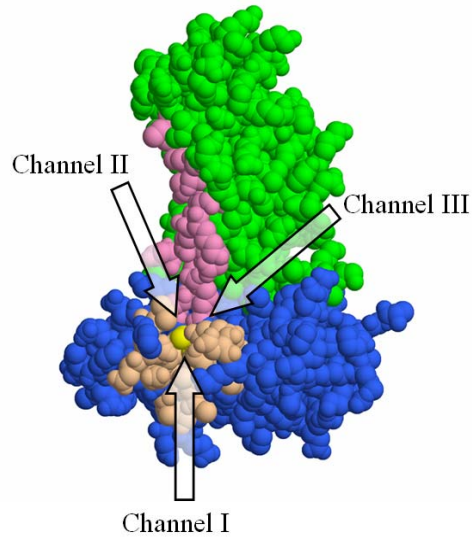


Figure 1-2. Overall structure of the human Ubc13-Mms2 heterodimer. 3-dimensional crystal structure co-ordinates were derived from the Protein Databank File “17JD” and RasTop 2.1 (www.geneinfinity.org) was used to create the molecular image. The Ubc13 active-site Cys is indicated in space-fill representation (yellow).

Each channel converges on the Ubc13 active-site, facilitating a multi-component scenario involving both a donor and acceptor Ub, and a putative exit path (Figure 1-3). Channel 1 corresponds to the typical E2 active-site where in this case, Ubc13 would bind the donor Ub through a covalent thioester bond. Because the Ubc13 structure does not appreciably change upon binding Mms2, it has been inferred that channel 1 behaves relatively independent of Mms2. In contrast, the remaining two channels are formed only after the asymmetrical heterodimer is created by the Ubc13-Mms2 interaction. Channel 2 runs steeply along one side of Mms2 toward the Ubc13 active-site, and is postulated to comprise the necessary link between donor and acceptor Ub, thus providing the key molecular framework for Lys63-linked poly-Ub chain assembly. In accordance, molecular docking programs lead to solutions whereby Mms2 specifically interacts with an acceptor Ub such that the Ub-Lys63 residue is made specifically available to the Ubc13 active-site through Channel 2. The last identifiable channel to converge on the Ubc13 active-site is also only apparent after Ubc13-Mms2 heterodimer formation. With the conjugation steps accounted for, Channel 3 has been speculated as an outgoing path for Lys63-linked Ub conjugates and follows in a relatively opposite direction to channel 2.

The predictions concerning channels 1 and 2 that were based on visualization of the heterodimer crystal structures were later supported by detailed NMR analyses (McKenna et al., 2003b). In these experiments, the chemical-shifts for every residue in Ubc13, Mms2, and Ub were monitored during all the possible binding combinations to create an elaborate interaction map for each of the individual protein surfaces.

A



B

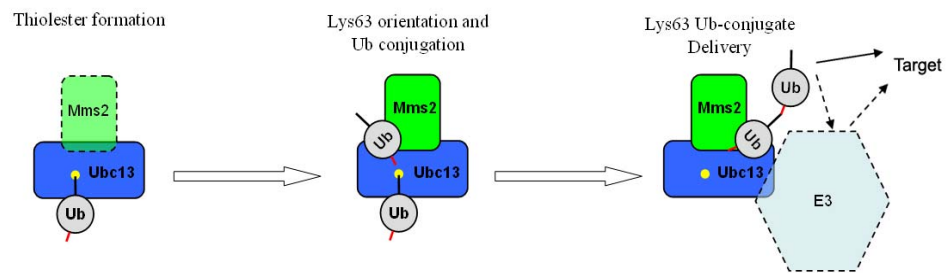


Figure 1-3. Channels created by the Ubc13-Mms2 heterodimer provide the framework for Lys63-linked Ub conjugation. (A) van der Waals space-fill representation of the Ubc13-Mms2 surface. Mms2 (green), Ubc13 (blue), Ubc13 active-site Cys (yellow). Residues undergoing chemical shift upon Ub-Ubc13 thiolester formation and Mms2-Ub non-covalent interaction are shown in tan and rose, respectively. Arrows indicate channels through which Ub is proposed to pass during ubiquitylation. (B) Cartoon representation showing the steps involved in Ubc13-Mms2-mediated ubiquitylation from left to right. Channel 1 involves thiolester formation with the donor Ub, Channel 2 orients the acceptor Ub for Lys63 conjugation, and Channel 3 aids in the delivery of the conjugate (direct or indirect) to the target.

The pooled data was then used to create an unbiased, data-driven, computer generated prediction of the Ub-Ubc13-Mms2-Ub tetrameric complex (Figure 1-4). The solution alleviated any speculation surrounding the mechanistic hypothesis proposed from visual inspection of the crystal structures alone. The results showed that the Mms2-bound Ub is oriented such that its Lys63 ϵ -amino nitrogen is placed within 4 Å of the carboxyl-terminus of Ub-Gly76 at the Ubc13 active-site. It is notable that in this model the surface of Ubc13 at the distal end of channel 3, which is proposed to bind E3s, remains completely available (McKenna et al., 2003b).

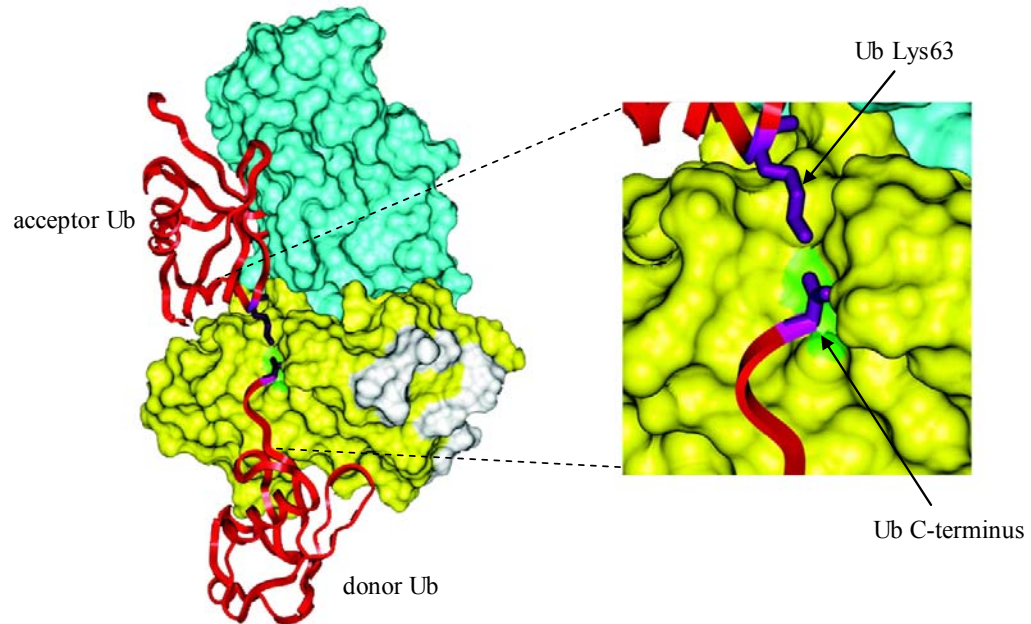


Figure 1-4. Model for the mechanism of Lys63-linked Ub conjugation by Ubc13-Mms2. The NMR-based structure on the left is adapted from McKenna *et al.*, 2003 showing the human Ubc13 (yellow and white) and Mms2 (blue-green) heterodimer oriented similar to Figure 1-3, and bound to two molecules of ubiquitin (red). Shown at right is a close-up view of the acceptor Ub bound by Mms2 such that its Lys63 ϵ -amino group is in close proximity to the C-terminus of a donor Ub bound at the Ubc13 active-site Cys (green).

The elegant and detailed model describing Lys63-linked Ub conjugation by the Ubc13-Mms2 (i.e. Ubc13-Uev) E2 complex is a unique case in the ubiquitylation field. Whereas the chemistry of ubiquitylation has been understood for quite some time (Haas and Rose, 1982; Hershko et al., 1983), the mechanistic basis behind the various steps remains somewhat unclear despite a wealth of structural data. One of the greatest difficulties is that, unlike the case for Ubc13-Mms2, the conjugation of one Ub molecule to another is generally expected to take place on the E3 or the target protein. Therefore, the variability of E3s (HECT, RING finger, U-box, multi-subunit, etc.), the sheer number of target proteins, and the lack of a ubiquitylation consensus sequence are a few of many features that make it difficult to present a unified model for Ub conjugation. Indeed, the structure-based models of Ub chain assembly so far suggest two very different general strategies in order to overcome the same apparent problem; a very large distance between the C-terminus of the Ub bound at the E2 active-site and its eventual conjugation site on the target (VanDemark and Hill, 2002). In the case of HECT-domain E3s, the problem is proposed to be overcome by mechanisms involving large conformational changes (Huang et al., 1999; Verdecia et al., 2003). In contrast, the structural data of the RING finger E3 c-Cbl (Zheng et al., 2000) and the multi-subunit E3 SCF (Hao et al., 2005; Zheng et al., 2002; Zheng et al., 2000) suggest that structural rigidity is important. The passing of Ub from the E2 active-site in these cases is instead proposed to involve the specific placement of the target within large gaps created in the E2-E3 structure. Most interestingly, neither of these current models explain how a particular Lys-specific Ub linkage is made. The clarity and precision of the mechanistic

model for Lys63-linked Ub-conjugation by Ubc13-Mms2 is likely to be a gold-standard in the ubiquitylation field for a long time to come.

1.9 Structure of Lys63-linked ubiquitin chains

With an elegant mechanistic model to explain Lys63-linked Ub chain formation, another important question involves the consequence that the unique chains have on the target. An obvious possibility is that Lys63-linked Ub chains result in a significantly different topology than Lys48 Ub chains, and are therefore presented to the cell as a distinct molecular signal. Indeed, several lines of evidence to date suggest that Lys63-linked Ub would signal for something other than proteasome-mediated degradation. First, cells expressing Ub-K63R as their sole source of Ub have no apparent deficiency in bulk protein turnover (Spence et al., 1995). Second, several studies suggest that the half-life of proteins conjugated by Lys63-linked Ub is not appreciably reduced (Arnason and Ellison, 1994; Fisk and Yaffe, 1999; Galan and Haguenuer-Tsapis, 1997; Spence et al., 2000) and the current cellular roles involving Lys63-linked Ub chains so far do not seem to involve proteasome-mediated degradation. For example, inhibition of the proteasome does not lead to a significant reduction in DNA damage tolerance activity (Hofmann and Pickart, 2001) or Ub-Lys63-dependent signaling (Deng et al., 2000). Also, Ub₄ is the minimum Ub-chain length recognized by the 26S proteasome (Thrower et al., 2000) and some *in vitro* evidence suggests that Ubc13-Mms2 predominantly synthesize Ub₂ (McKenna et al., 2001). Third, Lys63-linked Ub chains are structurally distinct from those linked through Lys48.

The 3-dimensional structures of Lys48-linked Ub₂ and Ub₄ have been solved by NMR (Varadan et al., 2003; Varadan et al., 2002) and X-ray crystallography (Cook et al., 1992; Cook et al., 1994; Phillips et al., 2001). Despite this wealth of data, the flexible nature of the Lys48-linked Ub-conjugates leaves some uncertainty surrounding the particular orientation to which the chain conforms. For example, Lys48-linked chains appear to orient themselves in “open” and “closed” conformations *in vitro*. The closed conformation is made possible through intermolecular Ub interactions mediated by hydrophobic patches. The Lys48-linked open conformation does not have such non-covalent contacts. The most recent and detailed NMR data suggests that Lys48-linked Ub chains predominantly exist in the closed conformation under physiological conditions; however, a small degree of conformational flexibility when binding other proteins *in vivo* is not ruled-out (Varadan et al., 2004). Nonetheless, the invariable feature of Lys48-linked Ub chains is that the connections between the C-terminal Gly residue of one Ub and the Lys48 residue of the next are at ~90° with respect to one another.

In a marked contrast to Lys48, the Ub-Lys63 residue is approximately 180° relative to the C-terminal Gly residue. As a result, these linkages can be envisioned to create a more linear or extended poly-Ub tertiary structure. Structural studies of Lys63-linked Ub₂ in solution are in accordance with this prediction (Varadan et al., 2004). In addition, the intermolecular binding of Lys48-linked poly-Ub chains is not observed for the Ub linkages via Lys63. Yet another distinction between Lys48- and Lys63-linked Ub chains was demonstrated through protein interaction studies using a Ub-binding protein. In the experiment a promiscuous Ub-binding domain was shown to bind to Lys63-linked

Ub chains in a manner similar to mono-Ub. In contrast, the interaction with Lys48-linked Ub chains was made in a different, albeit undetermined, high-affinity manner (Varadan et al., 2004). Future structural studies of Lys63-linked Ub chains, especially those for Ub₄, are expected to provide more evidence supporting the notion that different Ub chains lead to distinct chain topology and behavior.

1.10 Cellular roles of Lys63-linked ubiquitin chains

It is in some ways helpful to group the cellular roles of Lys63-linked poly-Ub chains into two categories; 1) those that clearly involve Ubc13-Uev-mediated ubiquitylation and 2) those that do not appear to involve Ubc13-Uev-mediated ubiquitylation, or where the data is insufficient or merely suggestive. Taken together, the number of cellular roles implicated with Lys63-linked Ub chains to date is still far fewer than those for Lys48-linked Ub chains.

1.10.1 Cellular roles of Lys63-linked ubiquitin chains generated by Ubc13-Uev

As discussed above, one of the best-characterized roles for Ubc13-generated Lys63-linked Ub chains is error-free DNA damage tolerance in *S. cerevisiae* (Broomfield et al., 2001; Pastushok and Xiao, 2004). Largely due to studies in our laboratory, there is strong evidence to suggest that the role of Ubc13-Mms2 and Lys63-linked Ub chains is conserved in error-free DDT throughout eukaryotes (Andersen et al., 2005; Ashley et al., 2002; Brown et al., 2002; Li et al., 2002; Wen, et al., in press). In addition, the cadmium sensitivity of a mouse neuroblastoma cell line induced by the expression of Ub-K63R is likely attributed to a deficiency in Ubc13-Mms2-mediated ubiquitylation in DDT

(Tsirigotis et al., 2001). A complicating factor in studying DNA repair in higher eukaryotes, however, is the occurrence of an additional Mms2 homolog called Uev1. Uev1A adopts a similar 3-dimensional structure to Mms2 (Zhang et al., 2005), binds with similar affinity to Ubc13 and Ub (McKenna et al., 2003a), and is able to function in place of *MMS2* in yeast DDT (Chapter 3 of this thesis). These similar features made it difficult to exclude the possibility that Uev1A could function like Mms2 with Ubc13 to generate Lys63-linked Ub chains in mammalian DDT. A recent publication by our laboratory was able to rule out this option by showing that the Ubc13-Mms2 complex functions in DNA repair, while the Ubc13-Uev1A complex is responsible for the activation of the NF- κ B signaling pathway (Andersen et al., 2005).

The activation of the NF- κ B pathway through Lys63-linked Ub chains is the other well-characterized role involving Ubc13 (Finley, 2001). NF- κ B is a vertebrate transcription factor that is responsible for the expression of numerous genes that govern various important biological processes such as cell differentiation and apoptosis, inflammation, and immunity (Baldwin, 1996; Chen et al., 1999; Chen, 2005; Krappmann and Scheidereit, 2005). Under non-stimulating conditions, an I κ B protein prevents the transcription function of NF- κ B by sequestering it in the cytosol. NF- κ B can be activated through a number of elaborate signal-transduction pathways that respond to various stimuli that are most often, but not always, detected by plasma-membrane receptors (Krappmann and Scheidereit, 2005). Transduction of the signal requires the action of various cytosolic proteins that eventually lead to the phosphorylation of I κ B by an activated I κ B kinase (IKK). Phosphorylated I κ B is ubiquitylated via Lys48-linked poly-Ub chains and subsequently degraded by the proteasome, leaving NF- κ B free to enter the

nucleus and elicit the appropriate transcriptional response (Chen et al., 1995; Scherer et al., 1995).

The connection between Ubc13-Uev1A and the NF- κ B pathway was originally made through the establishment of a cell-free system to monitor IKK activation by TRAF6 (tumor necrosis factor receptor-associated factor 6; Deng et al., 2000). TRAF6 is a RING finger E3 involved in the NF- κ B signal transduction pathway responding to the stimulation of interleukin-1 and Toll-like receptors. Using the *in vitro* cell-free assay, Deng et al. showed that TRAF6-dependent activation of IKK required a cell-extract fraction containing the Ubc13-Uev1A complex. Further analysis specifically demonstrated that IKK activation is dependent on Lys63-linked ubiquitylation by Ubc13-Uev1A, and that the ubiquitylation activity is promoted by TRAF6. The lack of proteasomes in the assay also suggested that the Lys63-linked poly-Ub-mediated activation of IKK is proteasome independent. In a follow-up study, it was reported that TRAF6 is actually a target of the Ubc13-Uev1A Lys63-linked Ub chains, in a step that is required for the activation of IKK (Wang et al., 2001).

Shortly after these novel findings, Ubc13-Uev1A and Lys63-linked Ub chains were demonstrated to be involved in the activation of several other signaling pathways employing the same general scheme; namely the transduction of a receptor-borne signal by TRAF-associated Lys63-linked poly-ubiquitylation by Ubc13-Uev1A. These signal transduction pathways included those for tumor necrosis factor receptors (Shi and Kehrl, 2003), endosome-associated Toll-like receptors (Luftig et al., 2003), and T-cell receptors (Sun et al., 2004; Zhou et al., 2004). Intriguingly, in the latter case, the final target of the Lys63-linked Ub chains was the γ subunit of IKK (NEMO), indicating that TRAF6 might

be a ubiquitylation intermediate instead of a *bone fide* target. However, it cannot be ruled out that TRAF6 and NEMO are both biologically relevant targets of Ubc13-Uev1A-mediated Ub conjugation.

In addition to DNA repair and cell signaling, a very recent discovery will likely uncover additional roles for Ubc13-Mms2/Uev1A-generated Lys63-linked Ub chains. A crystal structure has been reported for a trimeric complex consisting of Ubc13, Uev1A, and CHIP (C-terminal of Hsp70 interacting protein; Zhang et al., 2005). The physical interaction was confirmed through the co-purification of Ubc13-Uev1A and CHIP derived from human cell-extracts. In the crystal structure, CHIP binds directly to Ubc13 through a surface that is typical of E2-E3 interactions. Based on the visual comparison with the Ubc13-Mms2 heterodimer structure, the Ubc13-Uev1A interaction is apparently uninhibited by binding to CHIP (Moraes et al., 2001; VanDemark et al., 2001). Importantly, the physical interaction of CHIP with Ubc13-Uev1A does not appear to obstruct the surfaces necessary for the Lys63-linked Ub-conjugation model. In support of this fact, CHIP specifically facilitates Ubc13-Uev1A-mediated Lys63-linked Ub chain formation (Zhang et al., 2005).

CHIP normally exists as a dimeric U-box E3 that mediates interactions between E2s from the Ubc4/5 family and the molecular chaperones Hsp70 and Hsp90 (Ballinger et al., 1999). The physical connection between ubiquitylation machinery and protein chaperones suggests that CHIP plays a general role in protein quality control. Indeed, along with Ubc4/5, CHIP is responsible for the ubiquitylation of unfolded protein (Murata et al., 2001). Given the novel finding that CHIP is also involved with Ubc13-Uev1A-mediated Lys63-linked ubiquitylation, I propose a model whereby CHIP can

have two distinctly opposite roles in governing protein folding. In one role, a terminally unfolded protein could be marked for elimination through the CHIP-Ubc4/5 complex and modification by Lys48-linked Ub chains. In another role, the CHIP-Ubc13-Uev1A complex could target an unfolded protein with Lys63-linked Ub chains which would not lead to proteasome-mediated degradation. This could potentially allow for proper protein refolding through the affiliation of CHIP with Hsp70/90.

While the hypothesis involving Ubc13-Uev1A in protein folding is speculative, it is interesting to recall the discovery of Lys63-linked Ub chains *in vivo*. In the study, the authors identified that the *ub-K63R* mutation caused yeast cells to be sensitive to treatments that can cause protein misfolding (heat-shock and canavanine) (Arnason and Ellison, 1994). Other evidence that implicates Ubc13-Uev1A in protein folding is found via the physical association with CHIP. CHIP has been connected to the Lys63-linked ubiquitylation of tau, and the tau protein and associated insoluble protein aggregates are typical in Alzheimer's disease (Babu et al., 2005; Petrucelli et al., 2004; Shimura et al., 2004). CHIP is also found to physically interact with the RING finger E3 Parkin, which is involved with Lys63-linked Ub-conjugation by Ubc13-Uev1A (Doss-Pepe et al., 2005; Imai et al., 2002; Lim et al., 2005a). The mutation of Parkin can lead to the misfolding and aggregation of proteins which are characteristically found in Parkinson's Disease (Lim et al., 2005b). Taken together, a potential role for Ubc13 in general protein folding is plausible and the implication in neurodegenerative diseases is exciting.

1.10.2 Cellular roles implicated with Lys63-linked ubiquitin chains

Spanning a wide range of biological processes in several different organisms, Lys63-linked Ub chains have been implicated in poxvirus function (Huang et al., 2004), cell motility (Didier et al., 2003), photomorphogenesis (Yanagawa et al., 2004), a mitotic checkpoint (Bothos et al., 2003), mitochondrial inheritance (Fisk and Yaffe, 1999), ribosome function (Spence et al., 2000), and membrane permease endocytosis (Galan and Hagenauer-Tsapis, 1997; Springael et al., 1999). While these roles for Lys63-linked Ub chains are exciting, there is either insufficient or no evidence in these cases to support the involvement of Ubc13-Mms2/Uev1A.

In several of these instances the involvement of a Ubc13-Uev complex is implicated but the data is not conclusive. With poxvirus function (Huang et al., 2004), photomorphogenesis (Yanagawa et al., 2004), and the mitotic checkpoint (Bothos et al., 2003), the affiliation of Lys63-linked Ub chains with Ubc13-Uev is based solely upon *in vitro* ubiquitylation assays. It is notable that such experiments are sometimes prone to erratic behavior and possible false-positives. For example, the E2 UbcH5 has promiscuous Ub conjugation activities *in vitro* and can promote ubiquitylation reactions with numerous E3s that may not be physiologically relevant (Bothos et al., 2003). Also, *in vitro* ubiquitylation reactions involving Ubc13-Uev may be promoted by the simple addition of irrelevant peptide sequences (personal communication, T. Moraes, University of Alberta, Edmonton, AB). While the ubiquitylation involved with cell motility was monitored *in vivo*, the experimentation did not distinguish between a direct or indirect relationship with Ubc13 (Didier et al., 2003).

A second group of cellular roles attributed with Lys63-linked Ub chains has been discovered using the expression of *ub-K63R* to invoke various phenotypes. While the

Ub-Lys63 residue was shown to be important for mitochondrial inheritance (Fisk and Yaffe, 1999), ribosome function (Spence et al., 2000), and membrane permease endocytosis (Galan and Haguenaer-Tsapis, 1997; Springael et al., 1999), a connection between the *ub-K63R* phenotype and *ubc13* has not been made. In fact, there is evidence to suggest that Ub conjugation via Lys63 in at least two of these cases may be mediated by other ubiquitylation enzymes. For example, the Lys63-dependent ubiquitylation of the large ribosomal subunit *in vivo* is abolished in a *ubc4* Δ strain (Spence et al., 2000; Spence et al., 1995). Also, the modification of the uracil and general amino acid permeases requires Ub-Lys63 and the HECT domain E3, Rsp5 (Galan and Haguenaer-Tsapis, 1997; Galan et al., 1996; Springael et al., 1999). While neither Ubc4 or Rsp5 have been shown to genetically or physically interact with Ubc13, they have been documented to interact with one another (Horak, 2003; Nuber and Scheffner, 1999).

One of three possibilities is expected for the implicated roles for Lys63-linked Ub conjugation in this section; 1) they are experimental artifacts, 2) a definitive requirement for Ubc13-Uev will be demonstrated, or 3) an additional mechanism of Lys63-linked Ub conjugation will be discovered. Given the clear data-derived model for Lys63-linked Ub chain formation by Ubc13-Uev, my feeling is that the second possibility is most likely. I expect that phenotypes for *ubc13*, *mms2*, and/or *uev1* will eventually be linked to the cellular roles where *in vivo* Lys63-linked Ub chains are well-demonstrated.

1.11 Summary and significance

Ubiquitylation is a fundamental and indispensable covalent modification system found throughout eukaryotes. Conventional wisdom has held that ubiquitylation leads to

the conjugation of Lys48-linked Ub chains to various protein targets, which in turn signals for their specific degradation by the proteasome. The discovery of Ub chains linked through alternative Lys residues, such as Lys63, has presented new and exciting challenges in the field. Central questions concerning Lys63-linked Ub chains that arose were the identity of the E2(s) involved in creating them, the biochemical mechanism(s) employed, and in what cellular role(s) they function.

The revelation that a unique Ubc13-Uev heterodimer could provide the biochemical activity for Lys63-linked Ub chain formation came as a surprise. Through close collaboration, I had the pleasure of being involved in the landmark studies that carved out an elegant model for the mechanism behind Lys63-linked Ub conjugation by Ubc13-Mms2. Without an *in vivo* functional context, however, the proposal stands as a mere hypothetical *in vitro* model. This thesis serves to provide many detailed structure-function studies in order to help validate the Ubc13-Mms2 Ub conjugation model. Through the generation of additional hypotheses and careful experimentation, the molecular underpinnings behind the cellular functions of Ubc13-Mms2 were further uncovered.

Despite the proposed mechanism of Lys63-linked Ub conjugation by Ubc13-Uev, a connection between Lys63-linked Ub chains observed *in vivo* and Ubc13-Uev has not been found in some cases. In the final chapter of this thesis, I attempted to clarify one of these occurrences through the investigation of a novel direct interaction between Mms2 and a protein involved in a membrane-permease endocytosis pathway.

CHAPTER TWO MATERIALS AND METHODS

2.1 Strains, cell culture, transformation, and storage

2.1.1 Yeast

The *Saccharomyces cerevisiae* two-hybrid strains used in this study include PJ69-4A (*MATa trp1-901 leu2-3, 112 ura3-52 his3-200 gal4Δ gal80Δ P_{GAL2}-ADE2 LYS2::P_{GAL1}-HIS3 met2::P_{GAL7}-lacZ*), a gift from P. James (University of Wisconsin at Madison). The other two-hybrid strain used was Y190 (*MATa gal4 gal80 his3 trp1 ade2-101 ura3 LEU2::URA3 GAL1-LAC7 LYS2::GAL1-HIS3*), which was received from D. Gietz (University of Manitoba, Winnipeg, MB).

Most of the functional tests were performed using the haploid *S. cerevisiae* strain HK580-10D (*MATa ade-1 can1-100 his3-11,15 leu2-3, 112 trp1-1 ura3-1*) as the wild-type reference strain. The strain was received from H. Klein (New York University, New York, NY) and used as the recipient to delete the entire *MMS2* open reading frame (ORF) by a one-step gene replacement method (Rothstein, 1983) using an *mms2Δ::HIS3* cassette generated through PCR (polymerase chain reaction) amplification as previously described (Xiao et al., 1999). With the same approach, a *ubc13Δ* HK580-10D strain using a *ubc13Δ::HIS3* cassette (Brusky et al., 2000), a *mms2Δ ubc13Δ* HK580-10D strain using the *mms2Δ::HIS3* and *ubc13::hisG-URA3-hisG* cassettes, and a *mms2Δ rev3Δ* HK580-10D strain using *mms2Δ::HIS3* and *rev3::hisG-URA3-hisG* cassettes were also created.

The *rev3::hisG-URA3-hisG* was obtained using a *KpnI* restriction digestion of plasmid pDG347, received from D. Gietz (Roche et al., 1994).

The *rsp5* strain used in this study came from the allelic *mut2* strains that were received as a tetrad from a backcross (HP148-2A, 2B, 2C, 2D). The wild-type parental strain is XV185-14C (*MATa ade2-1, arg4-17, his1-7, hom3-10, lys1-1, trp5-48*) and all strains were provided as a gift from R.C. von Borstel (University of Alberta, Edmonton, AB).

SUB280 (*MATa, his3-Δ200, leu2-3,112, ura3-52, lys2-801, trp1-1, [am] ubi-Δ1::TRP1, ubi2-Δ2::ura3, ubi3-Δub-2, ubi4-Δ2::LEU2*) (Finley et al., 1994) and SUB413 (isogenic to SUB280) are specially engineered yeast strains for the exclusive expression of wild-type and K63R mutated ubiquitin, respectively. In SUB280, Ub is expressed from a gene on the multi-copy plasmid pUB39 which is under the control of a copper-inducible *CUP1* promoter. In SUB413, the wild-type Ub of pUB39 is replaced with a K63R mutant. SUB280 and SUB413 were received as gracious gifts from R. Haguenaer-Tsapis (Institut Jacques Monod, Université Paris, Paris).

A BY4741 (*MATa, his3Δ, leu2Δ, lys2Δ, ura3Δ fur4Δ*) strain was purchased from Research Genetics as part of a homozygous deletion library in *S. cerevisiae*. The strains were created using the protocol described at the Saccharomyces Genome Deletion Project (http://www-sequence.stanford.edu/group/yeast_deletion_project/deletions3.html). An otherwise isogenic strain with *trp1Δ* was used as the wild-type control.

Yeast cells were cultured at 30°C in a complete YPD medium (1% Bacto-yeast extract, 2% Bacto-peptone, 2% glucose) or in a synthetic dextrose (SD) medium (0.67% Bacto-yeast nitrogen base without amino acids, 2% glucose) supplemented with

necessary nutrients as required (20 mg/l of adenine, uracil, tryptophan, histidine, arginine, and methionine; 30 mg/l of tyrosine, lysine; 50 mg/ml leucine; 200 mg/ml threonine; Adames, 1997). To make solid plates, 2% agar was added to either YPD or SD medium prior to autoclaving and the molten agar was cooled in a 55°C water bath before being poured into Petri dishes.

Yeast cells were transformed using a modified dimethyl sulfoxide (DMSO)-enhanced protocol (Hill et al., 1991). For each transformation, approximately 1.5 ml of early log-phase yeast cells were pelleted and washed with 500 µl lithium acetate solution (LiOAc, 0.1 M lithium acetate, 10 mM Tris-HCl, pH 8.0). The suspension was pelleted once again and resuspended in 100 µl of LiOAc. The transforming DNA was then added along with 4 µl of denatured and sheared salmon sperm DNA (10 mg/ml stock). Prior to a 45 minute incubation at 30°C, 280 µl of 50% polyethelene glycol 4000 was added and each sample was mixed gently. After this incubation, 39 µl dimethyl sulfoxide was added and the cells were heat-shocked at 42°C for 5 minutes. Cells were pelleted, the supernatant was discarded, and 500 µl double-distilled water (ddH₂O) was used to resuspend and wash the cells. Cells were pelleted once again, the supernatant was discarded, and the cells were resuspended in 100 µl ddH₂O and the entire volume was spread evenly on an agar plate. Plates were incubated at 30°C for 72 hours to allow colony growth. Prior to experimental use, putative transformants were streaked onto selective medium and allowed to grow up once again. For short term storage, yeast cell plates were sealed and then placed at 4°C for up to two months. For long term storage, actively growing yeast cells were suspended in 15% sterile glycerol and then frozen and stored at -70°C indefinitely.

2.1.2 Bacteria

The bacterial strain used in this study for protein expression was BL21-CodonPlus (DE3)-RIL [F^- *ompT hsdS*(r_B^- m_B^-) *dcm*⁺ *Tet*^r *gal* λ (DE3) *endA* *Hte* (*argU ileY leuW* *Cam*^r)]. This strain carries extra copies of the *argU*, *ileY* and *leuW* tRNA genes to help overcome codon bias, and was purchased from Stratagene (#230245). For typical DNA plasmid propagation and isolation, *Escherichia coli* DH10B (F^- *mcrA* Δ (*mrr-hsdRMS-mcrBC*) ϕ 80*lacZ* Δ M15 Δ *lacX*74 *recA1 endA1 ara* Δ 139 Δ (*ara, leu*)7697 *galU galK* λ -*rpsL* (*Str*^R) *nupG*) or *Escherichia coli* DH5 α (F^- ϕ 80*dlacZ* Δ M15 Δ (*lacZYA-argF*) U169 *recA1 endA1 hsdR*17(r_k^- , m_k^+) *phoA supE*44 λ^- *thi-1 gyrA*96 *relA*1) purchased from GibcoBRL (now Invitrogen) was used. With the exception of the incubation temperatures used for protein expression (see below), bacterial cells were incubated at 37°C. Bacteria cultures were grown in Luria Broth (LB) (1% Bacto-tryptone, 0.5% Bacto-yeast extract, 1% NaCl, pH 7.0). LB agar plates were prepared by the addition of water to a ready-made stock powder (US Biological, #L1500) which was then autoclaved, cooled to 55°C, and poured into Petri plates. When required for plasmid selection, media cooler than 55°C was supplemented with ampicillin (amp) to a final concentration of 50 μ g/ml.

Transformation of competent bacterial cells was performed by chemical and electroporation methods. For an electroporation, a 25 μ l aliquot of competent DH10B cells was removed from -70°C and placed on ice to thaw. Approximately 0.01 μ g of plasmid DNA was added to the cells and incubated for 45 seconds on ice. The plasmid and cell mixture was then transferred to a pre-chilled Gene Pulser Cuvette (Bio-Rad, #165-2089) that was then loaded into a Bio-Rad *E. coli* Gene Pulser and administered a

1.80 kV electric pulse. 400 μ l of liquid SOC media (2% Bacto-tryptone, 0.5% Bacto-yeast extract, 0.05% NaCl, 20 mM glucose, 2.5 mM KCl, 10 mM MgCl₂, pH 7.0) was added to the electrocuted cells which were subsequently incubated in a 37°C water bath for one hour. 100 μ l of the cell suspension was then spread evenly onto an appropriate selectable agar plate for an overnight incubation at 37°C. For a chemical transformation, a 50 μ l aliquot of competent DH5 α cells was removed from -70°C and placed on ice to thaw. Approximately 0.1 μ g of plasmid DNA was added to the cells and after a 30 minute incubation on ice, the cells and DNA were heat-shocked at 42°C for 45 seconds, and 450 μ l of room-temperature SOC media was added. The tube was then incubated in a 37°C water bath for one hour after which 150 μ l of the cell suspension was spread evenly onto an appropriate selectable agar plate for an over night incubation at 37°C. All putative transformants were streaked onto selective medium prior to their experimental use. For short term storage, the bacterial cell plates were sealed and then placed at 4°C for up to one month. For long term storage, actively growing bacterial cultures were suspended in 10% DMSO and then frozen and stored at -70°C indefinitely.

2.2 Plasmids and DNA

2.2.1 UBC13 and MMS2

The human *UBC13* open-reading frame (ORF) was PCR amplified as an *EcoRI-SalI* fragment and cloned into pGBT9 (Bartel and Fields, 1995) to form pGBT-hUBC13, an N-terminal fusion to Gal4_{BD}. The same *UBC13* fragment was similarly cloned into pGEX6 (GE Healthcare, #27-4597-01) to form an N-terminal gene fusion to glutathione-S-transferase (GST) and named pGEX-*hUBC13*. Human *MMS2* cDNAs were isolated as

previously reported (Xiao et al., 1998). The ORF was PCR amplified as a *Bam*HI-*Sal*I fragment and cloned into pGAD424 (Bartel and Fields, 1995) to form an N-terminal fusion to Gal4_{AD}, named pGAD-hMMS2. The same *MMS2* fragment was cloned into pGEX6 to form an N-terminal fusion to GST, named pGEX-hMMS2. The pGEX6-hUBC13-Y34A, -L83A, and pGEX6-hMMS2-F13A clones were provided as gracious gifts from M. Ellison (University of Alberta, Edmonton, AB). pYEX-MMS2 and pYEX-UBC13 are yeast GST-fusion constructs that were purchased from Research Genetics as part of a yeast GST-fusion library, and encode yeast GST-Mms2 and GST-Ubc13, respectively. The pYEX constructs are under the control of the *CUP1* inducible promoter. The YCpL-MMS2 construct was cloned using a *Bgl*II restriction digest of yeast genomic DNA which releases a 1043 base pair (bp) fragment containing the entire yeast *MMS2* gene, corresponding to 246 bps downstream and 797 bps upstream of the start site. YCpL-MMS2-A and YCpL-MMS2-B represent the two orientations for the bi-directional cloning of the *Bgl*II DNA fragment. The human *MMS2* ORF was PCR amplified to generate a *Bam*HI-*Sal*I fragment without a stop codon that was subsequently cloned into pG4BD-1 (received from R.B. Brazas, University of California San Francisco, San Francisco, CA) to create a C-terminal fusion to Gal4_{BD} called pG4BD-hMMS2. pG4BD-yMMS2 was created in the same manner.

Yeast two-hybrid, GST-fusion, and yeast centromeric plasmids containing site-specific mutations within human *UBC13*, *MMS2*, or yeast *MMS2* were constructed by the mega-primer site-directed mutagenesis approach described below.

2.2.2 UEV1A and UEV1B

The GST-Uev1A and GST-Uev1B proteins were derived from PCR amplification of cDNA clones for *UEV1A* (obtained from Z.J. Chen, University of Texas Southwestern Medical Center, Dallas, TX) and *UEV1B* (obtained from S. Lin, Robert Wood Johnson Medical School, Piscataway, NJ); the resulting fragments were cloned into pGEX6 (GE Healthcare, #27-4597-01). For the yeast two-hybrid constructs, *UEV1A* and *UEV1B* coding regions without stop codons were amplified by PCR as *Bam*HI–*Sal*I fragments and cloned into pG4BD-1 as C-terminal fusions to Gal4_{BD}.

2.2.3 RSP5

For yeast *RSP5* protein expression, a yeast pES4 plasmid containing a C-terminal-truncated *Bgl*II–*Xho*I PCR fragment of yeast *RSP5* that retains the WW and HECT domains was received as a gift from T. Harkness (University of Saskatchewan, Saskatoon, SK). This construct, pES4-RSP5ΔC2, contains the *TRP1* gene for selection and is under the inducible expression of the *CUP1* promoter, which governs the expression of a Myc-tagged Rsp5 fragment that lacks the C2 domain. It is noted that a *Bgl*II–*Xho*I digestion only releases the *RSP5* fragment, and not the *MYC* portion.

To determine the domain(s) sufficient for Rsp5 interaction with Mms2, N-terminal and C-terminal deletion constructs were made as follows. The *RSP5* ORF was obtained by an *Eco*RI–*Xho*I digestion of pYES-RSP5 (as a gift from T. Harkness) which was then cloned into *Eco*RI–*Sal*I fragments of pGBT9 and pGAD424 to form pGBT-RSP5 and pGAD-RSP5, respectively. Plasmid pGBT-*RSP5* containing the entire coding sequence (for amino acids 1-809) or subsequent derivatives were used to create a panel of deletion constructs. Double restriction digestion was carried out to generate the desired

deletions, followed by filling of the cohesive ends by the Klenow fragment of DNA polymerase I where required. The resulting DNA was then self-ligated and a small DNA linker was used to restore the proper reading frame when necessary. pGBT-*RSP5* derivatives were made with the following restriction enzymes; Rsp5 Δ 1-180 (*EcoRI-EcoNI*); Rsp5 Δ 1-325 (*EcoRI-KpnI*); Rsp5 Δ 1-360 (*EcoRI-BamHI*); Rsp5 Δ 1-468 (*EcoRI-BsaBI*); Rsp5 Δ 326-809 (*KpnI-NotI*); Rsp5 Δ 468-809 (*BsaBI-NotI*); Rsp5 Δ 183-809 (*EcoNI-NotI*).

2.2.4 CHFR, TRAF6, and FUR4

A human *CHFR* gene construct, pGEX4T-1, was received from T.D. Halazonetis (University of Pennsylvania, Philadelphia, PA) encoding a GST-fusion to amino acids 281-543 of *CHFR*, which contains the entire RING-finger domain.

The full-length mouse *TRAF6* ORF was obtained from Z.J. Chen. The *mTRAF6* ORF was cloned as an *EcoRI-SalI* fragment into pGBT9 and pGAD424 to form pGBT-*mTRAF6* and pGAD-*mTRAF6*, respectively.

The multi-copy yeast plasmid YEp352fF (2 μ *LEU2*) carries the *FUR4* gene under its own promoter and encodes the yeast uracil permease (Galan et al., 1996). YEp352fF was received as a gracious gift from R. Haguenaer-Tsapis.

2.2.4 DNA cloning and analysis

Plasmid manipulations were performed using enzymes from Invitrogen and New England Biolabs as per manufacturer instructions. Plasmid DNA was normally propagated using a small-scale boiling method (Maniatis et al., 1982). Approximately

1.5 ml of overnight bacterial culture was pelleted and subsequently resuspended in 350 μ l of bacterial lysis solution (0.1M NaCl, 10mM Tris-HCl, 1mM EDTA, 5% Triton X-100, pH 8). 20 μ l lysozyme (10 mg/ml in 10mM Tris-HCl, pH 8) was then added, the suspension was gently mixed, and the tubes were immediately placed in boiling water for 45 seconds, and then spun in a bench-top centrifuge at high speed (\sim 16,000 x g) for 10 minutes. The cell debris pellet was discarded and ethanol precipitation was carried out. Plasmids were resuspended in ddH₂O and kept frozen at -20°C for storage at a working concentration of \sim 0.005 μ g/ μ l. Plasmid preparations requiring higher concentration, yield, and purity were created using a plasmid mini-prep kit (BioRad, #732-6100).

Plasmid DNA and DNA fragments were separated by agarose gel electrophoresis [0.75% agarose in 1X TAE buffer (24% Tris base, 5.7% glacial acetic acid, 10% EDTA, pH 8.0)]. Gels were loaded into an electrophoresis apparatus filled with 1X TAE buffer, and a constant current of <100 mA was applied until the desired migration was reached. Gels were stained in 0.5 μ g/ml ethidium bromide for 5-10 minutes and the DNA was viewed using a UV trans-illuminator. DNA to be isolated was cut from the agarose gel as thin as possible, and placed at -70°C in a 1.5 ml Eppendorf tube (E-tube) for at least 30 minutes. A sieve for the DNA fragment was then made by introducing a pin-point hole in the bottom of a 0.5 ml E-tube, into which a small amount of cheesecloth (representative of \sim 50 μ l volume) was packed. The frozen gel piece was added into the 0.5 ml E-tube, which was placed inside a 1.5 ml E-tube and spun in a table-top centrifuge for 10 minutes (\sim 16,000 x g). The flow-through was collected and subsequently treated with phenol/chloroform as required to remove contaminants from the DNA preparation, which was then precipitated in ethanol and resuspended in ddH₂O.

2.3 Polymerase chain reaction

Polymerase chain reaction was used to amplify DNA fragments for the purposes of cloning and mutagenesis. PCR reaction mixtures were created using the recipe guidelines in the instruction manual for the Pfu Turbo DNA polymerase (Stratagene, #600250), which was used in all reactions. A PTC-100 programmable thermal controller (MJ Research, Inc., Watertown, MA) was used as the thermocycler to carry out the various amplifications. As a program guideline, a denaturing temperature of 95°C for one minute was followed by an annealing temperature of 55°C for 45 seconds, and primer extension was carried out at 72°C for 1 minute per kilobase of DNA to be amplified. These three steps were repeated 25 times per reaction.

2.4 Site-directed mutagenesis

The site-directed mutagenesis of human *UBC13* and *MMS2* was performed using a modified form of the megaprimer site-directed mutagenesis approach (Figure 2-1) based on (Baretino et al., 1994). For the first round of PCR, the pGEX6-hUBC13 and -hMMS2 constructs were used as the templates in a PCR using the upstream primer pGEX6-5', and a relevant downstream mutagenic primer (see Table 2-1) to synthesize the mutagenic megaprimer. The megaprimer fragment was then gel purified and used in the second round of PCR where the pGBT-hUBC13 and pGAD-hMMS2 constructs were used as templates in their respective reactions, pGEX6-5' was re-added (to amplify the megaprimer), and hUBC13-3' and pGAD-3' were used as downstream primers for pGBT-hUBC13 and pGAD-hMMS2, respectively. The resultant *hUBC13* and *hMMS2*

fragments were cloned into pGBT9 and pGAD424, respectively. Point mutations were confirmed by automated DNA sequencing at the Plant Biotech Institute, Saskatoon, SK or by my own manual DNA sequencing using a T7 Sequencing Kit (USB Corporation, #27168201).

The site-directed mutagenesis of yeast *MMS2* was carried out using the original megaprimer site-directed mutagenesis approach (Landt et al., 1990). In the first PCR, the YCpL-yMMS2 construct in the “A” orientation was used as the template DNA, and an upstream M13 universal reverse and a downstream mutagenic primer were used to generate the megaprimer. In the second PCR, the same vector backbone was used but with *yMMS2* in the opposite orientation (YCpL-yMMS2-B) and the M13 universal reverse primer was re-added along with the megaprimer.

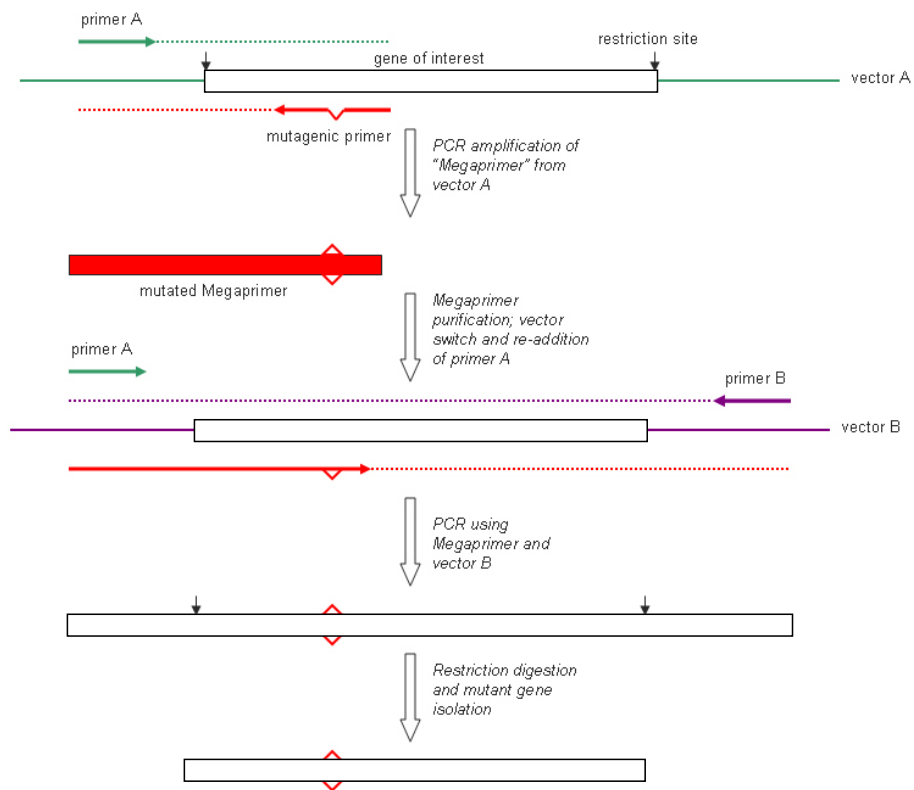


Figure 2-1. Site-directed mutagenesis strategy. A modified version of the megaprimer method of site-directed mutagenesis was employed. Of note is that two different vectors containing the same gene of interest is used. In the second round of PCR, a single primer specific for each vector allows the exponential amplification of the mutated DNA only.

Table 2-1. Oligonucleotides used for site-directed mutagenesis and PCR amplification.

Oligonucleotide*	Sequence (5'-3')
ohMMS2-Q23A	CGCCTACTCCTTTTGCTCCTTCTTCAAGTTC
ohMMS2-K24A	CGCCTACTCCTGCTTGTCCTTCTTCAAG
ohMMS2-S32A	CAAGGCCCCAGGCAACTGTACCGTC
ohMMS2-M49A	GGCCCAATAATCGCGCCTGTCCACC
ohMMS2-N12D	CCAACAAGCGAAAATCACGAGGAACTTT
ohMMS2-N12A	CCAACAAGCGAAACGAACGAGGAACT
ohMMS2-P10A	GCGAAAATTACGAGCAACTTTAACTC
ohMMS2-F13Y	CCAACAAGCGATAATTACGAGGAAC
ohMMS2-F13E	CCAACAAGCGCTCATTACGAGGAAC
ohMMS2-S64A	CTACTTTCAGGGCATATATTCTGTTTTC
ohMMS2-S64E	CTACTTTCAGCTCATATATTCTGTTTTC
ohUBC13-E55Q	GGAAGGAATAGTTGAAGTTTAAAAGTCCC
ohUBC13-F57E	TCTTCTGGAAGCTCTAGTTCAAGTTT
ohUBC13-F57Y	TCTTCTGGAAGGTATAGTTCAAGTTT
ohUBC13-E60Q	TGGGTATTCTTGTGGAAGGAATAG
ohUBC13-R70A	TTGGTCATGAAAGCTACTTTAGGTGC
ohUBC13-R70L	TTGGTCATGAAAAGTACTTTAGGTGC
ohUBC13-R70F	TTGGTCATGAAAATACTTTAGGTGC
ohUBC13-M64A	TTTAGGTGCTGCTGCTGGGTATTCTTC
ohMMS2-I62A	ACTTTCAGGCTATATGCTCTGTTTTTCATAATTT
oyMMS2-S27A	GCTAAACCATAAGCACATGATTCTGG
oyMMS2-I57A	GAAAGGGAATAGGCTCTGTTTTTCATG
M13 universal forward	GTAAAACGACGGCCAGT
M13 universal reverse	GGA AAC AGC TAT GAC CAT G
pGEX6-5'	CTG GCA AGC CAC GTT TG
pGAD-3'	GAA CTT GCG GGG TTT TTC
hUBC13-3	CCG TCG ACT TAA ATA TTA TTC ATG GC

*All oligonucleotides were ordered from Integrated DNA Technologies.

2.5 Recombinant protein expression and purification

BL21(DE3)-RIL (Stratagene, #230245) cells transformed with pGEX6-hMMS2, pGEX-hUBC13, or pGEX-CHFR were grown overnight at 37 °C in LB + amp media and then sub-cultured 1:10 into pre-warmed LB + amp the following day. Cells continued to grow to an optical density (OD) at 600 nm of between 0.6 and 0.8, and were then induced with 0.5 nM isopropyl- β -D-thiogalactopyranoside (IPTG) and transferred to a 30°C incubator for a 2 hour induction. Cells were harvested by centrifugation at 5000 x g and resuspended in phosphate-buffered saline (PBS, 140 mM NaCl, 2.7 mM KCl, 10 mM Na₂HPO₄, 1.8 mM KH₂PO₄, pH 7.3). Crude extracts were generated by passing the cells through a French Press at 10,000 psi and the soluble fraction was retained after centrifugation at 39,800 x g for 30 minutes. When needed, a bacterial protease inhibitor cocktail (Sigma, #P8465) was added as per the manufacturer guideline. All subsequent steps were performed at 4 °C. Soluble extracts were passed through a pre-packed 5 ml GStrap column (GE Healthcare, #17-5131-01), which was then washed with at least 5 column volumes of 1X PBS. GST-fusion proteins were eluted with reduced glutathione elution buffer (10 mM glutathione in 50 mM Tris-HCl, pH 8.0) and dialyzed extensively against cleavage buffer (50 mM Tris-HCl, 150 mM NaCl, 1 mM EDTA, 1 mM dithiothreitol, pH 7.0). If protein purity was not sufficient, the above purification steps were repeated. When needed, cleavage was performed by the addition of 2 units of Prescission Protease (GE Healthcare, #27-0843-01) per mg of fusion protein, followed by 16 hours incubation at 4°C with gentle rocking. Cleaved proteins were then applied to a GStrap column in order to remove the GST component from the cleaved protein of interest. When necessary, proteins were concentrated using Amicon Ultra centrifugal

filter devices (Millipore, #901024), and protein concentrations were determined using the BCA Protein Assay Kit (Pierce, #23227) as per the instruction manual. Purified proteins were kept at 4°C for short term use, or placed into <500 µl aliquots and were frozen quickly and kept at -70°C for long term storage. Purified Ub was purchased commercially (Sigma, #93950).

2.6 Protein analysis

Proteins were subject to sodium dodecyl sulfate polyacrylamide gel electrophoresis (SDS-PAGE) for visual analysis. In general, samples for SDS-PAGE were made by the addition of 2X protein sample buffer (125 mM Tris pH 6.8, 4% SDS, 10% glycerol, 0.006% bromophenol blue, 1.8% β-mercaptoethanol) to the protein solution. The protein samples were then placed in boiling water for 5 minutes, cooled, and then loaded onto the protein gel. Most commonly, 12% discontinuous (5% stacking, 12% separating) Tris-glycine polyacrylamide (37:1 acrylamide:bisacrylamide) gels were used (recipe in Maniatis *et. al*, 1989), with the exception that 10% polyacrylamide gels were used for the Fur4 membrane-protein analysis. Gels were stained with Coomassie Blue staining solution (0.025% Coomassie Brilliant Blue R250, 40% methanol, 7% acetic acid) for at least 30 minutes, followed by incubation in de-stain solution (40% methanol, 10% acetic acid) until proper protein band visibility was observed (1 hour to over night). The Mini-Protean 3 (Bio-Rad, #165-3301) gel apparatus was used for all SDS-PAGE.

In order to visualize proteins via Western blot, polyacrylamide gels from SDS-PAGE were equilibrated for 20 minutes in transfer buffer (0.037% SDS, 5.8% Tris-base, 3% (w/v) glycine, 10% methanol pH) along with equal-sized polyvinylidene fluoride

transfer membranes (Perkin-Elmer, #NEF1002) and filter papers. The components were assembled as described in manual for the Bio-Rad trans-blot semi-dry transfer cell, which was used for the blotting of proteins onto the PVDF membranes. Transfers were carried out for 1 hour at a constant current of 1 mA/cm². Membranes were then incubated in a blocking solution of (PBS, 3% non-fat milk powder) overnight at 4°C. The desired primary antibody was diluted in 10 ml PBST (PBS, 0.05% Tween-20, 1% non-fat milk powder) and the PBST solution was incubated with the membranes at room temperature for 1 hour with gentle rocking. The membranes were washed 3 times for 5 minutes with PBST. Subsequently, the desired secondary antibody was diluted in 10 ml PBST and incubated with the membranes as with the primary antibody. The membranes were then washed 3 times for 5 minutes with PBST and then 2 times with PBS to prepare for detection. The Western Lightning Chemiluminescence Reagent (Perkin-Elmer, #NEL101) was used as the substrate for the visualization of horseradish peroxidase-conjugated secondary antibodies. The detection of alkaline phosphatase-conjugated secondary antibodies was performed by a colourimetric reaction using the substrates nitroblue tetrazolium chloride and 5-bromo-4-chloro-3-indolyl phosphate diluted in alkaline phosphatase buffer (100 mM Tris, 100 mM NaCl, 5 mM MgCl₂, pH 8.5) to 330 µg/ml and 165 µg/ml, respectively.

2.7 GST pull-down assays

GST pull-downs were performed using MicroSpin GST Purification Modules (GE Healthcare, #27-4570-03). For the assays testing the interaction between human Ubc13 and Mms2, and Ubc13 and CHFR, 0.03 mg of purified GST fusion protein in 1X PBS

was loaded and incubated in the purification module for 1 h at 4°C with gentle rocking. The module was then washed three times with 500 µl PBS. Subsequently, 0.03 mg of purified, non-fused protein of interest in 1X PBS was added to the module and the incubation was continued for another hour at 4°C. The module was washed again three times with 500 µl PBS and 80 µl of reduced glutathione elution buffer was then added to elute the affinity-purified proteins. Eluted samples were subjected to SDS-PAGE and visualized by Coomassie Blue staining and/or Western Blot analysis.

The yeast protein GST pull-downs involving GST-Mms2, GST-Ubc13, and myc-Rsp5 were performed similar to the above but with the following differences. All proteins of interest were expressed from plasmids in *S. cerevisiae* cells and were harvested from total-cell extracts. The pES4-RSP5ΔC2 construct was co-transformed with pYEX-yMMS2 or pYEX-yUBC13 into *mms2Δ* or *ubc13Δ* yeast strains, respectively. The co-transformed cells were grown in selective media at 30°C until an OD at 600 nm of approximately 0.8 was reached. 0.5 mM CuSO₄ was then added to induce the expression of *GST-MMS2*, *GST-UBC13*, and *MYC-RSP5* for 2 hours at 30°C. Cells were then pelleted and resuspended in 1.5 x volume PBS with yeast protease inhibitor cocktail (Sigma, #P8215) as suggested. The suspension was then vortexed vigorously at 4°C in the presence 1 x volume of 0.5 mm glass beads for three 15 second bursts. The extract was then centrifuged at 4°C for 20 minutes at ~16,000 x g. 500 µl of the supernatant was applied to the Microspin GST Purification Modules and rocked gently for 2 hours at 4°C. The eluted proteins were visualized by Western Blots using α-GST and α-Myc Western blots.

2.8 Co-immunoprecipitation

The pES4-RSP5 Δ C2 construct was transformed into yeast cells and prepared as above (GST pull-down assays) to generate yeast cell extracts containing myc-Rsp5. In this case, N150 buffer (50 mM HEPES pH 7.8, 5 mM magnesium acetate, 10% glycerol, 0.005% NP40, 60 mM potassium acetate with 1 mM DTT) was used in place of PBS. Myc-Rsp5 was immunoprecipitated after the addition of 15 μ l of mouse α -Myc antibody to 1 ml of the yeast cell extract, followed by a 4 hour incubation at 4°C with gentle rocking. 100 μ l of Protein A Sepharose (Sigma, #P9424) was then added with 50 μ g of purified yeast Mms2 protein and the incubation was continued for another 4 hours at 4°C with gentle rocking. The suspension was centrifuged at low speed (2000 x g), the supernatant was removed (and saved as the input control), and 1 ml of N150 buffer was added to wash the beads. These wash steps were repeated 5 times except 200 μ l of protein sample buffer was added instead of N150 in the final step. The protein samples were then placed in boiling water for 5 minutes, cooled to room temperature, and the supernatant was loaded to a polyacrylamide gel. The co-immunoprecipitation of yMms2 was visualized by Western blot analysis using the cross-reacting mouse α -hMms2 polyclonal antibody.

2.9 Yeast two-hybrid assay

The yeast two-hybrid strains PJ69-4A (James et al., 1996) or Y190 (Zheng et al., 2002) were co-transformed with different combinations of Gal4_{BD} and Gal4_{AD} constructs. For each strain, the co-transformed colonies were initially selected on SD-Trp-Leu. For the PJ69-4A strain, a cell growth assay was performed where at least four independent colonies were grown in SD-Trp-Leu media and then replica plated onto either SD-Trp-

Leu-His alone or SD-Trp-Leu-His + 3-aminotriazole (3-AT) to test the activation of the *P_{GALI}-HIS3* reporter gene, or SD-Ade to test the activation of the *P_{GALI}-ADE* reporter gene. Plates were incubated for 48 hours at 30°C unless otherwise indicated. For the Y190 strain, a filter-lift assay was performed (Bartel and Fields, 1995) where at least four independent colonies were replica plated onto SD-Trp-Leu. White filter paper (3 mm) was then carefully overlaid onto the agar plate and the adhered yeast cells were then submerged in liquid nitrogen for 10 seconds. This filter paper was then overlaid, with the cells facing up, onto another filter paper pre-equilibrated in a Petri dish with a freshly mixed development buffer containing 1.8 ml of “buffer Z” (60 mM Na₂HPO₄, 40 mM NaH₂PO₄, 10 mM KCl, 1 mM MgSO₄), 45 µl X-gal (40 mg/ml stock in dimethylformamide), and 5 µl β-mercaptoethanol. The Petri dish was then sealed with parafilm and placed at 30°C until the desired signal was seen (4 hours to overnight).

2.10 Functional complementation assays

Gradient plate assays were performed for the semi-quantitative measurement of yeast cell sensitivity to MMS. At least three independent colonies for each strain were individually inoculated into 1 ml of SD minimal media and grown overnight. To prepare the gradient plates, molten YPD agar (30 ml) was mixed with the appropriate concentration of MMS to form a bottom layer. The gradient was created by pouring this layer into tilted square Petri dishes. After solidification for one hour, the Petri dishes were laid flat and 30 ml of the same molten agar without MMS was poured to form the top layer which was allowed to solidify for one hour. 0.1 ml of cells were then taken from the overnight cultures, mixed with 0.4 ml sterile water and 0.5 ml of 2% molten YPD

agar, and then immediately imprinted, using the edge of a microscope slide, onto the gradient plates that were made that day. Plates were incubated at 30°C for 48 hours (unless otherwise noted) before taking the photograph.

Dilution plate assays were performed for the semi-quantitative measure of yeast cell sensitivity to MMS and UV. 10 µl of overnight cell culture grown in selective minimal media was spotted as 10-fold dilutions in water, beginning with undiluted cultures, on selective minimal media agar plates containing MMS. For UV treatment, the spots were left to dry prior to dose administration. Plates were incubated at 30°C for 72 hours before taking the photograph.

2.11 Yeast membrane protein enrichment

The enrichment of yeast membrane proteins for SDS-PAGE was closely based on the method outlined by Galan et al., 1996. Yeast cells transformed with YEp352fF (encoding Fur4) were cultured in 100 ml of selective minimal media to an optical density at 600 nm of 0.8. Cell cultures were then centrifuged at 4,700 x g and the wet cell pellets were weighed. 300 µl of lysis buffer (0.1 M Tris-HCl, pH 7.5, 0.15 M NaCl, 5 mM EDTA) containing yeast protease inhibitor cocktail (Sigma, #P8215) was added for every 100 µg of wet cell pellet. All subsequent steps were performed at 4°C. A 1 x volume of glass beads was added and the tubes were vortexed vigorously in 1 minute intervals for a total of 3 minutes. The crude extract was then diluted 3X in lysis buffer and centrifuged at 0.4 x g for 1 minute. Leaving the pelleted cell debris and glass beads, the supernatant was removed and transferred to a separate tube, followed by centrifugation for 30 minutes at ~16,000 x g. This supernatant, representing the non-membrane-protein enriched

fraction, was saved for future analysis. The membrane enriched pellet was then suspended in 400 μ l lysis buffer plus 5 M urea, incubated on ice for 30 minutes, and centrifuged for 30 minutes at \sim 16,000 x g. The supernatant was discarded, and the pellet was resuspended in 400 μ l lysis buffer plus 10% trichloroacetic acid. A 15 minute centrifugation at \sim 16,000 x g was used to pellet the proteins once again. The supernatant was discarded and 10 μ l of 1 M Tris base was mixed with the pellet using a pipette tip. 40 μ l of 2X protein sample buffer was added, and the samples were heated at 37°C for 15 minutes, cooled to room temperature, and then loaded onto polyacrylamide gels.

2.12 Antibody generation and antibodies used

Mouse polyclonal antibodies against human Ubc13 and Mms2 proteins were generated as follows. Five eight-week-old female BALB/c mice were injected with an emulsion containing either purified human Ubc13 or Mms2. The emulsion was made by diluting the protein in PBS to 400 μ g in a final 1 ml volume. 1.1 ml of Freund's incomplete adjuvant was added to the 1 ml of protein, and the adjuvant and protein were emulsified with about 20 strokes of an emulsifier plunger. 2 ml of Tween 80 (1% in PBS) was added to the emulsified protein and 0.8 ml (\sim 80 μ g protein) of the mixture was injected into the intraperitoneal cavity of each mouse using 25 5/8 gauge needles. Three weeks later, a booster was given with the same procedure as before, except that half the amount of total protein was injected (\sim 40 μ g). Four weeks later, a second booster was given with the same protocol as the first booster. Five weeks later (a total of 12 weeks after the first injection), the mice were orbital bled, followed by cervical dislocation. Whole blood was placed on ice for 30 minutes, then centrifuged long enough (\sim 1 minute

at 13000 x g) so the supernatant (serum) could be removed for analysis. Anti-sera was dispensed in 50 µl aliquots and kept frozen at -70°C for long term storage. Non-injected mice were handled in parallel to provide negative control serum. A good working dilution for Western Blots containing ng quantities of protein was found to be 1:2500 and 1:1000 for the anti-Mms2 and anti-Ubc13 antibodies, respectively.

Other primary antibodies used in these studies were goat anti-GST (GE Healthcare, #27-4577-01), mouse anti-Fur4 (gift in kind from R. Haguenaer-Tsapis), and rabbit anti-Myc (Upstate, #06-549). Secondary antibodies used in these studies were alkaline phosphatase-conjugated anti-mouse (Calbiochem, #401212), horseradish peroxidase-conjugated anti-mouse (Upstate, #12-349), and alkaline phosphatase-conjugated anti-goat (Calbiochem, #401512). All antibodies were used at or above the manufacturer's recommended dilutions.

2.13 Ubiquitylation assays

A 0.5-ml conjugation reaction containing Uba1 (20 nM), ³⁵S-labeled Ub (2.5 µM), and Ubc13 or Mms2 (250 nM) in an ATP mixture (10 mM HEPES, pH 7.5, 5 mM MgCl₂, 5mM ATP, and 0.6 unit/ml inorganic phosphatase) was incubated at 30°C for 60 min. Reactions were terminated by the addition of trichloroacetic acid to a final concentration of 10% and processed for SDS-PAGE and subsequent analysis by autoradiography.

2.14 Surface plasmon resonance

Surface plasmon resonance (SPR) was performed using a Biacore X instrument. To create a chip for protein interaction analysis, a research grade CM5 sensor chip (Biacore, #BR-1000-12) was used to immobilize anti-GST antibody by amine coupling, according to instructions in the Amine Coupling (Biacore, #BR-1000-50) and GST Capture Kits (Biacore, #BR-1002-23). Approximately 15,000 response units (RU) of anti-GST antibody was immobilized to each of the two flow cells (Fc1 and Fc2). For all SPR experiments, GST-fusion or native proteins were purified to >95% homogeneity and dialyzed against HBS-P buffer (50 mM HEPES, 150 mM NaCl, 3 mM EDTA, 0.005% Surfactant P20, pH 7.5). All reagents were also degassed extensively and filtered immediately prior to use.

For the SPR studies involving GST-Ubc13 and GST-Mms2, a buffer flow rate of 20 μ l per minute and a 2 minute injection of 5 μ g/ml protein was used to capture ~1000 RU of the GST-fusion protein (ligand) in Fc2. For a control, purified recombinant GST (supplied in the GST Capture Kit) was similarly injected into the other flow cell to capture ~1000 RU in Fc1. All data generated were corrected for background in real-time (Fc2 – Fc1). To yield the binding curves, 10 μ l of the soluble protein (analyte) at various concentrations was then applied to the flow cells at 5 μ l per minute for 2 minutes. Regeneration of the sensor chip surface was accomplished with a 20 μ l per minute injection of 10 mM glycine, pH 2.2 for 2 minutes.

SPR studies of GST-Mms2 and Ub interaction were performed as those described above, except that only half (~600 RU) of the GST derivatives were immobilized to the sensor chip flow cells. To account for the slightly different amount of GST-Mms2

immobilized in each assay, the binding response to Ubc13 for each GST-Mms2 protein was measured, and the value was used as a factor for standardization.

For the determination of the Ubc13-Mms2 dissociation constant, Biacore BiaEvaluations software was used for fitting binding curves that were generated from analyte concentrations ranging from 1×10^{-8} to 5×10^{-8} M for Mms2, and 2.5×10^{-8} to 5×10^{-7} M for Ubc13. See Figure 2-2 for an example. With empirical knowledge (McKenna et al., 2001), a 1:1 molecular binding with mass transport was used as the interaction parameter in the software. The Chi^2 values were 5.2 and 2.3 for the GST-Mms2-Ubc13 and GST-Ubc13- Mms2 interactions, respectively. The data is deemed reliable by Biacore standards if Chi^2 is below 10.

Dissociation constants were also determined by manual calculation. Using plots of the response at equilibrium (RU_{eq}) vs. analyte (M), I was able to interpolate the maximum response (RU_{max}) for the interaction. Double-reciprocal plots of $1/\text{RU}_{\text{eq}}$ vs. $1/\text{analyte (M)}$ were then made and the K_d was calculated using the equation $K_d = \text{RU}_{\text{max}} \cdot \text{Slope}$. An example of these plots is shown for the GST-Mms2-Ub interaction in Figure 2-3.

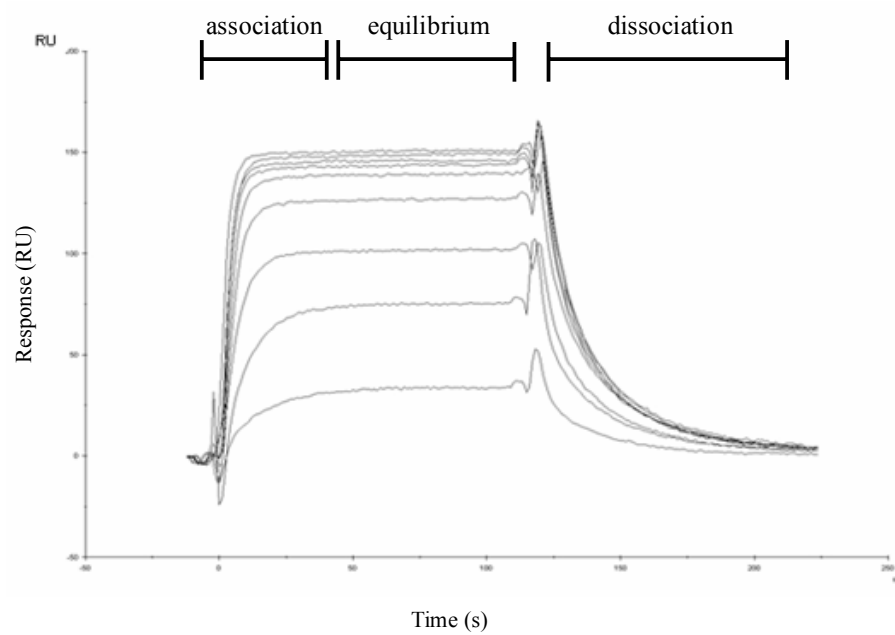


Figure 2-2. Example of binding curves used for computer-generated binding constant determination. Surface plasmon resonance was used to generate binding curves for the interaction between GST-Mms2 (ligand) and Ubc13 (analyte). Binding is depicted in a plot of the response (RU) vs. time (s) for various concentrations of analyte. These curves, along with the specific concentrations of protein used, were used in a curve-fitting algorithm provided by Biacore BiaEvaluations software to determine the dissociation constant of the GST-Mms2-Ubc13 interaction.

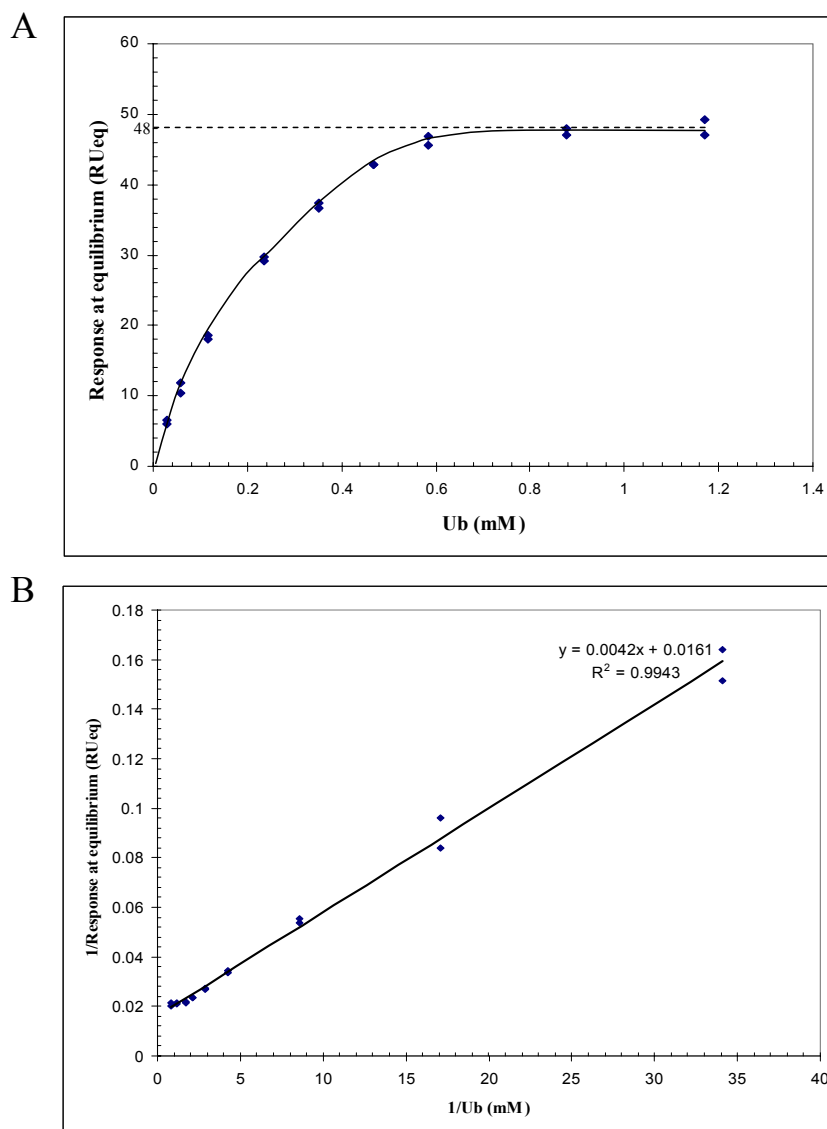


Figure 2-3. Example of plots used in the manual calculation of dissociation constants. (A) The interaction between GST-Mms2 (ligand) and various concentrations of Ub (analyte) are plotted as response at equilibrium (RU_{eq}) vs. analyte (mM). The maximum response (RU_{max}) was interpolated from the curve as 48. (B) A double-reciprocal plot of (A) is shown and the slope of the graph is determined to be 0.0358. Calculation of the dissociation constant was performed using values from (A) and (B), and the equation $K_d = RU_{max} \cdot \text{slope}$.

CHAPTER THREE FUNCTION OF HUMAN UBC13-UEV COMPLEXES IN YEAST DNA DAMAGE TOLERANCE

3.1 Rationale

The initial goal of this thesis was to establish a reliable experimental system for testing the structural and functional relationships of the human Ubc13 and Mms2 proteins. The preferred system would allow a quick and simple means to test the effect of various mutations on protein function. Given the extensive genetic characterization of *UBC13* and *MMS2* in *S. cerevisiae* DNA damage tolerance, it was felt that the most straight-forward approach would be to test the human *UBC13* and *MMS2* genes for functional complementation of their yeast counterparts in DDT. It should be noted here that unless otherwise indicated, the gene and protein names given throughout this thesis most often refer to the human counterparts, except in Chapter 5.

As discussed in chapter 1, DDT in *S. cerevisiae* is a branched pathway that includes at least one error-free and one mostly mutagenic component (Broomfield et al., 2001; Xiao et al., 1999; Figure 1-1). The *RAD6* and *RAD18* genes constitute the “stem” and are required for both sub-pathways, and their lack of function leads to the most severe DNA damage sensitivities of the DDT genes. It is for this reason that DDT is sometimes referred to as the *RAD6* DNA repair epistasis group. As compared with *rad6* or *rad18*, the mutation of genes involved in the error-free or mutagenic sub-pathways

cause a partial sensitivity to DNA damage. However, the abrogation of both sub-pathways with an *mms2Δ rev3Δ* strain, for example, leads to a DNA damage sensitivity that is nearly as severe as the *rad18* single deletion. Underscoring the requirement for Ub-mediated signaling in DDT, a strong DNA damage sensitive phenotype is also observed for point mutations that prevent Ub conjugation to PCNA. Because DDT is initiated by replication-blocking lesions, the genes involved in the pathway are sensitive to a wide array of DNA damaging agents.

Genetically speaking, error-free DDT activity is dependent on *UBC13*, *MMS2*, and Lys63-linked Ub chains (Hofmann and Pickart, 1999; Pastushok and Xiao, 2004). As a result, *ubc13*, *mms2*, and *ub-K63R* mutant strains are similarly sensitive to DNA damage. When this thesis work began, very little was known about the possible mechanisms of the Ubc13 and Mms2 proteins. The only insights came from a genetics-based inference that Lys63-linked Ub chains generated by Ubc13 and Mms2 were required for DDT, and a physical association that was observed between Ubc13 and Mms2 (Hofmann and Pickart, 1999). Soon after, we and our colleagues presented a model which outlined how a human Ubc13-Mms2 heterodimer is formed to generate Lys63-linked Ub chains (McKenna et al., 2001). As will be discussed in detail in chapter 4, the model implies that the function of Ubc13 and Mms2 in DDT is dependent on their ability to form a heterodimer and to conjugate Lys63-linked Ub chains. It was thus expected that a reliable system for testing the function of human *UBC13* and *MMS2* in *S. cerevisiae* would allow correlations to be drawn between heterodimer formation, Lys63-linked poly-Ub conjugation, and DDT function.

Using yeast DDT as a functional assay for structural studies of human Ubc13 and Mms2 has several advantages. First, *S. cerevisiae* offers many properties that make it an easy organism in which to perform molecular biology experiments, especially when compared to human cells. Those relevant to my studies include efficient plasmid transformation, an abundance of genetic markers, ease in creating gene knock-outs (cassette-targeted gene disruption), the availability and versatility of plasmid vectors, a fast rate of growth, and the relatively short time in which assays can be performed. Second, even to this day, the only known cellular function for yeast Ubc13 and Mms2 is error-free DDT, and no other phenotypes or growth defects have been observed for *ubc13* or *mms2* mutants. In contrast, the additional cellular roles attributed to mammalian Ubc13 and Mms2 as discussed in chapter 1 would likely complicate data interpretation and analysis. Last and most interestingly, the yeast system would be contingent on the heterologous function of Ubc13-Mms2 heterodimers. If the aforementioned mechanistic model is correct, the functional complementation in DDT by human *UBC13* or *MMS2* for its corresponding yeast mutant would require the yeast-human Ubc13-Mms2 heterodimer pairs to be compatible. Heterologous functions for Ubc13-Uev pairs have not been previously reported.

The plausibility of using human *UBC13* and *MMS2* genes in *S. cerevisiae* is seen in several ways. First, the yeast and human *UBC13* and *MMS2* genes share 68% and 47% protein sequence identity, respectively, and almost all of the other DDT genes have apparent homologs in higher eukaryotes (Table 3-1). Furthermore, most, if not all of the proteins listed have retained the functional domains or motifs that are seen in *S. cerevisiae* DDT proteins. The only exception is Rad5, which based upon protein

sequence analysis alone, does not have a true sequence homologue in higher eukaryotes. Nevertheless, several potential *RAD5* functional homologues are currently under investigation. Second, several genes isolated from higher eukaryotes are found to be capable of functionally complementing their corresponding DDT defects in budding yeast (Ashley et al., 2002; Koken et al., 1991; Xiao et al., 1998). Third, in a few limited cases, experimental inactivation of mammalian DDT genes in a cell line or in an animal model results in phenotypes reminiscent of the corresponding yeast mutants (Li et al., 2002; Roest et al., 1996; Tateishi et al., 2000). Finally, the Lys164 residue in PCNA appears to be conserved in all eukaryotic organisms examined so far (Pastushok and Xiao, 2004), suggesting that the mechanism of covalent modification of PCNA in DDT has been conserved throughout evolution. Indeed, the Rad18-dependent mono-ubiquitylation of mammalian PCNA has been observed (Watanabe et al., 2004) and mono-ubiquitylated PCNA signals for the preferential binding of a mammalian TLS polymerase after DNA damage (Kannouche et al., 2004; Watanabe et al., 2004).

Table 3-1. Sequence conservation of eukaryotic DDT proteins.

Protein (<i>S. cerevisiae</i>)	Organism	Protein name or accession number	% Identity*
Rad6	<i>H. sapiens</i>	E2a, E2b	69, 69
	<i>M. musculus</i>	Ube2a, Ube2b	69, 68
	<i>A. thaliana</i>	Ubc2	65
	<i>D. melanogaster</i>	Dhr6	68
	<i>C. elegans</i>	Ubc-1	61
	<i>S. pombe</i>	Rhp6	77
Rad18	<i>H. sapiens</i>	Rad18	14
	<i>M. musculus</i>	Rad18	15
	<i>A. thaliana</i>	n/a	-
	<i>D. melanogaster</i>	n/a	-
	<i>C. elegans</i>	n/a	-
	<i>S. pombe</i>	NP_595423	23
Ubc13	<i>H. sapiens</i>	Ubc13	68
	<i>M. musculus</i>	Ubc13	68
	<i>A. thaliana</i>	Ubc13a, Ubc13b	66, 65
	<i>D. melanogaster</i>	Bendless, NP_609715	70, 68
	<i>C. elegans</i>	Ubc13	66
	<i>S. pombe</i>	Ubc13	70
Mms2	<i>H. sapiens</i>	Mms2, Uev1a	47, 46
	<i>M. musculus</i>	Mms2	47
	<i>A. thaliana</i>	Uev1a, Uev1b, Uev1c, Uev1d	53, 51, 53, 52
	<i>D. melanogaster</i>	NP_647959	46
	<i>C. elegans</i>	Uev1	45
	<i>S. pombe</i>	Mms2	65
PCNA	<i>H. sapiens</i>	PCNA	35
	<i>M. musculus</i>	PCNA	35
	<i>A. thaliana</i>	PCNA	39
	<i>D. melanogaster</i>	PCNA	35
	<i>C. elegans</i>	PCNA	38
	<i>S. pombe</i>	PCNA	45

* DDT proteins from *S. cerevisiae* were applied to BLAST analysis and the highest scoring homologs from various model organisms were included in the table and shown with % amino acid sequence identity. n/a, not applicable (no sufficient homology found). Note: BLAST search with Rad5 failed to identify sufficient sequence homologs from any organisms examined in the database to date.

3.2 Results

3.2.1 Human *UBC13* and *MMS2* are able to function in *S. cerevisiae*

Early genetic studies on yeast *UBC13* and *MMS2* demonstrated that both genes are indispensable for error-free DDT (Broomfield et al., 1998; Brusky et al., 2000; Hofmann and Pickart, 1999). Therefore, the first functional complementation approach was to use double transformations of human *UBC13* and *MMS2* in *ubc13 mms2* double-deletion yeast strains to test for DDT activity. The experimental assay used an agar plate that is made with an increasing concentration of an alkylating agent, MMS, to induce DNA damage. On these gradient plates, the *ubc13Δ mms2Δ* strain was unable to grow at higher MMS concentrations due to a DNA repair deficiency, and functional complementation was observed as a relief of the MMS sensitivity. Figure 3-1 shows that the *ubc13Δ*, *mms2Δ*, and *ubc13Δ mms2Δ* yeast strains exhibited a roughly equivalent sensitivity to MMS. However, a double transformation containing both human *UBC13* and *MMS2* complemented the DNA damage sensitivity of the *ubc13Δ mms2Δ* strain. On the other hand, the single transformation of human *UBC13* or *MMS2* did not restore drug resistance in the double mutant.

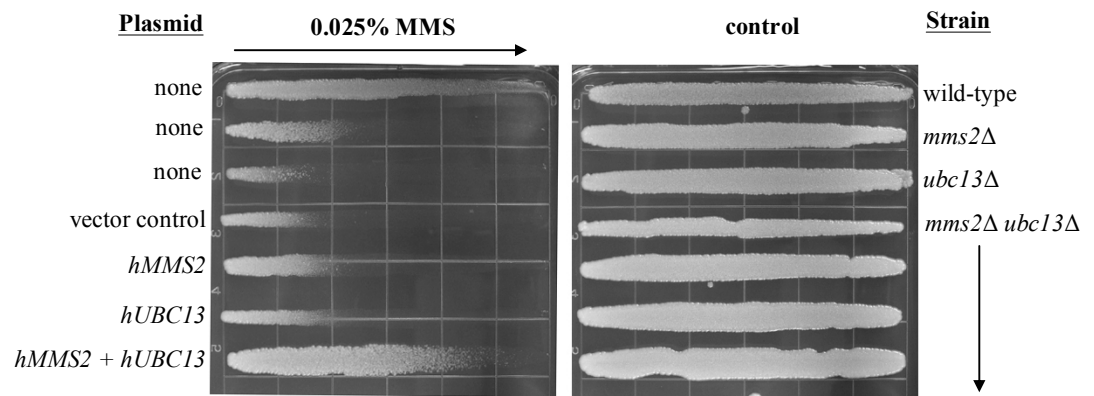


Figure 3-1. Functional complementation of yeast *ubc13 mms2* double deletion strains by their corresponding human genes. The function of human *UBC13* and *MMS2* double transformations is reflected in the ability to protect the yeast *ubc13 mms2* double-deletion strain from killing by MMS. Overnight cell cultures were printed on YPD plates containing a gradient of 0.025% MMS, and cells with a greater ability to survive DNA damaging treatment grew further along the gradient. Incubation was carried out for 48 hours at 30°C before taking the photograph. The arrow indicates an increasing MMS concentration. Test plasmids were pGAD-*hMMS2* and pGBT-*hUBC13*.

3.2.2 Human *UBC13* and *MMS2* complement their corresponding genes in *S. cerevisiae*

With the success of the double transformation approach above, it was desirable to see if single transformations of human *UBC13* and *MMS2* could provide complementation for their single-mutant counterparts. Figure 3-2 shows that transformation of the human *UBC13* and *MMS2* genes is able to provide MMS resistance in the *ubc13* Δ and *mms2* Δ strains, respectively. The inability of human *UBC13* to provide full complementation as compared with the wild-type strain is likely due to the nature of the plasmid-based gene fusion and not the actual gene itself. For example, a similar plasmid construct of the yeast *MMS2* gene does not provide full DDT complementation in the *mms2* Δ yeast strain (data not shown).

Given that MMS gradient plates are an important experimental assay in this thesis, a comparison with another method used to evaluate the sensitivity of cells to a drug treatment was performed. In this case, a dilution-plate assay was performed with the same strains as the gradient plate shown in Figure 3-2. In these assays, a plate with a single drug concentration is made onto which a 10-fold dilution series of cells is spotted. As seen in Figure 3-3, the complementation by human *UBC13* and *MMS2* in the dilution plates is visually comparable to that observed in the gradient plates.

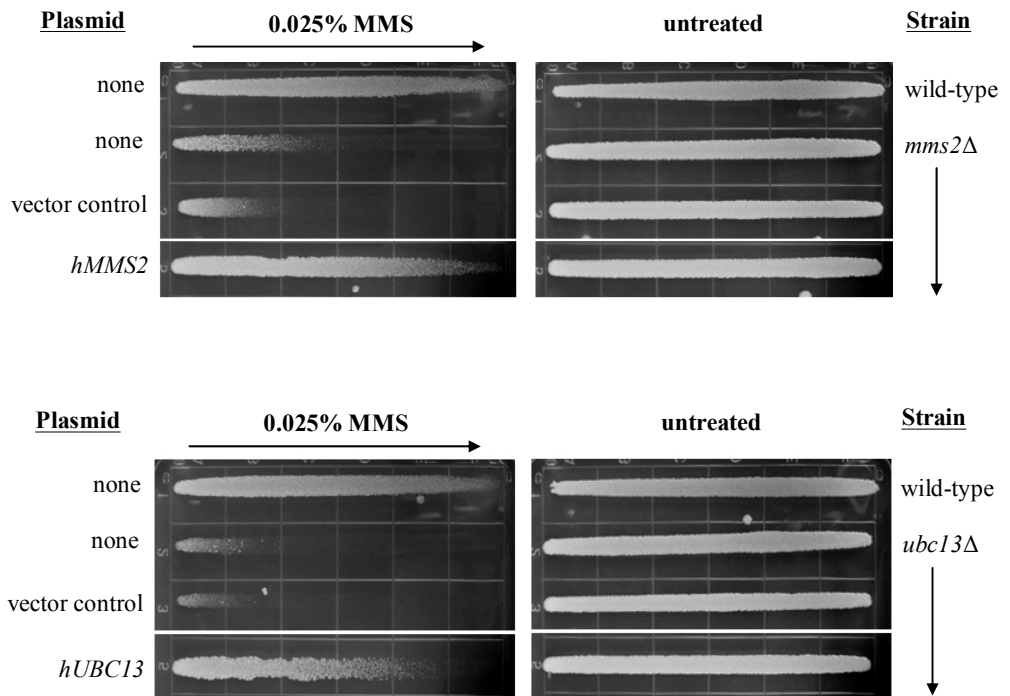


Figure 3-2. Functional complementation of yeast *ubc13* and *mms2* single deletions by their corresponding human genes. The function of human *MMS2* (upper panel) or *UBC13* (lower panel) is reflected in the ability to protect its corresponding yeast deletion mutant from killing by MMS. Overnight cell cultures were printed on YPD plates containing a gradient of 0.025% MMS, and cells with a greater ability to survive DNA damaging treatment grew further along the gradient. Incubation was carried out for 48 hours at 30°C before taking the photograph. The arrow indicates an increasing MMS concentration. Test plasmids were pGAD-hMMS2 and pGBT-hUBC13. The white line indicates that the data was taken from a different region on the same plate.

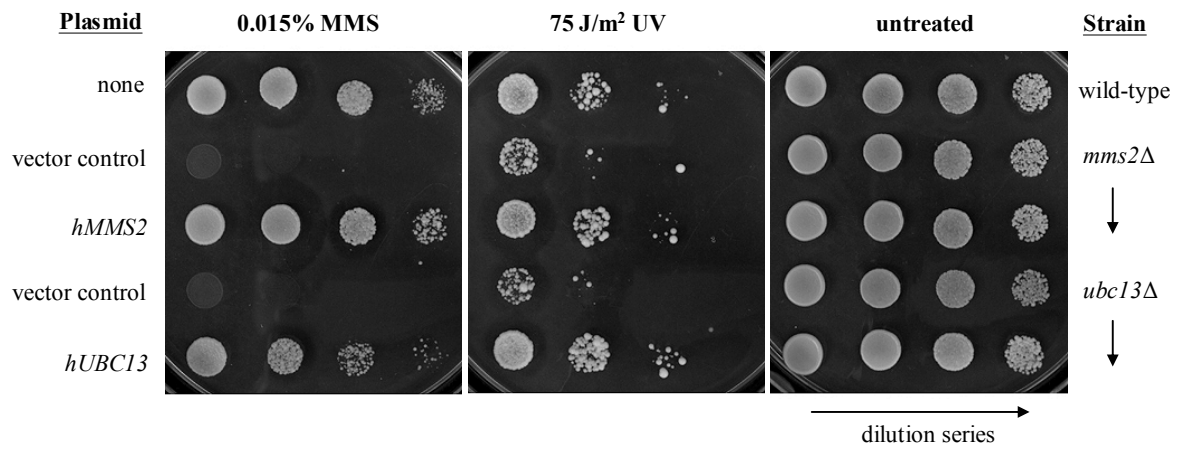


Figure 3-3. Dilution plate analysis of the functional complementation of yeast *ubc13* and *mms2* single deletions by their corresponding human genes. The function of human *UBC13* or *MMS2* is reflected in the ability to protect its corresponding yeast deletion mutant from killing by MMS or UV irradiation. Overnight cell cultures were spotted as serial dilutions on selective minimal media that contained either 0.015% MMS or was exposed to 75 J/m² of UV radiation. 10-fold dilutions increased from left to right and cells with a greater ability to survive DNA damaging treatment grew at higher dilutions. Incubation was carried out for 72 hours at 30°C before taking the photograph. Test plasmids were pGAD-hMMS2 and pGBT-hUBC13.

MMS is a commonly used alkylating agent that generates DNA damage, but the molecular targets that it can affect are not limited to nucleic acids. This is reflected by microarray analysis in yeast which shows that hundreds of genes are responsive to MMS treatment in *S. cerevisiae*, but most of them have no identifiable role in DNA repair processes (Jelinsky et al., 2000; Jelinsky and Samson, 1999). In order to help ensure that the complementation observed by human *UBC13* and *MMS2* is due to DNA repair and not an unrelated secondary effect, a parallel experiment to the MMS dilution plate was performed but with a very different DNA damaging agent. In this case, a dilution series containing the same strains as in the MMS assay was plated and the cells were subsequently treated with ultraviolet (UV) radiation. The plates were incubated in the dark until analysis in order to prevent the direct reversal of DNA damage through photoreactivation by DNA repair photolyases. As with the MMS treatment, the *ubc13Δ* and *mms2Δ* strains were sensitive to UV irradiation, and the sensitivity was alleviated after transformation with human *UBC13* and *MMS2*, respectively (Figure 3-3).

3.2.3 Functional complementation by human *MMS2* homologs in *S. cerevisiae*

Although there are no other apparent sequence homologs of *MMS2* in yeast, a search for *MMS2* homologs in human databases reveals the gene *UEVI* (also known as *CROC-1* and *CIRI*; Xiao et al., 1998). *UEVI* was originally isolated by its ability to trans-activate the promoter of the human proto-oncogene, *FOS* (Rothofsky and Lin, 1997). Shortly thereafter, studies by independent groups found that *UEVI* is down-regulated in cells undergoing differentiation (Sancho et al., 1998), but up-regulated in cells undergoing immortalization (Ma et al., 1998). *UEVI* resides in the human

chromosomal region 20q13.2 which is frequently amplified in many cancer types (Sancho et al., 1998; Savelieva et al., 1997) and *UEVI* transcripts are also abundant in numerous tumor-derived human cell lines (Ma et al., 1998).

UEVI is transcribed as one of two predominant splice variants in human cells, termed *UEVIA* and *UEVIB*. The Uev1A and Uev1B proteins are aptly named because like Mms2, they contain a Ubc-variant domain. The Uev domain in each case shares greater than 90% amino acid sequence identity with human Mms2. Beyond this core region of homology with Mms2, Uev1A and Uev1B have 33 and 84 residue amino-terminal extensions, respectively. Mms2 consists of the Uev domain alone and does not have such an extension. Although the Uev domains of Uev1A and Uev1B are completely identical, the amino terminal extensions are encoded by different exons and bear no apparent sequence similarity to one another, or to any other peptides in the databases used for the Basic Local Alignment Search Tool (BLAST) at the time of writing this thesis.

Given the high degree of similarity between human *MMS2* and *UEVI*, and the ability of human *MMS2* to complement its yeast counterpart (Figure 3-2 and Xiao et al., 1998), I was prompted to test whether *UEVIA* and *UEVIB* could similarly function in yeast DDT. Figure 3-4 shows that *UEVIA* is able to provide the *mms2* Δ strain with a resistance to MMS that is equivalent to human *MMS2*, whereas *UEVIB* does not. In fact, *UEVIB* provides no additional MMS resistance whatsoever.

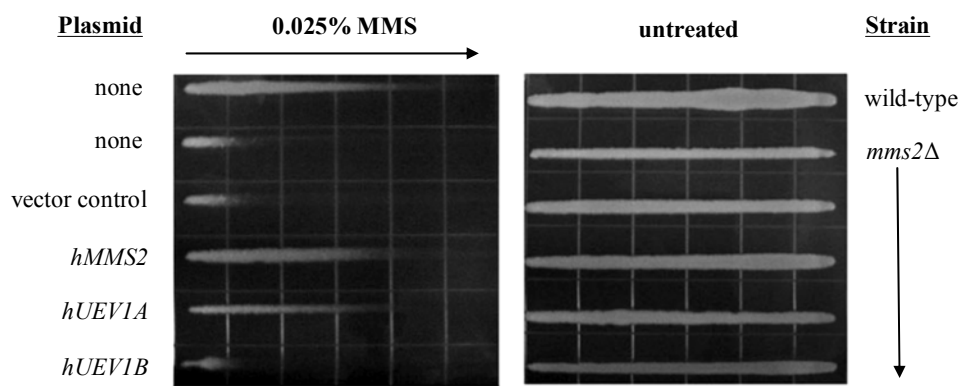


Figure 3-4. Heterologous functional complementation of human *UEV* genes in yeast. The function of human *MMS2*, *UEV1A*, and *UEV1B* in place of yeast *MMS2* is reflected in the ability to protect the *mms2* deletion strain from killing by MMS. Overnight cell cultures were printed on YPD plates containing a gradient of 0.025% MMS, and cells with a greater ability to survive DNA damaging treatment grew further along the gradient. Incubation was carried out for 36 hours at 30°C before taking the photograph. The arrow indicates an increasing MMS concentration. Test plasmids were pG4BD-*hMMS2*, pG4BD-*hUEV1A*, pG4BD-*hUEV1B* and pGAD-*hUBC13*.

3.2.4 Physical interactions between Ubc13-Uev proteins

In order to better understand how human *UBC13* and *MMS2* are able to function in yeast DDT, it was desirable to determine if physical interactions occur between the two proteins. Because Gal4_{AD} and Gal4_{BD} fusion constructs were used in the complementation tests, the easiest approach to employ was the yeast two-hybrid assay (Fields and Song, 1989). In addition to making use of the same constructs as for the complementation tests, the yeast two-hybrid assay offered other advantages. The yeast two-hybrid assay is an *in vivo* protein interaction test performed in the same organism used in the functional assays. In addition, while the nuclear localization of test proteins in the yeast two-hybrid assay is often undesirable, the Ubc13-Mms2 interaction is expected to occur in the nucleus anyway. Indeed, yeast Ubc13 and Mms2 both localize to the nucleus after DNA damage treatment (Ulrich and Jentsch, 2000). The auxotrophic markers in the yeast two-hybrid assay strain also allowed optimization of binding sensitivity such that low-affinity (or transient) and high-affinity (stable) interactions could be better detected.

As seen in Figure 3-5A, a physical interaction between Ubc13 and Mms2 was detected. An interaction between Ubc13 and Uev1A was also seen, even at the most stringent assay condition used (growth on medium lacking Ade). Perhaps with some future functional significance, I observed that the Ubc13-Mms2 interaction gave a stronger signal than the Ubc13-Uev1A interaction. On the other hand, a detectible interaction was not seen for Ubc13 and Uev1B. Due to the prevalence of false negatives in the yeast two-hybrid assay, I decided to confirm the interaction data in a completely different way using *in vitro* GST pull-downs.

A

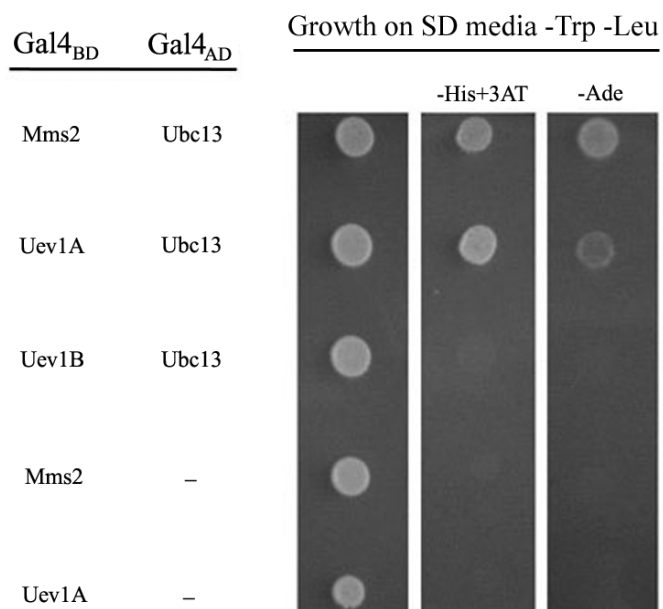


Figure 3-5. Ubc13–Uev physical interactions. (A) Yeast two-hybrid analysis of Ubc13–Uev physical interactions using the growth assay method. Physical interaction of the hybrid proteins causes the expression of the *HIS3* and *ADE* reporters which allows growth on minimal medium lacking His and Ade, respectively. Co-transformed plasmids were maintained with Trp and Leu markers and are indicated on the left. The plates were incubated at 30°C for 72 hours before taking the photograph. The assay was performed in triplicate, but only one representative transformant from each combination is shown. Test plasmids were pG4BD-hMMS2, pG4BD-hUEV1A, pG4BD-hUEV1B and pGAD-hUBC13. Cells co-transformed with pG4BD-hUEV1B + pGAD424 and pG4BD + pGAD-hUBC13 were also negative (not depicted).

B

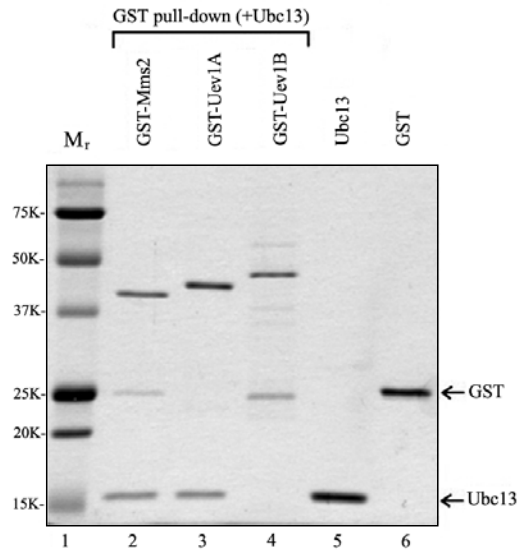


Figure 3-5. Ubc13-Uev physical interactions. (B) *In vitro* GST pull-down assay. Proteins of interest in each GST pull-down (Lanes 2 to 4) are indicated at the top. GST-hUev fusion proteins were immobilized on glutathione sepharose 4B columns and subsequently incubated with non-fused hUbc13. The physical interaction of test proteins allows their co-purification and is visualized by the presence of Ubc13 in eluted samples. A denaturing protein gel stained with Coomassie blue is shown. Lanes 5 and 6 were samples of purified hUbc13 and GST, respectively. It is noted that repeated handling (i.e. freeze-thawing) of the GST-Mms2 and GST-Uev1B samples caused some slight spontaneous cleavage of the fusion protein.

In the GST pull-down assays, purified GST fusion proteins were immobilized onto Glutathione Sepharose and subsequently incubated with purified human Ubc13 protein. After washing away the unbound portion, the bound proteins were eluted, run on a denaturing protein gel, and visualized after Coomassie blue staining (Figure 3-5B). This approach enabled the detection of stable protein interactions between Ubc13-Mms2 and Ubc13-Uev1A, however, a protein-protein interaction was not observed between Ubc13 and Uev1B. The results from the *in vitro* pull-down were thus in agreement with those of the *in vivo* two-hybrid assay.

Based on the human Ubc13-Uev interaction studies in Figure 3-5 and because the *in vitro* ubiquitylation activity of yeast Ubc13 and Mms2 is dependent on their co-purification (Hofmann and Pickart, 1999), the physical binding of Ubc13-Mms2 is expected to be required for their function in DDT. If this is indeed true, heterologous yeast-human Ubc13-Mms2 heterodimers would be expected in the single-gene complementation studies above where only a single human *UBC13* or *MMS2* gene was provided. To help confirm that this is the physiologically relevant situation, the yeast two-hybrid assay was used to test for protein interactions between human Ubc13 and yeast Mms2, and *vice versa*. In Figure 3-6, the human-yeast pairings for Ubc13 and Mms2 are seen to physically interact. Furthermore, the signal generated was apparently as strong as the yeast-yeast and human-human protein interactions themselves (Figure 3-6).

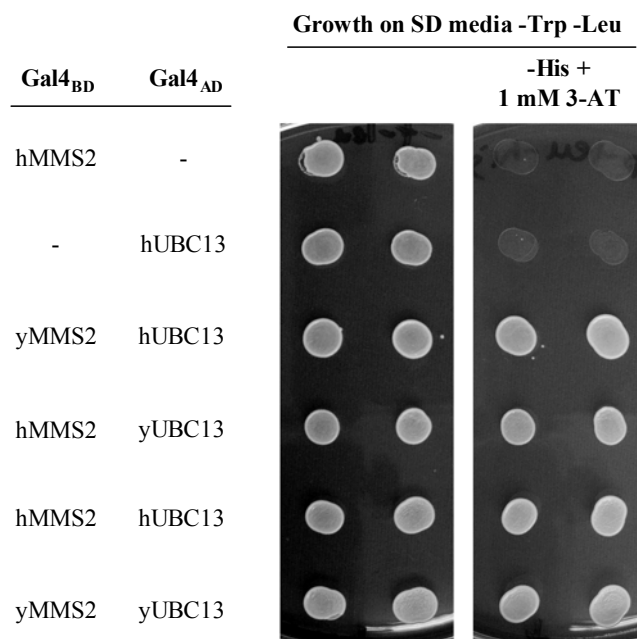


Figure 3-6. Heterologous Ubc13–Mms2 complex formation. Yeast two-hybrid analysis of Ubc13–Mms2 protein interactions by the growth assay method. Physical interaction of the hybrid proteins causes the expression of the *HIS3* reporter which allows growth on minimal medium lacking His. Co-transformed plasmids were maintained with Trp and Leu markers and are indicated on the left. The plates were incubated for 48 hours at 30°C before taking the photograph. Two representative transformants from each combination is shown. Cells co-transformed with Gal4_{BD}-yMMS2 + Gal4_{AD} and Gal4_{BD} + Gal4_{AD}-yUBC13 were also negative (not depicted). Test plasmids were pG4BD-hMMS2, pG4BD-yMMS2, pGAD-hUBC13, and pGAD-yUBC13.

3.3 Discussion

With the overall focus of my thesis work being structure-function studies of human Ubc13-Mms2, my initial goal was to develop a reliable assay to provide the basis for testing prospective mutant protein function. Several important factors as discussed in the rationale prompted me to test whether the budding yeast *S. cerevisiae* could be used to evaluate human *UBC13* and *MMS2* function. In this system, the alkylating agent MMS was used to generate DNA damage and plasmid-based copies of *UBC13* and *MMS2* (or the *UEV1A* and *UEV1B* homologs) were tested to see if they could function in DDT in place of their corresponding yeast mutants. The data presented in this chapter demonstrate that *S. cerevisiae* DNA damage tolerance is indeed a valid system for testing the function of the human *UBC13* and *MMS2* genes. Furthermore, the detailed protein interaction studies helped to suggest that heterologous Ubc13-Uev complexes are functional in DDT.

I first demonstrated the ability of simultaneous human *UBC13* and *MMS2* transformations to provide DDT function in a *ubc13Δ mms2Δ* double-deletion yeast strain. Perhaps surprisingly, I observed nearly complete complementation (Figure 3-1). The finding suggests that the human proteins are able to effectively retain the DDT activities of their yeast counterparts. A logical extension of this result is that the human Ubc13 and Mms2 proteins should be receptive to the upstream events or signals in yeast DDT, and are also able to effectively cause or execute the appropriate downstream events as well. The finding is particularly significant with respect to the yeast protein Rad5, which is required for Ubc13-Mms2-mediated error-free DDT in *S. cerevisiae* (Ulrich and Jentsch, 2000). Experimental evidence in *S. cerevisiae* supports a model whereby Rad5

interacts with Ubc13 and Rad18 (Ulrich and Jentsch, 2000) to provide a physical bridge between the E2 complexes Rad6-Rad18 and Ubc13-Mms2, so they can be localized at the ubiquitylation target in DDT, PCNA (Hoegge et al., 2002). However, no apparent protein sequence homolog for Rad5 exists in higher eukaryotes. The ability of human Ubc13 and Mms2 to function in yeast DDT is suggestive that there is indeed a functional Rad5 homolog (i.e. analog) in higher eukaryotes. Another highlight of this first experiment is that single transformations of *UBC13* or *MMS2* were not able to provide DNA damage resistance in the *ubc13Δ mms2Δ* mutant strain. The finding suggests that the role for Mms2 in DDT is dependent on Ubc13, such that a different E2 cannot function in place of Ubc13 in DDT. Reasons for the *UBC13* and *MMS2* co-dependence and the structural basis behind them will be addressed in chapter 4 of this thesis.

Similar to the double transformation approach, single gene transformations of human *UBC13* or *MMS2* were able to complement the DDT deficiency of their corresponding mutant strains. With respect to future experimentation, it is notable that the extent of complementation by both *UBC13* and *MMS2* was significant and easily noticeable in the assays. There was a clear and large difference between the complemented and non-complemented strains. It was felt that this would provide a good future opportunity to discern between Ubc13 and Mms2 mutants that might only partially reduce DDT activity.

Because they were used throughout the structure-function studies, two experiments were carried out to justify the use of the MMS gradient plate assays. The first showed that the gradient plate assay is as visually effective as the more commonly used dilution plate assay. As can be seen when comparing the single-gene

complementation studies in Figure 3-2 and 3-3, both assay methods allow the same conclusions to be drawn. My preference is for the gradient plate assay because growth on dilution plates can be difficult to interpret when cell colony size between strains is variable. The second experiment helped to ensure that the functional complementation observed by human *UBC13* and *MMS2* is attributed to DNA damage tolerance. As can be seen in Figure 3-3, functional complementation was also observed after UV DNA damaging treatment. However, the MMS dilution plate more clearly shows the differences between complemented and non-complemented cells. The result suggests that the relief of MMS sensitivity in the *ubc13Δ* and *mms2Δ* strains by the human *UBC13* and *MMS2* genes is attributed to processes related to DNA repair (i.e. DDT), and not an unrelated secondary biological process.

With the successful complementation of function by the human *MMS2* yeast two-hybrid construct, the human *MMS2* homologs *UEV1A* and *UEV1B* were tested to see if they could similarly function in yeast DDT. Indeed, it was found that *UEV1A* can alleviate the MMS sensitivity of the *mms2Δ* strain to the same extent as *MMS2* itself. On the other hand, *UEV1B* did not provide a detectible relief of DNA damage. The result is somewhat surprising because Uev1A and Uev1B differ only in their amino-termini which extend 33 and 84 residues beyond the region of Mms2 homology, respectively. To better understand the possible reasons why human *MMS2* and *UEV1A* complement the *mms2Δ* strain but *UEV1B* did not, the ability of each protein to physically interact with Ubc13 in the yeast two-hybrid assay was tested. Using the same constructs as in the functional complementation tests, physical interactions were detected between Ubc13 and Mms2, and Ubc13 and Uev1A. However, an interaction was not observed between Ubc13 and

Uev1B. The absence of a detectible interaction because of a false negative in the yeast two-hybrid assay can be due to several factors. A possible reason could be due to the production of recombinant protein in *S. cerevisiae*, such as poor protein expression or insolubility. In addition, the nature of the Gal4 fusion could lead to steric hindrance that would not be present in the native protein. Also, it cannot be ruled out that the interaction itself is simply below the detectable limits of the assay. In order to address some of these problems, purified proteins were used in *in vitro* binding experiments testing the same interactions as in the yeast two-hybrid assay. In accordance, the GST pull-down assays showed that Ubc13-Mms2 and Ubc13-Uev1A form direct, stable protein interactions, whereas Ubc13 and Uev1B do not.

The ability of *UEV1A* to function in place of *MMS2* in yeast DDT is a very interesting finding. The high degree of protein sequence similarity between Uev1A and yeast Mms2 suggests that they might be orthologs (proteins representing genetic variation across species but usually retaining the same biological function). However, a role for *UEV1A* in DNA repair would be at odds with *UEV1* studies to date, which characterize *UEV1* as a gene involved in the promotion of cell immortalization and tumorigenesis. Because genome instability is often at the root of cancer formation, DNA repair proteins are generally expected to have a role in preventing tumorigenesis. These facts are more fitting with the suggestion that human Mms2 and Uev1 are paralogs which arose from an *MMS2* gene duplication sometime during evolution, and have since undertaken divergent cellular roles. Indeed, the studies in this chapter were a part of a recent publication which showed that human Mms2 and Uev1A are involved in very different cellular roles (Andersen et al., 2005). Taken together, the ability of Uev1A to function in yeast DDT is

best attributed to an evolutionarily conserved physical interaction with Ubc13 and an ability to promote Lys63-linked Ub chain formation, like Mms2.

The inability of *UEV1B* to function in place of *MMS2* in yeast DDT was an observation initially seen in our laboratory (Xiao et al., 1998). With this in mind and the initial observations that yeast Ubc13 and Mms2 form a complex *in vitro*, the possibility that *UEV1B* could act as a dominant-negative regulator of *UBC13* DDT activity was tested. The premise was that if Uev1B could out-compete Mms2 for binding Ubc13, then DDT activity would be correspondingly reduced. However, through rigorous experimentation a dominant-negative effect was not observed (data not shown). The reason came to light through the protein interaction studies above involving Ubc13 and the various UeVs. Ubc13 and Uev1B did not physically interact in either the *in vivo* yeast two-hybrid assay or the *in vitro* GST pull-down assay and as such, a dominant-negative could not be exerted on Ubc13. Taken together, the data in this chapter provided the first clues that an interaction between Ubc13 and its cognate Uev is absolutely required for its cellular function. This idea was more definitively addressed through the detailed Ubc13-Mms2 mutagenesis studies in chapter 4 of this thesis.

To support the idea that a direct Ubc13-Uev physical complex is required for DDT function, Ubc13 and Mms2 proteins from yeast and humans were tested for their physical interaction with each other. It was felt that the yeast-human heterologous protein interactions would better reflect the actual physiological situation in the single-gene complementation studies performed above. Indeed, strong interactions were observed between yeast Ubc13 and human Mms2, and between human Ubc13 and yeast Mms2. Furthermore, heterologous complexes were detected as readily as the yeast-yeast

and human-human pairs themselves. The result suggests an evolutionary conservation of the molecular determinants that designate the specificity and affinity of Ubc13 for Mms2. The heterologous abilities of Ubc13 and Mms2 as demonstrated in this chapter set a precedent for the quick and efficient testing of putative Ubc13 and Uev orthologs throughout eukaryotes.

CHAPTER FOUR STRUCTURE-FUNCTION CHARACTERIZATION OF UBC13-MMS2

4.1 Introduction

In the chapter one of this thesis, the Ubc13-Mms2/Uev1A heterodimer was introduced as a unique E2 complex that generates Lys63-linked Ub chains. Based on various *in vitro* assays and on structural information, a reasonable model was suggested for how the atypical Ub-Lys63 linkages can be made. In accordance, the phenotypes associated with *ubc13* and *mms2* mutations in yeast DDT seemed to fit well with the mechanistic proposal. However, despite a couple of small exceptions, *in vivo* functional evidence to support the model was lacking. Therefore, a rational site-directed mutagenesis approach was performed to determine how the structure of Ubc13 and Mms2 relates to their cellular function. Using the experimental systems demonstrated in chapter 3 of this thesis, I was able to functionally address four integral features of the Ubc13-Mms2 structure and mechanistic model. As indicated in Figure 4-1, they are: 1) the Ubc13 active-site, 2) the Ubc13-Mms2 interface, 3) the Mms2-Ub interface and 4) the Ubc13-E3 interface. In each case I was able to create point mutations that led to detectable functional consequences, allowing various conclusions regarding structure-function relationships. The findings provide evidence in favour of the prevailing mechanistic model for Lys63-linked Ub chain formation by Ubc13-Mms2, while also further uncovering the structural basis behind the cellular functions of Ubc13 and Mms2.

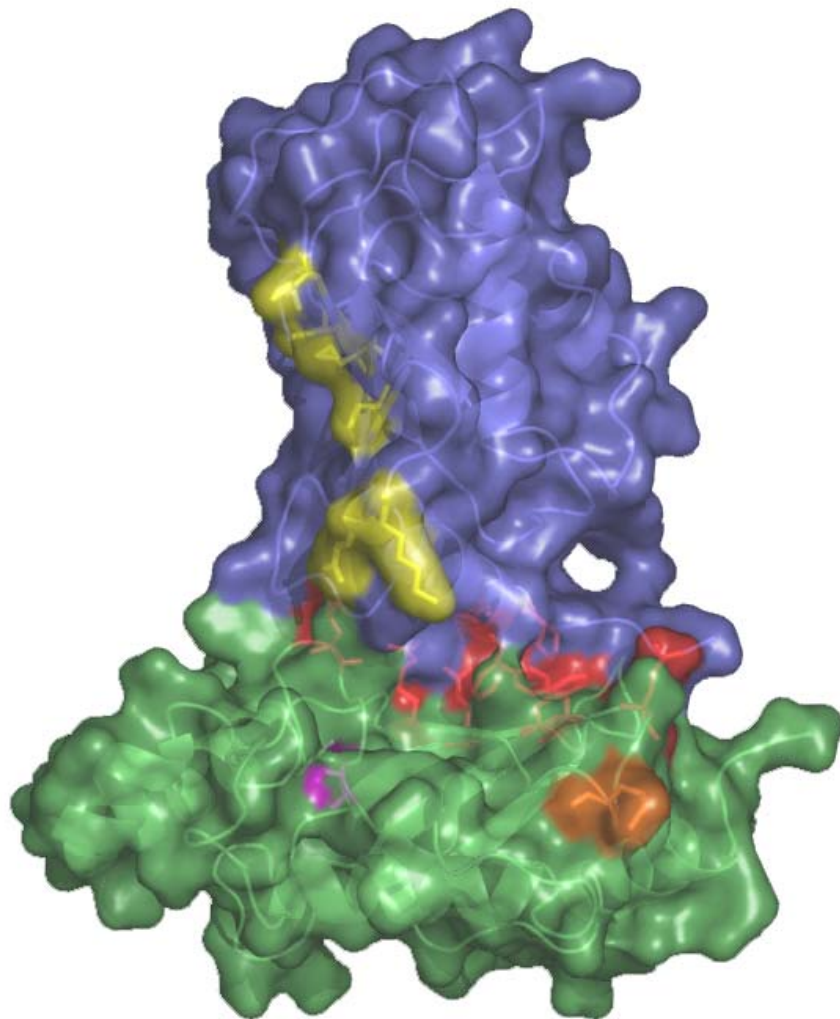


Figure 4-1. Residues mutated in Ubc13-Mms2 structure-function studies. A molecular structure of the Ubc13 (green) and Mms2 (blue) heterodimer was generated using PyMol v0.98 (DeLano, W.L., www.pymol.org). To determine the key regions of the Ubc13-Mms2 heterodimer, point mutations were made at residues corresponding to the Ubc13 active-site (violet), the Ubc13-E3 interface (orange), the Mms2-Ub interface (yellow), and Ubc13-Mms2 interface (red).

4.2 Ubc13 active-site results

The first structure-function analysis was performed to determine if that the Ub-conjugating activity of human Ubc13 is required for its function in yeast DDT. At least a few lines of evidence at the time, albeit indirect, indicated that this was the case. First, the study that made the first link between Ubc13, Mms2, and Lys63-linked Ub conjugation reported that the *ubc13Δ*, *mms2Δ*, and *ub-K63R* mutants all shared a similar sensitivity to DNA damage (Hofmann and Pickart, 1999). Second, the genetic dependence on *MMS2* by *UBC13* in DDT (Brusky et al., 2000) is in agreement with the role of Mms2 to promote poly-Ub chain formation by Ubc13 *in vitro* (McKenna et al., 2001). Third, based on sequence alignments with other E2s, Ubc13 seems to contain the conserved Cys residue (Cys87) required for an E2 active-site (Figure 4-2). Fourth, Ubc13-Cys87 is situated in a cleft that is surrounded by residues that undergo chemical shift upon the Ub-Ubc13 interaction *in vitro* (McKenna et al., 2003a; McKenna et al., 2003b).

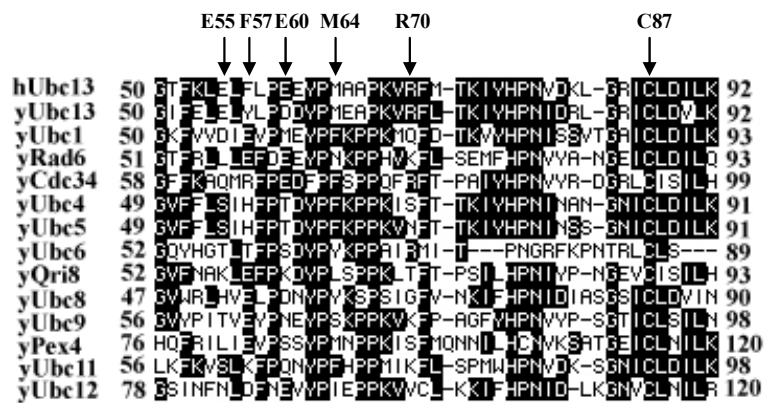


Figure 4-2. Protein sequence alignment of the E2 homologs in *S. cerevisiae* and human Ubc13. An alignment was generated using the CLUSTAL algorithm with default parameters. Only a portion of the entire protein sequences is shown. Residues exactly matching the hUbc13 consensus are shaded black. The residues indicated with arrows correspond to the human Ubc13 residues mutated in these studies.

4.2.1 The Ubc13 active-site Cys residue is required for function in DDT

In order to test if the putative active-site Cys residue of Ubc13 is required for DDT, a conservative Ubc13-C87S point mutation was created. The Cys to Ser mutation has been used successfully to abrogate the Ub-conjugating activity of other E2 enzymes (Sullivan and Vierstra, 1993; Sung et al., 1991b). The human *UBC13-C87S* construct was then transformed into a *ubc13Δ* yeast strain and then analyzed by an MMS gradient plate assay. Figure 4-3A shows that in contrast to wild-type *UBC13*, the *C87S* mutant is unable to functionally complement the yeast *ubc13* deletion after DNA damaging treatment. To help ensure that the Ubc13-C87S protein is actually expressed and folded properly, the identical *UBC13-C87S* construct was tested for physical interactions with Mms2 in the yeast two-hybrid assay (Figure 4-3B). The Ubc13-C87S mutant interacted with Mms2 as well as wild-type Ubc13.

Based on the results, it can be concluded that the Ubc13 active-site Cys residue is required for its function in DDT. Because of a unique property inherent to the particular mutation generated, it can be further inferred that DDT requires Ub conjugation by Ubc13, and not merely Ubc13-Ub ester formation. The Cys-Ser mutation enables an E2-Ub ester to be formed *in vitro* and *in vivo* (similar to the Cys thioester), however, the intermediate is metabolically stable and does not allow Ub to be conjugated to the target (Sullivan and Vierstra, 1993; Sung et al., 1991b). In this regard, the Ubc13-C87S substitution might be useful in future studies involving intermediate steps in Ubc13-Mms2-mediated Ub-conjugation.

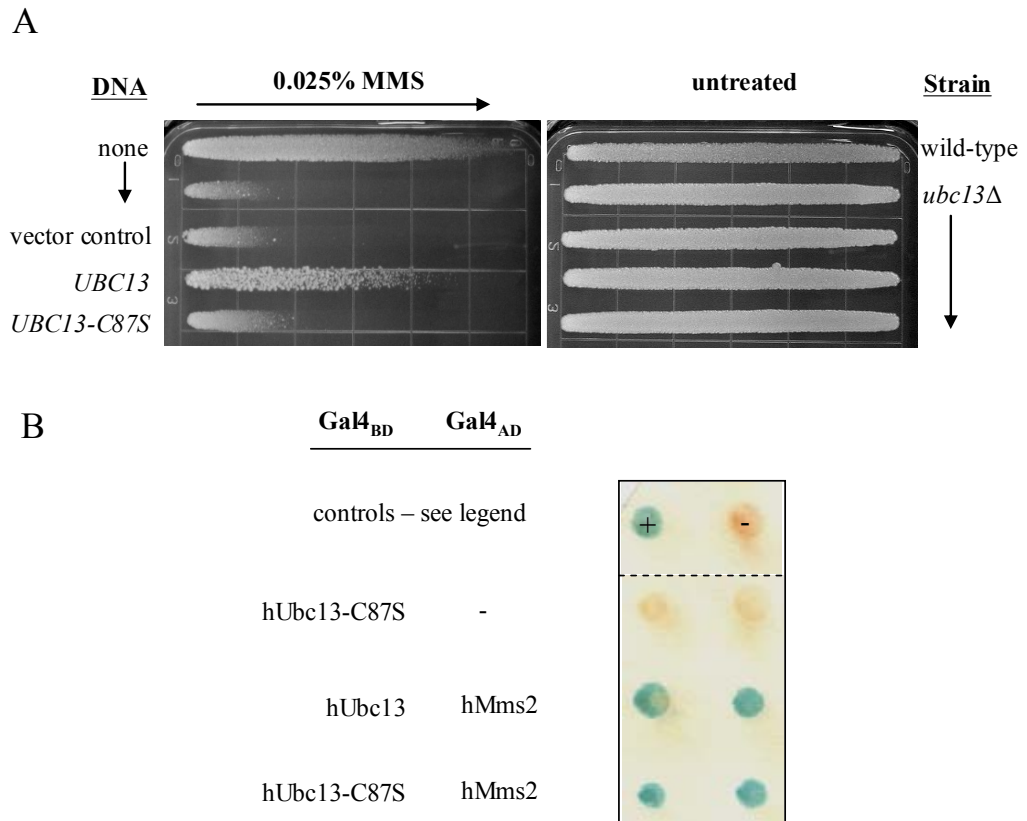


Figure 4-3. The Ubc13-C87S substitution abrogates its function in yeast DDT but not its physical interaction with Mms2. (A) The *in vivo* function of human *UBC13-C87S* is reflected in the ability to protect a *ubc13^Δ* yeast strain from killing by MMS. Overnight cell cultures were printed on YPD plates containing a gradient of 0.025% MMS, and cells with a greater ability to survive DNA damaging treatment grew further along the gradient. Incubation was carried out for 48 hours at 30°C before taking the photograph. The arrow indicates an increasing MMS concentration. (B) Yeast two-hybrid analysis of the Ubc13-C87S-Mms2 protein interaction using the β -galactosidase filter-lift detection method. Physical interaction of the Gal4 hybrid proteins leads to the expression of the β -galactosidase gene which causes blue colour development in the assay. Co-transformed plasmids were maintained with Trp and Leu markers and are indicated on the left. The picture was taken after 4 hours of colour development. Two representative transformants from each combination is shown except for the top-most experimental controls where a single transformant was used to show a positive (+) and negative (-) assay result for *Gal4_{BD}*-hUbc13 + *Gal4_{AD}*-hMms2 and *Gal4_{BD}* + *Gal4_{AD}*-hMms2, respectively. Dotted line indicates data taken from a different part of the same assay filter. Test plasmids were pGBT-hUBC13, pGBT-hUBC13-C87S, and pGAD-hMMS2.

4.3 Ubc13-E3 interface results

As discussed in chapter one, the model for Lys63-linked Ub conjugation identifies at least three possible channels for Ub binding and/or transfer. The third channel is generated after the formation of the Ubc13-Mms2 heterodimer, and roughly extends outward from the Ubc13 active-site (the site of Lys63-linked Ub conjugation) along the β -sheet residues of Ubc13 and the α -1 helix and N-terminus of Mms2 (Figure 1-2 and 1-3). The relevance of channel 3 in Ubc13-Mms2 ubiquitylation is suggested by two separate crystal structures showing the detailed aspects of E2-E3 physical interactions.

One of the structures shows a physical interaction between UbcH7 and a RING finger E3, c-Cbl (Zheng et al., 2000). The binding of the two proteins is predominantly mediated through contacts belonging to the RING finger domain of c-Cbl and a surface on UbcH7 that corresponds to the region on Ubc13 that is proximal to channel 3. Functional relevance for the involvement of this type of E2-E3 interaction in mediating ubiquitylation has been demonstrated through mutations that destroy the Zn^{2+} cross-bridge of the E3 RING finger. Such mutants abrogate the ability of E3s to physically interact with E2s and as a result, the cellular target is not ubiquitylated (Freemont, 2000; Joazeiro and Weissman, 2000; Waterman et al., 1999).

The second crystal structure involves a protein from the other predominant class of E3s which are marked by the HECT domain. The HECT domains differ functionally from RING finger domains in that it forms thioesters with Ub, whereas the RING finger domains do not. The HECT domain also conforms to a very different 3-dimensional structure than the RING finger domain. It is thus surprising that the manner in which the HECT domain E3, E6AP, binds to UbcH7 is strikingly similar to the UbcH7-RING

finger domain interaction (Huang et al., 1999). Apparently the same UbcH7 surface is required for the physical interaction with both the HECT and RING finger domains. Although Ubc13-Mms2 (or Ubc13-Uev1A) has not been found to interact with HECT domain E3s to date, these findings implicate that channel 3 of Ubc13-Mms2 could be used to transfer Ub through HECT and RING finger domain E3s.

There is no direct experimental evidence to date to support the necessity of channel 3 for Ubc13-Mms2 function in DDT. However, the physical interaction between Ubc13 and the RING finger E3 Rad5 (Ulrich and Jentsch, 2000), and the requirement for *RAD5* in error-free DDT (Xiao et al., 2000) suggest a functional relevance *in vivo*. To address this problem, a point mutation was created within the Ubc13 surface that is typical of general E2-E3 interactions as explained above. Furthermore, the point mutation lies within the aforementioned channel 3. It was hypothesized that a mutant causing the disruption of the Ubc13-E3 interaction would lead to the inability of Ubc13-Mms2 to pass Lys63-linked Ub chains to the target. The consequence could be measured phenotypically in yeast, for example, by the inability of the *UBC13* mutant to complement *ubc13Δ* in DDT.

4.3.1 Design of a Ubc13-M64A mutant

In order to determine which residue(s) to mutate, the UbcH7-c-CBL crystal structure was used as a 3-dimensional template for human Ubc13. Given the high degree of structural conservation among E2s, I was able to accurately replace the position of UbcH7 in the E2-E3 structure with Ubc13. The result is a hypothetical structure of Ubc13 interacting with a RING finger domain (Figure 4-4A). Using this model, the

visual determination of which Ubc13 residues are likely to come into close contact with the RING finger domain of an E3 was possible (space-fill residues in Figure 4-4A). These residues were then compared in alignments using the UbcH7 and several Ubc13 protein sequences. The analysis revealed that all but one potential E2-RING finger interface residue was conserved between UbcH7 and Ubc13. Furthermore, this residue, corresponding to human Ubc13-Met64, is exposed to solvent and completely conserved throughout all Ubc13 sequences (Figure 4-4B and personal communication, Janet Hill, Plant Biotechnology Institute, Saskatoon, SK). Given that Ubc13 and UbcH7 do not share cellular functions or physical partners, the human Ubc13-Met64 residue (Phe63 in UbcH7) was a good candidate for Ubc13-E3 interaction specificity. This is supported by the suggestion that the UbcH7-Phe63 residue is likely important for specifically interacting with the E3s c-Cbl (Zheng et al., 2000) and E6-AP (Huang et al., 1999).

The Ubc13-M64A point mutation for chosen for several reasons. First, Ala substitutions are typical for “scanning” mutagenesis because alanine has a small non-polar R-group that is relatively unassuming and unlikely to introduce large structural changes. Second, the Met to Ala substitution is significant enough from a size standpoint, and would likely eliminate the Met contacts with the surface of the E3 RING finger domain. Third, a protein sequence alignment of all E2s in yeast reveals that no other E2 has a small non-polar residue that corresponds to Ubc13-M64 (Figure 4-2).

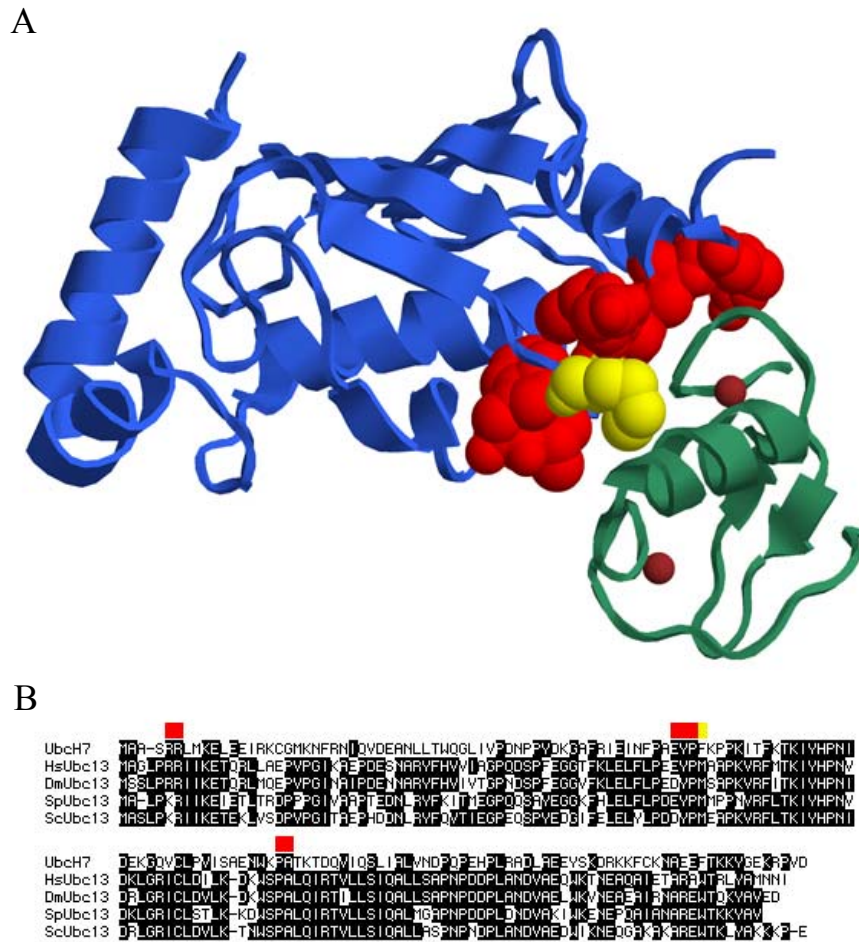
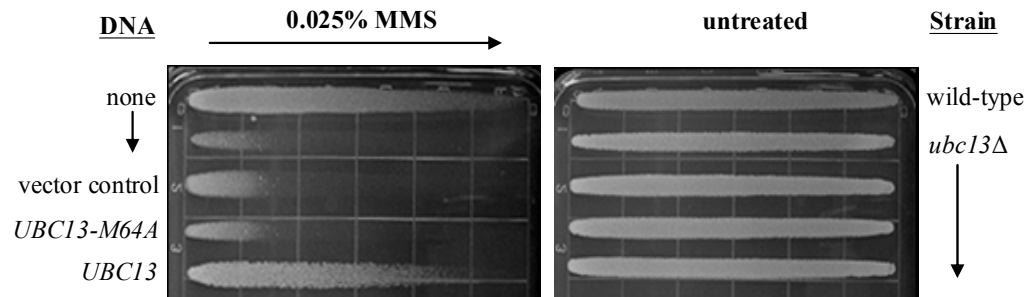


Figure 4-4. Identification of a Ubc13 residue of putative importance in binding RING finger domains. (A) Ubc13 surface predicted to interact with a RING finger domain. The Ubc13 structure (blue) is oriented in place of UbcH7, based on the heterodimer structure of UbcH7-c-Cbl. Only the RING finger portion of c-Cbl (green) is shown, with zinc atoms shown in maroon. Ubc13 residues shown in space-fill representation are those that fall in proximity to the Ubc13-RING finger interface. Residues coloured red are conserved between UbcH7 and Ubc13, whereas the yellow residue (Met64) is unique to Ubc13 (correspondingly indicated in (B)). (B) Amino acid sequence alignment of Ubc13 from *Homo sapiens* (Hs), *Drosophila melanogaster* (Dm), *Schizosaccharomyces pombe* (Sp) and *Saccharomyces cerevisiae* (Sc) against UbcH7.

4.3.2 The *UBC13-M64A* mutant does not function in DDT

The *UBC13-M64A* mutant was transformed into *ubc13Δ* yeast strains and tested for its ability to function in error-free DDT. Unlike wild-type *UBC13*, the *UBC13-M64A* mutant did not relieve the *ubc13Δ* strain from MMS sensitivity (Figure 4-5A). *UBC13-M64A* demonstrated a phenotype in the functional assay that was indistinguishable from the negative control. The surprisingly strong effect prompted testing to ensure that the human Ubc13-M64A protein could be expressed and folded properly in yeast cells. Because the Ubc13-Met64 residue lies in a region that is visibly distinct from the Ubc13-Mms2 interface, I tested the binding of Ubc13-M64A to Mms2 in the yeast two-hybrid assay. Figure 4-5B shows that Ubc13-M64A is indeed proficient in binding to Mms2.

A



B

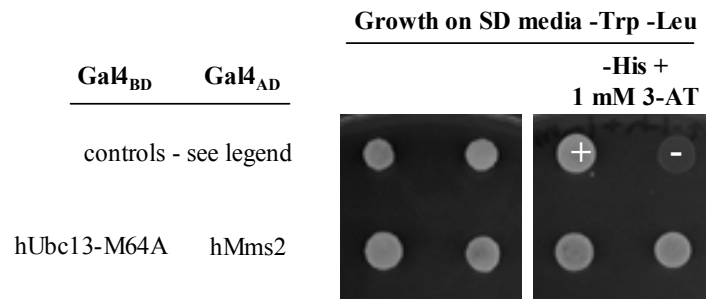


Figure 4-5. The Ubc13-M64A substitution abrogates its function in yeast DDT but not its physical interaction with Mms2. (A) The *in vivo* function of human UBC13-M64A is represented in the ability to protect a *ubc13Δ* yeast strain from killing by MMS. Overnight cell cultures were printed on YPD plates containing a gradient of 0.025% MMS, and cells with a greater ability to survive DNA damaging treatment grew further along the gradient. Incubation was carried out for 48 hours at 30°C before taking the photograph. The arrow indicates an increasing MMS concentration. (B) Yeast two-hybrid analysis of the Ubc13-M64A-Mms2 protein interaction using the cell growth method. Physical interaction of the Gal4 hybrid proteins leads to the expression of the *HIS3* gene which allows growth on SD media lacking His. Co-transformed plasmids were maintained with Trp and Leu markers and are indicated on the left. Two representative transformants are shown except for the experimental controls where a single transformant was used to show a positive (+) and negative (-) assay result for Gal4_{BD}-hUbc13 + Gal4_{AD}-hMms2 and Gal4_{BD}-hUbc13-M64A + Gal4_{AD}, respectively. Cells co-transformed with Gal4_{AD}-MMS2 + Gal4_{BD} were also negative in the assay (not depicted). Test plasmids were pGBT-hUBC13, pGBT-hUBC13-M64A, and pGAD-hMMS2.

4.3.3 Ubc13-M64A disrupts physical interaction with RING finger E3s

Due to the requirement of *RAD5* in error-free DDT (Ulrich and Jentsch, 2000) and its postulated role in acting as a physical bridge between E2 complexes (Hoegge et al., 2002), the inability of *UBC13-M64A* to provide resistance to DNA damage treatment strongly suggested that the mutation impairs a heterologous physical interaction between human Ubc13 and yeast Rad5. The yeast two-hybrid assay was used to test this possibility. Indeed, a detectible physical interaction was observed between human Ubc13 and yeast Rad5. However, the interaction was no longer detected when the Ubc13-M64A mutant was used (Figure 4-6). The Ubc13-M64A protein is apparently expressed and folded properly in the assay because it was completely able to physically interact with Mms2 (Figure 4-5).

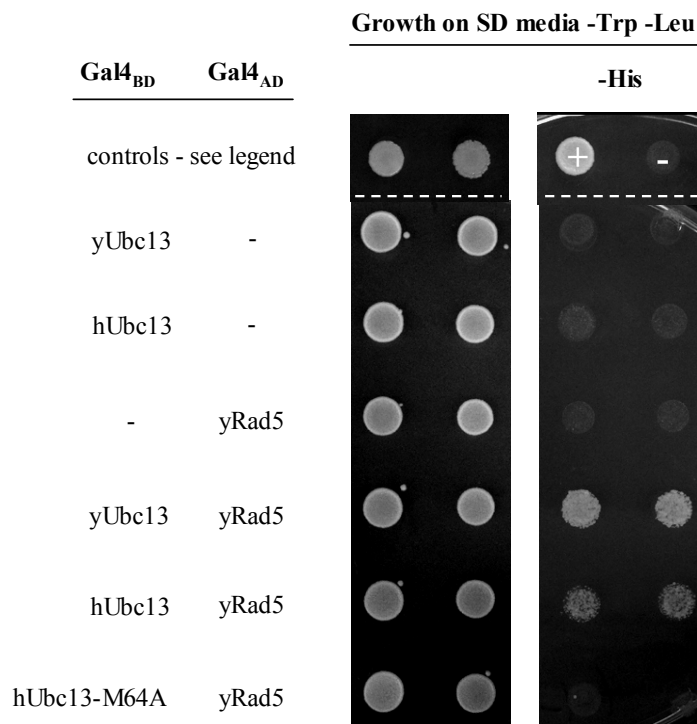


Figure 4-6. The Ubc13-M64A substitution abolishes its interaction with Rad5. Yeast two-hybrid analysis of the hUbc13-M64A-yRad5 protein interaction using the cell growth method. Physical interaction of the Gal4 hybrid proteins leads to the expression of the *HIS3* gene which allows growth on SD media lacking His. Co-transformed plasmids were maintained with Trp and Leu markers and are indicated on the left. Two representative transformants are shown except for the experimental controls where a single transformant was used to show a positive (+) and negative (-) assay result for Gal4_{BD}-hUbc13-M64A + Gal4_{AD}-hMms2 and Gal4_{BD}-hUbc13-M64A + Gal4_{AD}, respectively. Plates were incubated for 72 hours at 30°C before the picture was taken. Dotted line indicates data taken from a different part of the same assay plate. Test plasmids were pGBT-hUBC13, pGBT-hUBC13-M64A, pGBT-yUBC13 and pGAD-yRAD5.

The ability of the Ubc13-M64A mutation to abrogate the interaction with Rad5 prompted the testing of two other Ubc13-E3 physical interactions. As discussed in chapter 1, Lys63-linked Ub chains generated by Ubc13-Uev are required for TRAF6-dependent activation of the NF- κ B pathway (Deng et al., 2000). Because TRAF6 is a RING finger E3, it was originally expected that a physical interaction might occur between Ubc13 and TRAF6. Using the sensitivity of the yeast two-hybrid assay several years later, our laboratory was able to show a physical interaction between mouse TRAF6 and human UBC13 (Wooff et al., 2004). It is notable that the human and mouse Ubc13 amino acid sequences are identical. As seen in Figure 4-7, human Ubc13 and mouse TRAF6 yield a positive signal in the yeast two-hybrid assay. On the other hand, when the human Ubc13-M64A mutant was tested, a physical interaction with TRAF6 was not detected even though Ubc13-M64A was still proficient in binding to Mms2 (Figures 4-5 and 4-7).





Gal4_{AD} Fusion	Gal4_{BD} Fusion	
hMMS2	hUBC13	
mTRAF6	hUBC13	
mTRAF6	hUBC13-M64A	
hMMS2	hUBC13-M64A	

Figure 4-7. The Ubc13-M64A substitution abolishes its physical interaction with TRAF6. Yeast two-hybrid analysis of the hUbc13-M64A-mTRAF6 protein interaction using the β -galactosidase filter-lift detection method. Physical interaction of the Gal4 hybrid proteins leads to the expression of the β -galactosidase gene which causes blue colour development in the assay. Co-transformed plasmids were maintained with Trp and Leu markers and are indicated on the left. Two representative colonies from each treatment are shown after a 36 hour incubation at 30°C. Cells co-transformed with Gal4_{AD}-mTRAF6 + Gal4_{BD}, Gal4_{AD} + Gal4_{BD}-hUbc13-M64A, and Gal4_{AD} + Gal4_{BD}-hUbc13 were negative in the assay (not depicted). Test plasmids were pGAD-hMMS2, pGAD-mTRAF6, pGBT-hUBC13, and pGBT-hUBC13-M64A.

Another putative Ubc13 physical interaction occurs with a novel human mitotic checkpoint pathway protein named CHFR (checkpoint with fork-head associated and RING finger domains). CHFR is a RING finger E3 that delays mitosis through an unknown mechanism after treatment with microtubule poisons (Scolnick and Halazonetis, 2000). Through various *in vitro* ubiquitylation assays, it was observed that CHFR functions to promote Lys63-linked Ub chain formation by Ubc13-Mms2 (Bothos et al., 2003). Point mutations that destroy the CHFR RING finger domain abolished the Ub-conjugation activity attributed to Ubc13-Mms2. The findings were best explained by a RING finger dependent physical interaction between CHFR and Ubc13-Mms2. In order to test this idea directly, a purified GST-CHFR derivative containing the RING finger domain was used to perform *in vitro* GST pull-downs assays with wild-type and Ubc13-M64A proteins. As seen in Figure 4-8, CHFR was able to bind to wild-type Ubc13 but not Ubc13-M64A.

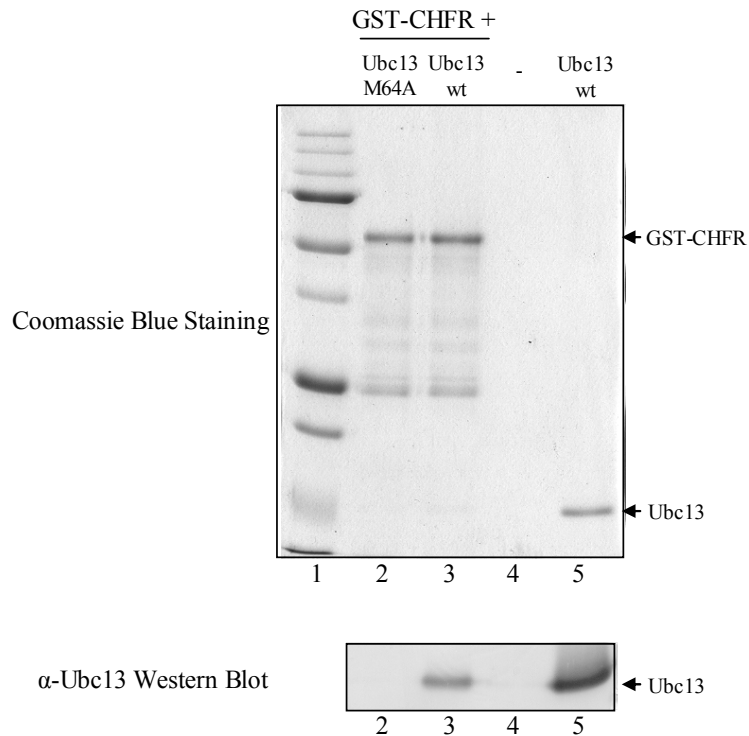


Figure 4-8. The Ubc13-M64A substitution abolishes its physical interaction with CHFR. A GST pull-down was used to test the *in vitro* binding of GST-hCHFR to non-fused wild-type (wt) hUbc13 (Lane 2) and hUbc13-M64A (Lane 3). Physical interaction of the test proteins allows their co-purification and subsequent detection in denaturing protein gels, as shown above. The binding of GST-CHFR to Ubc13 was not detected in the upper panel (the Coomassie blue stained gel). For increased sensitivity, an α -Ubc13 Western Blot of the same samples is shown in the bottom panel. Lane 1 (protein marker); Lane 4, negative control (resin-only) pull-down of Ubc13; Lane 5, Ubc13 protein only. It is noted that some degradation of the GST-CHFR fusion occurred during the assay (Lanes 2 and 3, upper panel).

4.3.4 Discussion of the Ubc13-E3 interface

Through the above analysis, a structure-based approach was used to generate a point mutation (Ubc13-M64A) that was predicted to lie within a putative Ubc13-E3 interface. Moreover, the Ubc13-Met64 residue is located near the distal end of a channel that has been proposed, based on structural analysis, to provide an outgoing route for Lys63-linked Ub conjugated by Ubc13-Mms2. These ideas present a conceptual link between the Ubc13-Mms2 Ub-conjugation event and the subsequent transfer to the E3-bound target.

When testing the functional consequence of the *UBC13-M64A* mutation in yeast DDT, no complementation of the *ubc13Δ* strain was observed. However, the Ubc13-M64A protein was fully capable of binding to human Mms2 *in vivo*, which indicated that the mutation did not affect the overall structure of Ubc13. The striking phenotypic effect of the point mutation was presumably due to the abrogation of a required Ubc13-E3 interaction (i.e. Ubc13-Rad5 in error-free DDT). Indeed, a physical interaction between the human Ubc13 and yeast Rad5 proteins was detected, and the finding helps to explain why the human *UBC13* gene is functional in yeast DDT. The result also suggests that an unidentified functional equivalent to *RAD5* will be found in higher eukaryotes. In accordance with the lack of complementation by *UBC13-M64A*, the Ubc13-M64A substitution was seen to abolish the physical interaction with Rad5 in the yeast two-hybrid assay. The Ubc13-M64A mutation was also shown to have the same effect on abolishing the Ubc13-TRAF6 interaction, indicating that the Ubc13-Met64 residue might be a general specificity requirement for the physical interaction of Ubc13 with its various cognate E3s. In this light, it might be interesting to determine if the Ubc13-M64A

mutation leads to interactions with other E3s that do not normally physically associate with Ubc13.

Whereas Rad5 and TRAF6 could not be used to demonstrate an *in vitro* physical interaction with Ubc13 (data not shown), the human RING finger E3 protein CHFR was used in a GST pull-down experiment with human Ubc13. A novel protein interaction between Ubc13 and CHFR was successfully shown. Furthermore, the same experiment showed that the physical interaction with CHFR was completely disrupted with the Ubc13-M64A mutant. The physical interaction between Ubc13 and CHFR, and the abrogation by the Ubc13-M64A mutant has been since confirmed in our laboratory using the yeast two-hybrid assay (data not shown).

The finding that different E3s interact with Ubc13 through the same residue suggests that the conjugation activity of Ubc13 can be exclusively sequestered in different cellular pathways. Moreover, the conservation of the physical interaction suggests a conserved biochemical mechanism for the delivery of Lys63-linked Ub to the target via “channel 3” of Ubc13-Mms2. Further structural analysis of Rad5, TRAF6, and CHFR, and the identification of additional Ubc13-specific E3s will undoubtedly shed more light on this possibility. It will also be interesting to determine whether Mms2 or Uev1A can facilitate the Ubc13-E3 interactions demonstrated above. While Ubc13 may be sufficient, Mms2 and Uev1A might provide additional binding affinity or specificity to a particular Ubc13-E3 interaction. The relatively weak interaction strengths observed for Ubc13-Rad5 and Ubc13-TRAF6, and the fact that the Ubc13-M64A mutation reveals a separate binding site on Ubc13 for Mms2, suggests that this is a possibility.

4.4 Mms2-Ub interface results

Based on the studies in this chapter so far, it has been shown that the binding of Ubc13 to Ub (at its active-site) and the interaction between Ubc13 with an E3 are both important functional aspects of Ubc13-Mms2. However, two other protein interactions are also fundamental to the model for Lys63-linked Ub chain assembly, and they provided the opportunity to conduct novel structure-function studies of Ubc13-Mms2. One such interaction involves the specific binding of Mms2 to Ubc13. The important determinants of the Ubc13-Mms2 interface and the functional consequences will be addressed in detail below. The other critical interaction is based on NMR chemical-shift data which suggest that Mms2 orients Ub to promote linkages through Ub-Lys63. In order to provide functional evidence to support this idea, appropriate mutations in Mms2 that abolish the interaction with Ub were desired. If the mechanistic model was to be upheld, it was hypothesized that such mutations would abolish Lys63-linked Ub conjugation by Ubc13-Mms2, and lead to DNA damage-sensitive phenotypes. Because the Mms2 binding sites for Ub and Ubc13 were proposed to be independent, such mutations can potentially act as dominant-negative regulators of Ubc13 Lys63-dependent Ub conjugation.

4.4.1 NMR-directed design of Mms2 surface mutations

The first probe into the putative Mms2-Ub interaction surface began with information taken from detailed NMR analyses of human Mms2 and Ub (S. McKenna, University of Alberta, Edmonton, AB, personal communication). It was discovered that certain Mms2 residues undergo changes in chemical environment upon incubation with

Ub *in vitro*. These so-called chemical-shifts are indicative of localized changes that can be caused by protein-protein interactions. However, while the sensitivity of the approach allows the detection of low-affinity or transient interactions (as was expected for Mms2-Ub), it also led to an abundance of candidates for Mms2 mutagenesis (Figure 1-3, pink residues). Therefore, only the residues which had undergone the largest chemical perturbation shifts and that were also representative of the entire putative interaction surface were mutated (S. McKenna, personal communication). These residues, corresponding to Mms2-Glu23, -Lys24, -Ser32, and -Met49, were substituted with Ala and are indicated in Figure 4-12.

In testing the effects of these mutations, two factors prompted the use of a more sensitive variation of the DDT functional complementation approach as performed in other parts of this thesis. One factor was that I expected the affinity of the Mms2-Ub interaction to be very weak in order to facilitate the efficient release of acceptor Ub after conjugation. Second, the large number of Mms2 residues that underwent a chemical shift upon interacting with Ub suggested that the affinity might be the sum of many small contributions from numerous residues. There was a concern that even the strongest phenotypes of individual mutations would go undetected in the typical functional complementation assays.

The more sensitive functional complementation assay variation took advantage of the synergistic relationship between *mms2* and *rev3* in DDT. The assays were nearly identical to those used to demonstrate that human *MMS2* functions in yeast DDT, except that the strain used in this case was an *mms2 rev3* double-deletion strain, instead of the *mms2* Δ single. With this approach, a very slight MMS-sensitive phenotype (reminiscent

of *rev3Δ* alone) would be observed in the case of full complementation by an *MMS2* transformation. On the other hand, a synergistic sensitivity to MMS would be observed in *MMS2* mutants that have impaired function in error-free DDT. However, none of the mutants caused a DNA damage sensitive phenotype in the assay (data not shown). In order to generate a stronger disruption of the surface, two of the mutations were combined to generate *MMS2-Q23A/M49A*. However, the double-mutant functioned as well as wild-type *MMS2* in the enhanced error-free DDT complementation assay (data not shown).

4.4.2 Mutagenesis of a putative Mms2 phosphorylation site

In another attempt to identify residues that might be important for Mms2 function through binding to Ub, a more directed approach involving the mutation of a putative Mms2 phosphorylation site was used. Initial sequence analysis in 1999 had identified that the Mms2 family of Uevs contained a conserved phosphorylation consensus sequence. With updated databases, this possibility was re-evaluated and the existence of such a site was confirmed. Most striking is that this consensus sequence (Arg-Ile-Tyr-Ser-Leu) is situated on the face of Mms2 that is proposed to interact with Ub. It was reasoned that a functional link between phosphorylation and ubiquitylation was possible. In accordance, preliminary observations indicated that mammalian Mms2 is phosphorylated *in vivo* (N. Syed, University of Saskatchewan, Saskatoon, SK, personal communication).

Visualization of the apparent phosphorylation consensus sequence in the human Mms2 crystal structure indicated that the hydroxyl group of the Tyr residue is not completely solvent-exposed, and is thus unlikely to be accessible for phosphate

modification. On the other hand, the Ser64 residue was a good candidate because it is conserved in Mms2 sequence alignments from yeast and mammals (Figure 4-13) and has an R-group that is directed outwards from the Mms2 interior. When comparing the NMR data (McKenna et al., 2003a) for the residues in the consensus sequence, the residues immediately flanking Ser64 (Tyr63 and -Leu61) were found to undergo chemical-shift upon Mms2-Ub interaction; however, no such change was observed for Mms2-Ser64. It was thus hypothesized that the phosphorylation of Mms2-Ser64 might prevent Ub from contacting Mms2-Tyr63 and -Leu61, thus interfering with the Mms2-Ub interaction. This was expected to inhibit the Lys63-linked Ub conjugation by Ubc13-Mms2 and lead to a measurable reduction in DDT activity. In this model, the biochemical activity of Ubc13-Mms2 could be regulated by a DNA-damage-responsive de-phosphorylation event. The fact that Mms2 proteins expressed in bacteria are proficient in ubiquitylation reactions is in accordance with this thought.

To address the hypothesis experimentally, two different mutations of the Mms2-Ser64 residue were created. Mms2-S64E was the first mutant, and was designed to mimic constitutive phosphorylation by the substitution to a larger and negatively charged residue. It was hoped that the mutant would inhibit the Mms2-Ub physical interaction in the manner proposed for phosphorylation. Despite using the aforementioned enhanced functional complementation approach, *MMS2-S64E* behaved like wild-type *MMS2* (data not shown). To cover the possibility that the phosphorylation of Mms2-Ser64 plays a positive role in Ubc13-Mms2-mediated Ub conjugation, an Mms2-S64A mutation was made to prevent phosphorylation. However, *MMS2-S64A* had no effect as observed in the functional complementation assay (data not shown).

4.4.3 Identification of Mms2 surface mutants defective in binding Ub *in vitro*

The inability to detect a phenotypic change for any of the Mms2 mutants in the functional assays above could be due to several reasons. One possibility is that the residues chosen for mutagenesis are not as important as the NMR data suggests, or that the Ala substitutions were not significant enough to disrupt the Mms2-Ub interactions. Another possibility is that the proposed model for Mms2-Ub binding is an *in vitro* phenomenon (or artifact) that does not actually occur inside the cell. A more favourable reason is that the Mms2-Ub interaction occurs with low-affinity over a large surface area and cannot be sufficiently abrogated by individual point mutations. The latter possibility is considered to be particularly likely because slight phenotypic differences could have been masked by the multi-copy vector and strong promoter used to constitutively express the *MMS2* derivatives in the assays.

The likelihood that the phenotypic changes went undetected became even more probable following a publication which used a completely different approach to address the putative Mms2-Ub interaction of the yeast proteins (Tsui et al., 2005). The authors began with mutations on the surface of Ub, instead of Mms2, and performed *in vitro* ubiquitylation reactions with purified Ubc13-Mms2 proteins. Through the analysis it was identified that Ub-Ile44 is necessary for the efficient conjugation of Lys63-linked di-Ub. However, the result was not particularly surprising because Ub-Ile44 was previously shown to be a common feature in protein-protein interactions involving Ub. Computerized docking of Ub to the Mms2 surface revealed that the Ub-Ile44 residue could potentially interact with Mms2-I57. Indeed, a yeast Mms2-I57A mutation caused a

greater than 10-fold reduction in di-Ub formation and behaved as a weak competitor in wild-type yeast Ubc13-Mms2 Ub-conjugation reactions (Tsui et al., 2005). Furthermore, the authors of the yeast protein study were able to demonstrate a partial DNA damage-sensitive phenotype *in vivo* for a *MMS2-I57A* mutant. It was realized that the success of the yeast protein study was likely because a single-copy plasmid employing the native yeast *MMS2* promoter was used.

In order to re-evaluate the Mms2 mutations created in this thesis work, it was felt that a protein-protein interaction approach might be more successful. Possibly due to an inherently low binding strength or physical hindrance from the Gal4_{BD} fusion, the yeast two-hybrid assay could not be used to detect a physical interaction between Mms2 and Ub (data not shown). As an alternative, surface plasmon resonance (SPR) was used as an *in vitro* approach to detect the Mms2-Ub physical interaction. SPR technology can be used as a sensitive tool for the real-time measurement of protein-protein interactions, and the data can often be used to determine kinetic parameters and binding constants (Szabo et al., 1995). In this particular experiment, GST-Mms2 was immobilized to the SPR sensor chip, purified Ub was then introduced as the soluble-phase analyte, and the binding response for GST-Mms2-Ub was subsequently monitored. A range of Ub concentrations was used in order to generate a series of binding curves for the calculation of the Mms2-Ub dissociation constant (K_d). Using the manual calculation approach as described in chapter 2 (Figure 2-3), the K_d of the Mms2-Ub interaction was determined to be approximately 200 μ M. The value is in good agreement with the NMR-derived K_d from our collaborators who determined it to be approximately 100 μ M (McKenna et al.,

2003a). The higher K_d as determined in this thesis may be due to the use of GST-Mms2 fusion proteins in the experimentation.

Given the ability to detect the Mms2-Ub interaction by SPR, all but one of the mutant human Mms2 proteins (Mms2-K24A) were purified and expressed. Preliminary analysis by SPR indicated that the Mms2-Q23A/M49A, -S64A, and S64E mutants did not affect binding with Ub when compared to wild-type, however, the Mms2-S32A mutation caused an appreciable decrease in affinity for Ub (data not shown). In order to put this finding in perspective, a human Mms2-I62A mutation was made which corresponds to the yeast Mms2-I57A substitution that was reported to interfere with Mms2-Ub binding and function (Tsui et al., 2005). For further comparison, an Mms2-S32A/I62A double-mutant was also created to help determine the relationship between the Mms2-Ser32 and -Ile62 residues in binding to Ub. The results in Figure 4-9 show that the Mms2-I62A mutation caused a decreased affinity for Ub, but apparently not to the extent as Mms2-S32A. Based on the results of each individual mutant, a reduction in Ub-binding by the Mms2-S32A/I62A double-mutant was also expected. Indeed, the ability of Mms2-S32A/I62A to bind Ub was decreased further than either of the single mutations alone. It is worth noting that throughout these experiments, no expression or solubility problems with any of the Mms2 derivatives were seen, suggesting that they were expressed and folded properly. In accordance, SPR was used to confirm that each of the Mms2 mutants retained an ability to bind purified Ubc13 (data not shown).

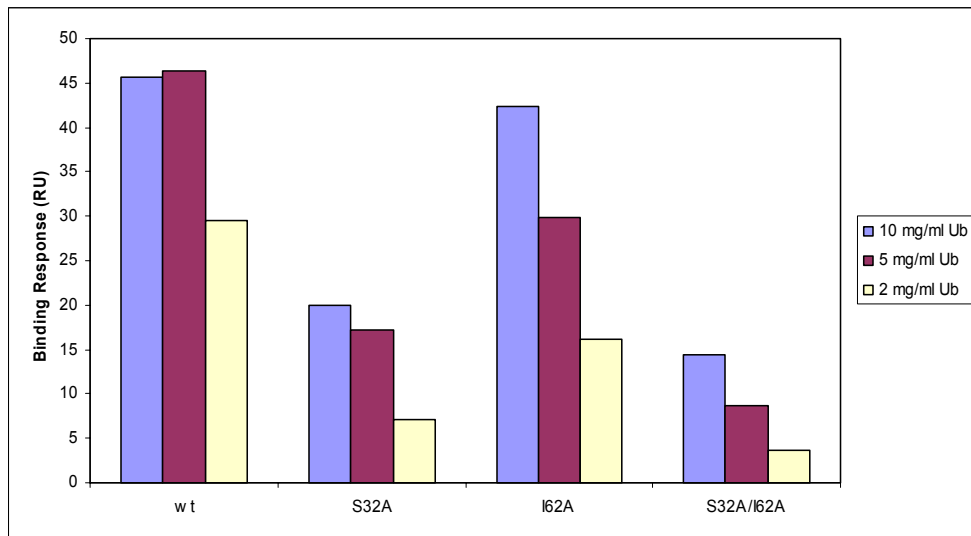


Figure 4-9. The mutation of the Mms2-Ub interface disrupts its binding with Ub *in vitro*. Surface plasmon resonance was used to measure the binding response of GST-hMms2 derivatives (indicated at the bottom) with various concentrations of Ub. It is noted that 5 mg/ml Ub yielded a maximum binding response for wild-type (wt) Mms2. Data shown is the average of three independent experiments.

4.4.4 Functional complementation in DDT is impaired by Mms2-Ub interface mutations

In order to determine the relationship between *in vitro* Ub binding and DDT function, the yeast equivalents of the human Mms2 mutants above causing lowered Ub-binding were generated. The yeast *MMS2-S27A*, *-I57A*, and *-S27A/I57A* mutations correspond to human *MMS2-S32A*, *-I62A*, and *-S32A/I62A*, respectively. Each of the yeast mutants was created in a single-copy plasmid employing the native yeast *MMS2* promoter. The ability of each of these constructs to provide functional complementation in the *mms2Δ rev3Δ* yeast strains after DNA damage treatment by MMS was then tested. Figure 4-10 shows that *MMS2-S27A* and *MMS2-I57A* have comparable deficiencies in DDT function. Strikingly, while the reduction in DDT is moderate in each of the single mutants, the *MMS2-S27A/I57A* mutant displayed a strongly additive decrease in DDT function. The phenomenon is more easily seen when comparing the same strains on dilution plates containing MMS. In fact, the *MMS2-S27A/I57A* mutant is nearly as sensitive to DNA damage as the negative control (Figure 4-11).

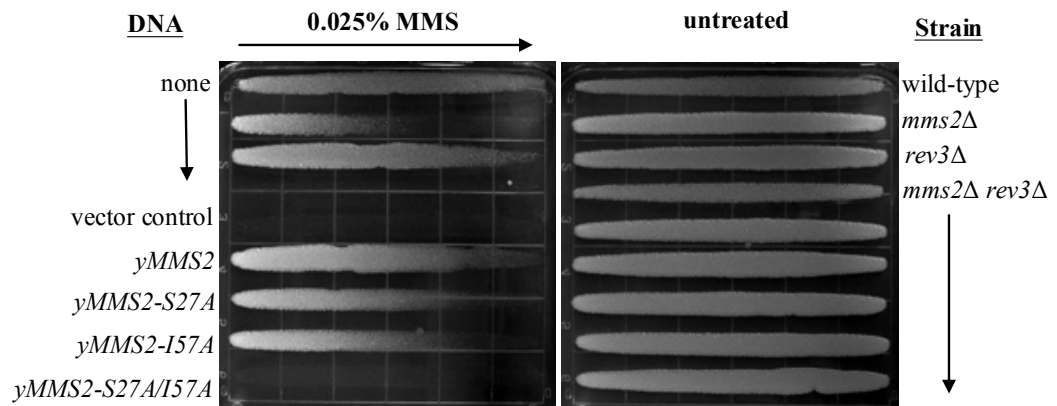


Figure 4-10. The mutation of the Mms2-Ub interface disrupts the *in vivo* function of *MMS2*. The *in vivo* function of yeast *MMS2* mutants is reflected in the ability to alleviate an *mms2 rev3^Δ* yeast strain from killing by MMS. Overnight cell cultures were printed on YPD plates containing a gradient of 0.025% MMS, and cells with a greater ability to survive DNA damaging treatment grew further along the gradient. Incubation was carried out for 48 hours at 30°C before taking the photograph. The arrow indicates an increasing MMS concentration. Test plasmids were YCpL-yMMS2, YCpL-yMMS2-S27A, YCpL-yMMS2-I57A, YCpL-yMMS2-S27A/I57A.

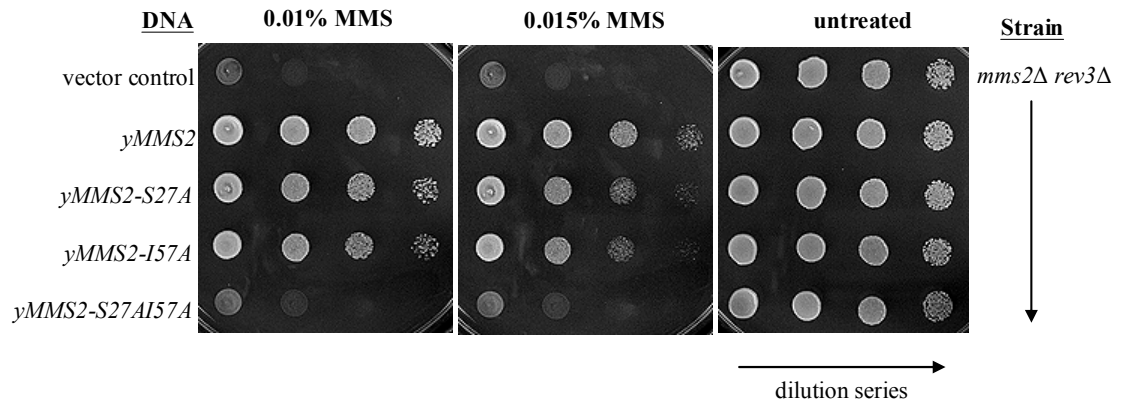


Figure 4-11. The *MMS2-S27A/I57A* double-mutant causes an additive MMS sensitive phenotype. The *in vivo* function of yeast *MMS2* mutants is reflected in the ability to alleviate an *mms2[?] rev3[?]* yeast strain from killing by MMS. Overnight cell cultures were spotted as dilutions on selective minimal media that contained either 0.01% or 0.015% MMS. 10-fold serial dilutions increased from left to right and cells with a greater ability to survive DNA damaging treatment are able to grow at higher dilutions. Incubation was carried out for 48 hours at 30°C before taking the photograph. Test plasmids were YCpL-*yMMS2*, YCpL-*yMMS2-S27A*, YCpL-*yMMS2-I57A*, YCpL-*yMMS2-S27A/I57A*.

4.4.5 Discussion of the Mms2-Ub interface

The mechanistic model of Ubc13-Mms2-mediated ubiquitylation suggests that an acceptor Ub is non-covalently bound by Mms2 in a manner that favours the specific linkage of Ub molecules through Lys63. In order to provide functional evidence to support the model, a number of site-directed mutations of Mms2 were generated within the putative Mms2-Ub interface. Thus, mutations that disrupt the Mms2-Ub interface would be expected to reduce the ability of Mms2-Ubc13 to conjugate Lys63-linked Ub chains, leading to a measurable error-free DDT-deficient phenotype.

Despite the targeted design of Mms2 mutations based on NMR data and a putative phosphorylation consensus sequence within the suspected Mms2-Ub interface, phenotypic changes were not observed in initial, albeit extra-sensitive, functional complementation assays. As a result, a potentially more sensitive *in vitro* method was used to evaluate the consequence of the mutations on Mms2-Ub interaction strength. Using SPR, a dissociation constant for the wild-type Mms2-Ub interaction was calculated to be approximately 200 μ M. Subsequent analysis of the relative binding strength of various Mms2 mutants with Ub revealed that an Mms2-S32A mutation was unique in causing a decrease in Mms2-Ub interaction strength. To put the finding in perspective, a human Mms2-I62A mutant was generated as the equivalent of a yeast point mutation shown by another group to affect Mms2-mediated Ub conjugation *in vitro* and error-free DDT *in vivo* (Tsui et al., 2005). In the SPR binding assay, the Mms2-I62A mutation was also found to impair the Mms2-Ub interaction but not to the extent of the Mms2-S32A mutant. Interestingly, the generation of both mutants in the same protein (Mms2-S32A/I62A) caused an additive decrease in affinity for Ub.

In an attempt to correlate Mms2-Ub affinity with *in vivo* DDT function, the human Mms2 mutations that decreased Ub affinity were correspondingly created in yeast Mms2. These yeast mutants were then cloned into single-copy plasmids employing the native *MMS2* promoter. Testing them in functional complementation assays, it was determined that both the yeast *MMS2-S27A* and *-I57A* single mutants caused a slight defect in DDT activity. On the other hand, the *yMMS2-S27A/I57A* double mutant caused a very surprising synergistic defect in error-free DDT. The finding that each of the single mutants is able to function somewhat in DDT provides indirect evidence that the *yMms2-S27A/I57A* protein is expressed and folded properly *in vivo*. It is also noted that the corresponding human Mms2-S32A/I62A mutant was able to efficiently bind Ubc13 in the SPR experiments.

Taken together, the Mms2 mutations yielded results that were somewhat surprising because a strong correlation between *in vitro* Ub binding and *in vivo* functional complementation was expected; however, some disparity was observed between the *in vitro* and *in vivo* data. For example, the *yMMS2-S27A* single mutation caused a barely detectible phenotype in the functional assay, whereas the *yMMS2-S27A/I57A* double mutation caused a phenotype almost indistinguishable from the negative control. When the corresponding hMms2 proteins were tested for their ability to bind Ub *in vitro*, the difference between these single and double mutants was not nearly as pronounced (Figures 4-10, 4-11 vs. 4-9).

A possible explanation for the disparate results is apparent when considering the orientation of acceptor and donor Ub molecules in the Ubc13-Mms2 Ub conjugation model. Most notable is the precise placement of the Mms2-bound Ub such that its Lys63

is within 4 Å of the Ubc13 active-site. The single point mutations can be envisioned to cause a slight repositioning of acceptor Ub on the large Mms2-Ub interface. This slight adjustment may be done in such a way that the ε-amino group of Ub-Lys63 is still in close enough proximity to the Ubc13 active-site for efficient conjugation. The hypothetical phenotype could be a reduction in Mms2-Ub binding affinity *in vitro* that is overcome by the successful conjugation of Lys63-linked Ub chains *in vivo*. On the other hand, although the Mms2 double mutation could also retain some affinity to Ub as observed in the *in vitro* assays, the resultant placement of acceptor Ub might not permit Lys63-linked Ub conjugation. The result is a DDT deficient phenotype. It is noted that the hypothesis might be easily addressed through comparisons of the *in vitro* ubiquitylation activity of each of the mutant Mms2 proteins. The inability to conjugate Lys63-linked Ub chains may be expected of the yMms2-S27A/I57A double mutant.

The structure-based studies of the Mms2-Ub interface above provided strong functional support for the proposed mechanism of Ubc13-Mms2 Lys63-linked Ub conjugation. From another perspective, the results also allowed a more fundamental question concerning Mms2 and Ub to be addressed.

In the simplest sense, Mms2 goes about its mechanistic role with Ubc13 by acting as a Ub-binding domain (Ubd). Ubds are found in Ub-binding proteins (also called Ub receptors) and act as autonomous non-covalent Ub-binding modules that are indispensable components of the ubiquitylation process (Hicke et al., 2005). For example, the molecular signals generated by the Ub-modification of targets would simply go undetected without Ubds. Nine distinct Ubds have been characterized to date, and they are found within hundreds of different proteins throughout eukaryotes. The length

of the Ubd can range in size from about 20 to 150 amino acids, and various crystal structures reveal that they generate vastly different structural conformations. Despite these core differences, the specific surface on Ub that they each interact with is completely conserved (Hicke et al., 2005). The critical region for interaction in all cases to date surrounds a small hydrophobic patch on Ub that is marked by Ile44. Another notable feature of Ubds is that their affinity for Ub is weak ($K_d = 2\text{-}500 \mu\text{M}$ range), but binding may be strengthened by the occurrence of multiple Ubds in tandem, which may even cause the preferential binding to Ub chains over mono-Ub.

The calculation of the Mms2-Ub dissociation constant in these studies to be $\sim 200 \mu\text{M}$ helps to confirm that human Mms2 is a *bona fide* Ubd. Moreover, the results of the Mms2 mutations provide additional insight which suggests that different UeVs may use different surfaces to interact with Ub. A crystal structure of Tsg101 bound to Ub reveals that its Uev domain, like the other characterized Ubds, specifically interacts with the hydrophobic patch surrounding Ub-Ile44 (Sundquist et al., 2004). The apparent interaction between yeast Mms2-Ile57 and Ub-Ile44 suggests that the Uev-Ub interaction is conserved in this regard (Tsui et al., 2005). However, the identification of a second important residue (yMms2-Ser27) for the Mms2-Ub interaction significantly adds to the conventional wisdom for how the Mms2 family of UeVs interacts with Ub. Specifically, the spacing of the yMms2-Ser27 and -Ile57 residues helps to map a hypothetical Mms2-Ub interface, for which a crystal structure has yet to be reported. As seen in Figure 4-12, the surfaces of the Uev domains of Mms2 and Tsg101 that are used to interact with the same surface on Ub are apparently distinct. When the residues that were shown to be important for the Mms2-Ub interaction are correspondingly highlighted on Tsg101, it is

revealed that they are localized independent of the Tsg101-Ub interface. This reasoning might provide an additional explanation for the mechanistically distinct functions and cellular roles performed by the two predominant Uev families represented by Mms2 and Tsg101. Also, it cannot be ruled out that each Uev domain contains two surfaces capable of binding to Ub. A crystal structure of Mms2 bound to Ub would undoubtedly help to clarify these possibilities.

Another significant conclusion from the results in this section involves the Mms2-Ser32 (yeast Mms2-Ser27) residue in particular. The Mms2-Ser32 residue was found to be important for interacting with Ub and enabling Mms2 to function in DDT, in a manner that is consistent with the model of Lys63-linked Ub chain synthesis by Ubc13-Mms2. The decrease in Ub-binding in the Mms2-S32A mutant is a novel finding that suggests an important role for polar contacts in the Mms2-Ub interaction. This result challenges the current understanding of Ubd-Ub interactions in general which claim that the predominant interactions are mediated through hydrophobic contacts in and around Ub-Ile44 (Hicke et al., 2005). Among all the residues mutated in these studies, including Mms2-Ile62 which is speculated to contact Ub-Ile44, the residue corresponding to human Mms2-Ser32 is the only one that is absolutely conserved in Mms2 and Uev1 sequence alignments (Figure 4-13 and data not shown).

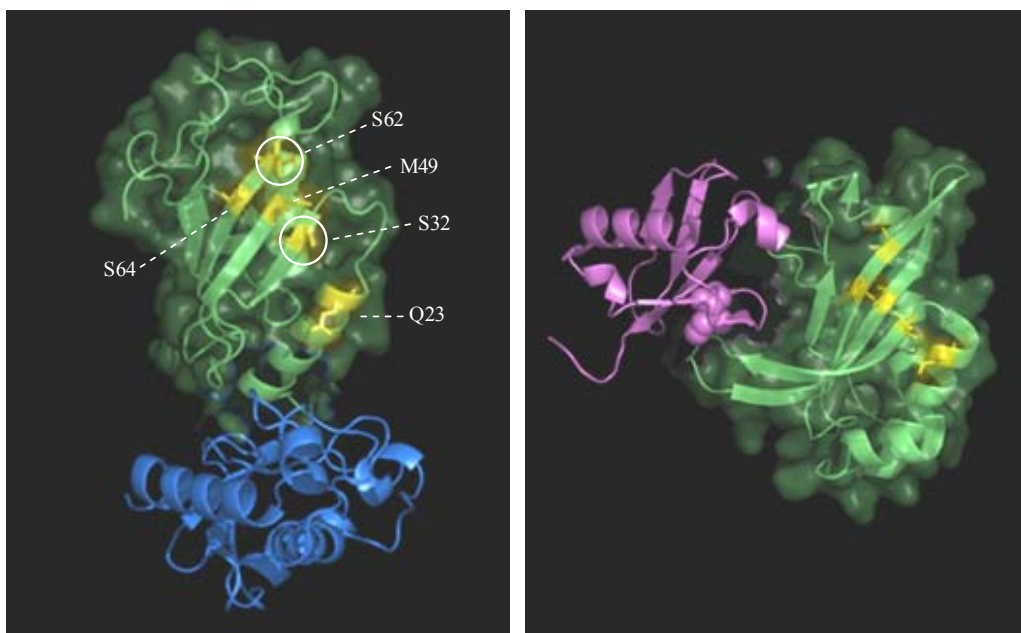


Figure 4-12. The Uev domains of human Mms2 and Tsg101 use different surfaces to physically interact with Ub. The Uev domains of Mms2 (left panel, green) and Tsg101 (right panel, green) are orientated similarly and are bound to Ubc13 (blue) and Ub (violet), respectively. The Mms2 residues mutated in the Mms2-Ub physical interaction studies and the corresponding Tsg101 residues are shown in yellow. The two residues shown in this study to be important for the Mms2-Ub interaction (left panel, white circles) do not visibly correspond to the same surface used for the Tsg101-Ub interaction (right panel).

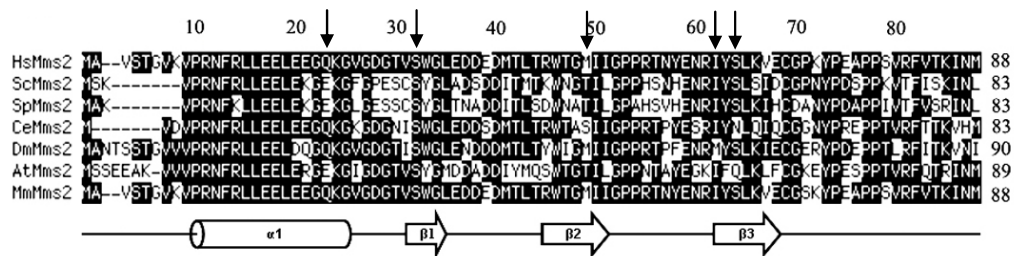


Figure 4-13. Protein sequence alignment of Mms2 proteins from various organisms.

Alignment of Mms2 protein sequences from various model organisms using the CLUSTAL method. Residues identical to the HsMms2 sequence are shaded black and residues corresponding to the hMms2-Ub interface that were mutated in this study are indicated with arrows. Hs, *Homo sapiens*; Sc, *S. cerevisiae*; Sp, *Schizosaccharomyces pombe*; Ce, *Caenorhabditis elegans*; Dm, *Drosophila melanogaster*; At, *Arabidopsis thaliana*; Mm, *Mus musculus*.

4.5 Ubc13-Mms2 interface results

The structure-function studies above have addressed three main features of Ubc13 and Mms2. They include the Ubc13 active-site, the Ubc13-E3 interaction, and the Mms2-Ub interaction. The experimental results have helped to draw conclusions pertaining to each of these separate yet important features; however, the model of Lys63-linked Ub conjugation holds that these features are brought together functionally by the formation of a unique Ubc13-Mms2 heterodimer. Therefore, the most intensive and meaningful structure-function studies of this thesis were focused upon the Ubc13-Mms2 interface. The main goals were to identify important residues for the Ubc13-Mms2 interaction, to demonstrate a correlation between Ubc13-Mms2 binding and function, and to determine why Mms2 forms a specific complex with Ubc13, and not other E2s.

4.5.1 Structure of the Ubc13-Mms2 interface

The overall structure of the human Ubc13-Mms2 heterodimer is shown in Figure 4-14A. Each molecule adopts the characteristic α/β E2 fold and exhibits a very similar three-dimensional structure, with the main exception that Mms2 lacks two C-terminal α -helices as compared with Ubc13. The highlighting feature is that Mms2 packs against Ubc13 to form a unique asymmetrical structure that creates a long channel which buries ~1500 Å² of solvent-accessible surface area (Moraes et al., 2001; VanDemark et al., 2001).

Oriented similarly as in Figure 4-14A, a closer look at the Ubc13-Mms2 heterodimer is shown in Figure 4-14B and reveals the residues in close proximity to the interface. Due to the large number of candidate residues, several factors became

important in determining which amino acids to mutate. First, initial studies on heterodimer formation (McKenna et al., 2001) indicated that the Ubc13-Mms2 complex is stable in high salt concentrations, suggesting a large contribution by hydrophobic contacts. Visible inspection reveals that a significant number of these hydrophobic contacts likely surround a region that corresponds to a two residue insertion (Mms2-Asn12 and -Phe13) near the amino-end of the α 1 helix of Mms2. Interestingly, this insertion is a distinguishing characteristic of Uev sequences when compared to canonical E2s. Second, a localized change in the orientation of the human Mms2 N-terminus upon heterodimer formation with Ubc13 was previously identified (Moraes et al., 2001), implicating an importance for the Ubc13 residues in proximity to the Mms2 N-terminus. Last, each of the residues mutated are completely conserved or very similar in multiple protein sequence alignments of Ubc13 and Mms2 proteins from various model organisms (Figure 4-14C).

A

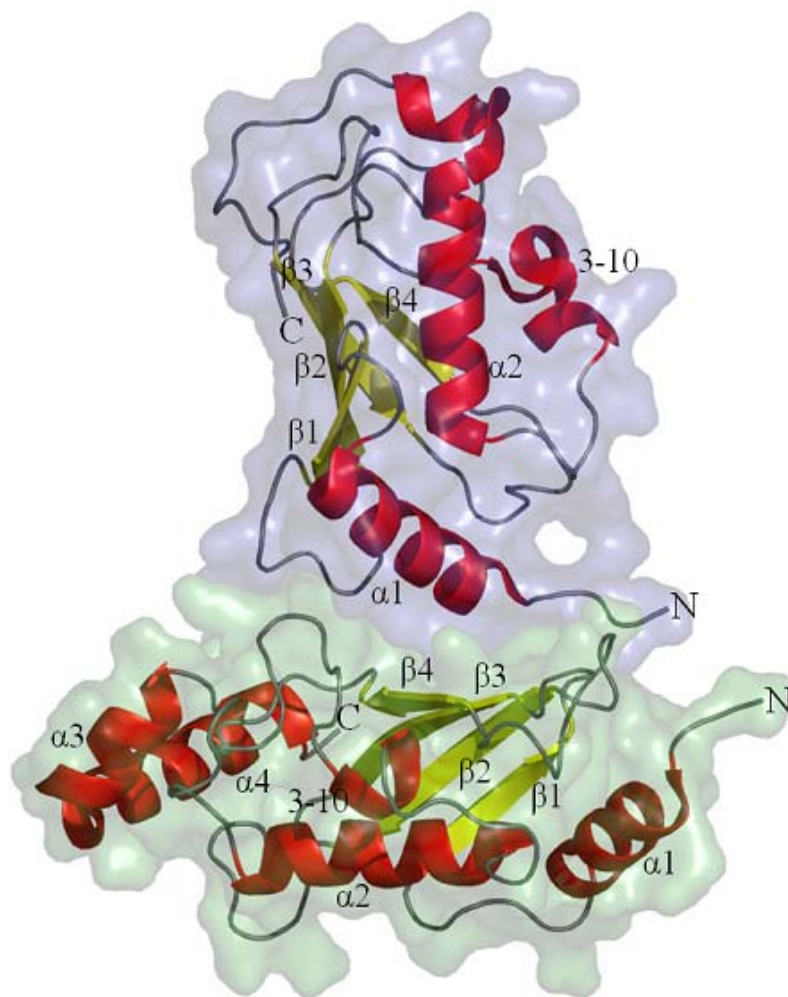


Figure 4-14. Secondary and tertiary structures of Ubc13 and Mms2. (A) Overall structure of the human Ubc13-Mms2 heterodimer. Ubc13 (bottom, green shading) and Mms2 (top, blue shading). The molecular structure was created using PyMOL version 0.96 by DeLano Scientific (<http://pymol.sourceforge.net/>) and the protein databank file 17JD.

B

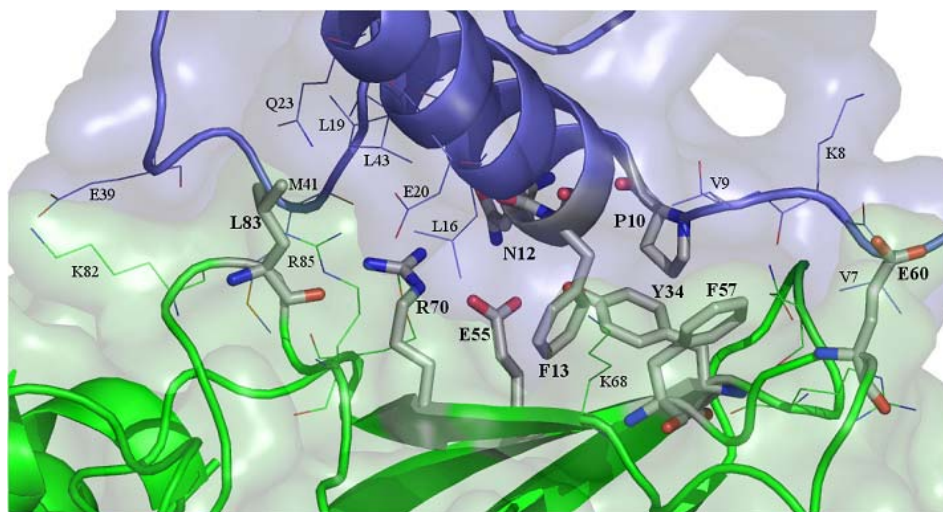


Figure 4-14. Secondary and tertiary structures of Ubc13 and Mms2. (B) Close-up view of residues in proximity to the Ubc13 (green) -Mms2 (blue) interface. Residues addressed by mutagenesis in these studies are indicated in bold and shown in stick (as opposed to line) representation. The complex is oriented as in Figure 4-14A.

C

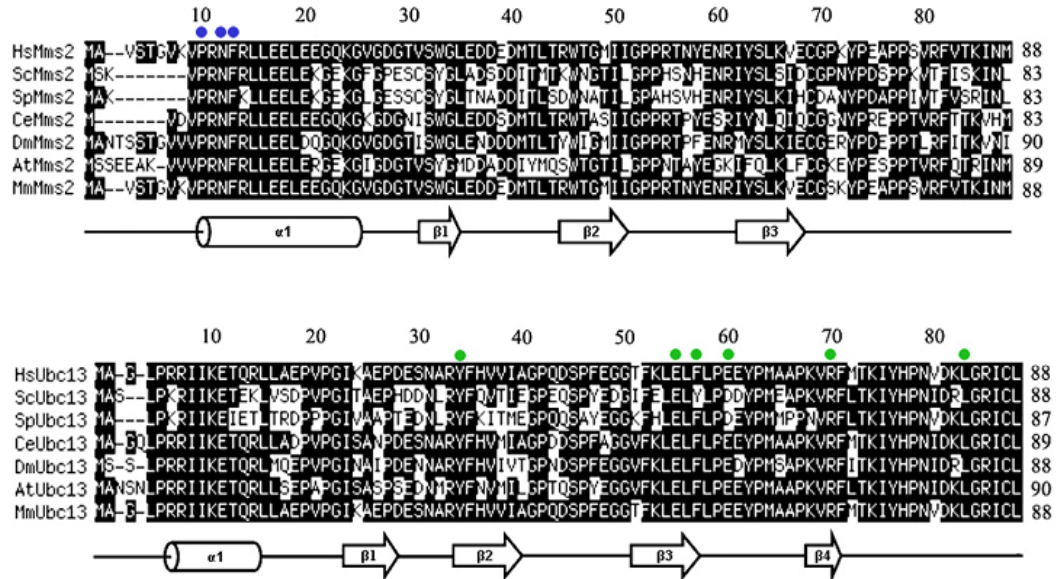


Figure 4-14. Secondary and tertiary structures of Ubc13 and Mms2. (C) Alignment of Mms2 (upper panel) or Ubc13 (lower panel) protein sequences from various model organisms using the CLUSTAL method. Identical residues are shaded black and residues mutated in this study are indicated with a dot. Hs, *Homo sapiens*; Sc, *S. cerevisiae*; Sp, *Schizosaccharomyces pombe*; Ce, *Caenorhabditis elegans*; Dm, *Drosophila melanogaster*; At, *Arabidopsis thaliana*; Mm, *Mus musculus*. Only the regions which span the interface residues are shown.

4.5.2 Design of Ubc13 mutants and their interaction in the yeast two-hybrid assay

Because all the evidence to date suggests a specific complex between Mms2 and a single E2 (Ubc13), the initial site-directed mutagenesis focused on residues of Ubc13. It was anticipated that this approach would narrow down the search for key residues because various E2s, despite often being involved in very different cellular roles, always have very conserved core domain sequences. Therefore, those Ubc13 residues that visibly interact with Mms2 in the crystal structure and are not conserved with other E2s were seen as good candidates for mutagenesis.

Before selecting mutants to test *in vivo*, two readily-available Ala substitutions (Ubc13-Y34A and -L83A) were tested for their binding to Mms2 *in vitro* using GST pull-down assays. These residues had been previously suggested (Moraes et al., 2001) to contribute hydrophobic contacts at two separate regions of the interface (Figure 4-14B). However, neither mutation had a significant effect on binding to Mms2 as determined by the GST pull-down assay (data not shown) and isothermal titration calorimetry experiments (T. Moraes, personal communication), suggesting that residues presumed to contribute hydrophobic contacts would have to be changed more drastically. With this in mind, the Ubc13-Phe57 residue of the putative hydrophobic core was targeted through the design of a non-conservative substitution to Glu, which would introduce a charged polar group into the region.

In another attempt to address this same central region of the interface, the role of the Ubc13-Glu55 residue was probed. Crystal structure data implicates a dual role whereby the beta and gamma-carbons of Glu55 can provide hydrophobic contacts for Mms2-Phe13, while the carboxyl group is used to H-bond with Mms2-Asn12 (Moraes et

al., 2001; VanDemark et al., 2001; Figure 4-14B). The only Ubc13 mutant studied to date was the corresponding Glu55 in yeast Ubc13 (VanDemark et al., 2001), for which Ala was substituted, resulting only in a small titration-dependent effect on binding and function (Ulrich, 2003). Therefore, a conservative E55Q mutant was created that was expected to disrupt the H-bonding with Mms2-Asn12, while maintaining approximate size and the putative hydrophobic contacts with Mms2-Phe13.

The last of the initial Ubc13 mutagenesis focused on Ubc13-Glu60, which is situated near the N-terminus of Mms2. While it is not resolved in the human structure, the yeast Ubc13-Mms2 heterodimer shows an H-bond formed between Ubc13-Glu60 and Mms2-Ser2. It was predicted that a conservative Ubc13-E60Q mutation would disrupt the bond and address the importance of the Mms2 N-terminus in binding to Ubc13.

In order to determine the effect of these interface mutations on complex formation in the cell, the yeast two-hybrid assay was employed as a qualitative measurement of physical interaction strength. Figure 4-15 shows the effects of these Ubc13 mutations. The Ubc13-E60Q mutation did not affect the Ubc13 interaction with Mms2; however, the Ubc13-E55Q and Ubc13-F57E mutations resulted in the complete disruption of heterodimer formation as visualized in the assay. The severe consequences of the Ubc13-Glu55 and -Phe57 mutants prompted the investigation of another residue in this area, Ubc13-Arg70.

The Arg70 residue is absolutely conserved among Ubc13 sequences (Figure 4-14C). While it has been suggested that Arg70 can provide hydrophobic contacts in the yeast heterodimer structure (VanDemark et al., 2001), another predominant contribution to the interface is noted as an H-bond with the carbonyl carbon of Mms2-Met41 (Figure

4-14B). To address this bond a Ubc13-R70A mutant was generated and its binding to Mms2 was tested in the yeast two-hybrid assay. As seen in Figure 4-15, Ubc13-R70A caused an impairment of the Ubc13-Mms2 interaction.

		Growth on SD media	
Gal4 _{AD} Fusion	Gal4 _{BD} Fusion	-Trp-Leu	
		-His+1mM 3AT	-Trp-Leu
Vector	Ubc13		
Mms2	Ubc13		
Mms2	Ubc13-E55Q		
Mms2	Ubc13-F57E		
Mms2	Ubc13-E60Q		
Mms2	Ubc13-R70A		
Mms2	Vector		
Mms2	Ubc13		
Mms2-F13E	Ubc13		
Mms2-F13Y	Ubc13		
Mms2-N12A	Ubc13		
Mms2-N12D	Ubc13		

Figure 4-15 *In vivo* interaction of mutated Ubc13 and Mms2 with wild-type partners by a yeast two hybrid assay. Yeast cells transformed with Gal4_{AD} and Gal4_{BD} fusion constructs were used to test the strength of the Ubc13-Mms2 interaction. Association of the Gal4 fusion proteins turns on the *GALI* promoter which transcribes the *HIS3* reporter gene. Positive interactions are observed by growth on media without His plus 1 mM 3-AT, after 48 hours at 30°C. Plasmids were maintained in the cell by growth on media without Trp and Leu. At least four colonies from each combination were tested and two representative colonies are shown. It is noted that the left-most colony of the duplicate for the Mms2-Ubc13-R70A pairing did not grow well and is not reflective of the other replicates for this combination. Test plasmids were pGAD-hMMS2 (and mutant derivatives) and pGBT-hUBC13 (and mutant derivatives).

4.5.3 Design of Mms2 Mutants and their interaction in the yeast two-hybrid assay

The finding that all of the substitutions of Ubc13 residues which affect binding lie in close proximity prompted the narrowing of the search for key interface residues in Mms2. The Mms2 residues that seemed to most closely correspond to these Ubc13 residues were Mms2-Asn12 and -Phe13, which correspond to a two amino acid insertion unique to Uevs when aligned against E2s (VanDemark et al., 2001).

Visualization of the Ubc13-Mms2 heterodimer shows an apparent insertion of the Mms2-Phe13 residue into a hydrophobic region, created mainly by the Ubc13 residues mutated above. As with Ubc13-F57E, it was decided to exploit this area with an aggressive Mms2-F13E substitution to introduce a charged polar group that would likely impinge upon the apparent hydrophobic contacts.

Unlike Phe13, Mms2-Asn12 does not contribute to the hydrophobic core but forms H-bonds with the Ubc13 residues Glu55 and Tyr34. However, because only the Ubc13-E55Q mutation showed an effect on binding, a possible pairwise interaction between with Mms2-Asn12 was tested. Two Asn12 mutations were thus created; one as a conservative N12D substitution and a second mutation, N12A, in order to abolish any H-bonding possibilities with Ubc13-E55Q.

When testing these Mms2 mutants in the yeast two-hybrid assay, it was found that neither Mms2-N12A nor -N12D had a detectable effect on inhibiting complex formation as compared to wild-type Mms2 (Figure 4-15). In contrast, the Mms2-F13E mutation seemed to completely disrupt the Ubc13-Mms2 interaction.

Because the mutagenesis of Ubc13 yielded mutants that resulted in severe (Ubc13-E55Q and Ubc13-F57E) and slight (Ubc13-R70A) disruption of the Ubc13-

Mms2 physical interaction, it was desired to have a complement of Mms2 mutants with similar effects. Because the aggressive introduction of a charged group at Mms2-Phe13 (F13E) caused a severe effect on interaction, it was hypothesized that a more conservative F13Y mutation that simply introduces a small polar hydroxyl group might cause a moderate effect. Indeed, the Mms2-F13Y mutant did not interact with Ubc13 as strongly as wild-type Mms2, nor did it completely abolish the yeast two-hybrid interaction either (Figure 4-15).

Taken together, the yeast two-hybrid data showed that two mutations (Mms2-F13Y and Ubc13-R70A) cause weakened interactions between Ubc13 and Mms2, and three mutations (Mms2-F13E, Ubc13-E55Q, and Ubc13-F57E) cause the complete disruption of the Ubc13-Mms2 interface, as detected in these assays.

4.5.4 The *in vivo* function of *MMS2* and *UBC13* interface mutants correlates with their *in vivo* interaction

Throughout this thesis, the human *MMS2* and *UBC13* genes were shown to functionally complement their yeast counterparts in error-free DDT. In chapter 3, it was experimentally suggested that a Ubc13-Uev physical interaction is necessary for *in vivo* function. The creation of Ubc13-Mms2 interface mutations that disrupt heterodimer formation to different degrees allowed this idea to be tested. As seen in Figure 4-16, the Asn12 mutants of *MMS2* that did not reduce the Mms2-Ubc13 interaction in the yeast two-hybrid assay appeared to be fully functional in yeast DDT. On the other hand, the mutations at Mms2-Phe13 which address the core hydrophobic region, caused a slight (F13Y) and drastic (F13E) decrease in the protection of cells against DNA damaging

treatment by MMS (Figure 4-16). The partial phenotypes for *MMS2-F13Y* and *-F13E* were reminiscent of their effects on binding to Ubc13 in yeast two-hybrid assay.

As in the yeast two-hybrid assay, the *UBC13-E60Q* mutant behaved no differently than the wild-type control in the functional complementation test (Figure 4-16). However, each of the Ubc13 mutants in proximity to Mms2-Phe13 led to a decrease in DDT activity. Most strikingly, *UBC13-E55Q* and *UBC13-F57E* provided no detectable protection against MMS treatment when compared with the negative control. This correlated perfectly with the complete loss of a detectable yeast two-hybrid interaction between Mms2 and each of the Ubc13-E55Q and -F57E mutations. The Ubc13 mutation that was designed to destroy H-bonding with the Mms2 backbone, *UBC13-R70A*, led to an incomplete loss in the ability to complement the *ubc13Δ* deletion. This was in agreement with the yeast two-hybrid assay results, which showed that the Ubc13-R70A mutation caused a moderate reduction in binding to Mms2.

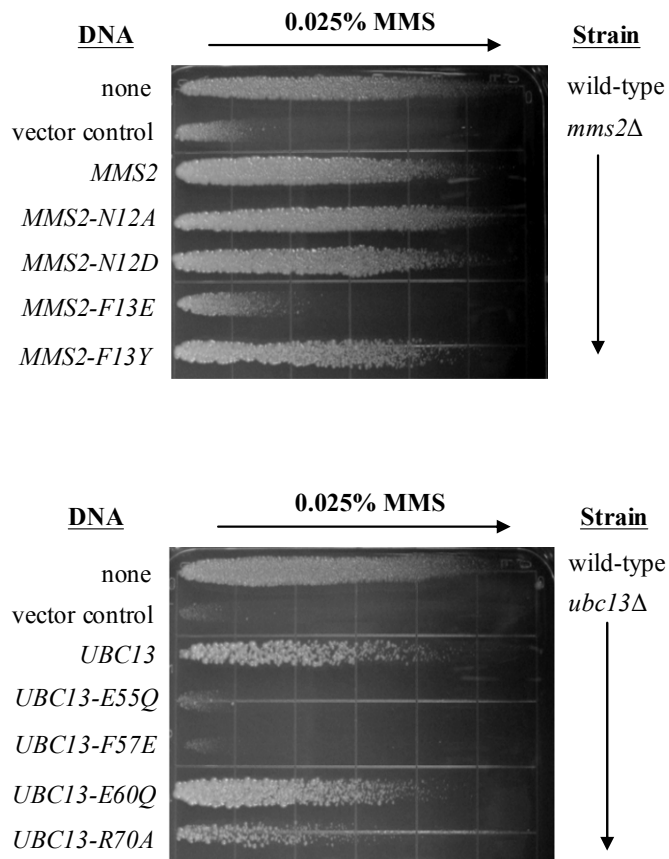


Figure 4-16. Functional complementation of yeast *ubc13* and *mms2* mutants by corresponding human genes and their derivatives . The function of human Ubc13 or Mms2 is reflected in the ability to protect their corresponding yeast deletion mutants from killing by MMS. Cells were printed on YPD plates containing 0.025% MMS and cells with a greater ability to survive DNA damaging treatment grew further along the gradient. Incubation was carried out for 48 hours at 30°C. All cells grew equally well on YPD plates without MMS (data not shown). Test plasmids were pGAD-hMMS2 (and mutant derivatives) and pGBT-hUBC13 (and mutant derivatives).

4.5.5 Binding ability of interface mutants by *in vitro* pull-down

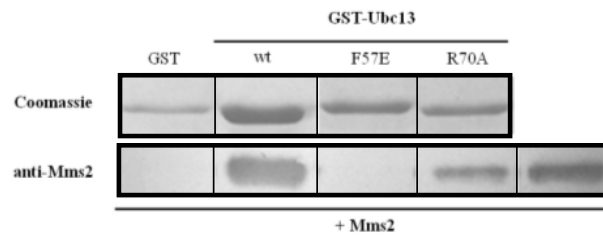
The yeast two-hybrid assay provides a good qualitative indication of binding strength but several assay factors already discussed in this thesis can hinder final conclusions. Therefore, to address and confirm the *in vivo* interaction data, it was desirable to quantitatively evaluate the effects of Ubc13 and Mms2 mutations on binding *in vitro*. Wild-type and mutant proteins were thus expressed and purified as GST fusions from bacteria. When needed, the fusion protein was cleaved and the native, non-fused Ubc13 or Mms2 protein was isolated. The recombinant bacterial expression approach is advantageous because prokaryotes do not have ubiquitylation enzymes that can provide background interference. The lack of post-translational modifications during bacterial expression was not a concern because *in vitro* binding and ubiquitylation experiments using recombinant protein from bacterial sources have been successful (Hofmann and Pickart, 1999; McKenna et al., 2001).

In addition to the wild-type proteins, two groups of mutants from each of Ubc13 and Mms2 were purified. These include those which resulted in reduced binding and functional complementation (Mms2-F13Y and Ubc13-R70A) and those that seemed to completely abolish the binding and function (Mms2-F13E and Ubc13-F57E). Despite rigorous attempts, GST-Ubc13-E55Q could not be retrieved in soluble form from bacteria. To show that the lack of *in vivo* binding and function in this mutant was not due to insolubility in yeast cells, the ability of Ubc13-E55Q and the other Ubc13 mutants to interact with mouse TRAF6 was tested in the yeast two-hybrid assay. The physical interaction between wild-type Ubc13 and TRAF6 was previously shown in Figure 4-7. As discussed above and in Woof et al., 2004, the Ubc13-TRAF6 interface is likely

independent of the Ubc13-Uev interface. Therefore, the Ubc13-E55Q mutation was not expected to affect the ability of Ubc13 to bind to TRAF6. Indeed, all of the Ubc13 mutants were able to interact with TRAF6 with a binding strength comparable to wild-type Ubc13 (data not shown).

As a first approach toward verifying the *in vivo* interaction data, the purified proteins were used in *in vitro* GST pull-downs. Wild-type or mutant GST-Ubc13 or GST-Mms2 was immobilized and subsequently incubated with non-fused Mms2 or Ubc13, respectively. In order to enhance the sensitivity of the assay, co-purified proteins were visualized by Western Blot. Whereas Ubc13-F57E was unable to interact with Mms2, Ubc13-R70A retains an ability to bind Mms2 (Figure 4-17). Similarly, Mms2-F13E apparently does not bind Ubc13 in the assay, whereas Mms2-F13Y was able to co-purify with Ubc13 (Figure 4-17). The results are in agreement with the *in vivo* interaction data above (Figure 4-15).

A



B

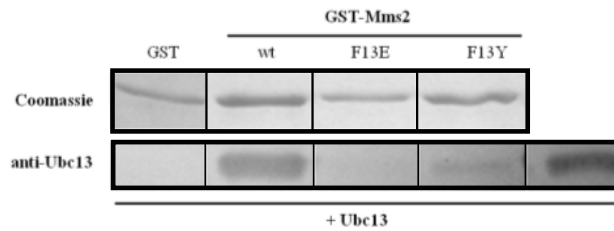


Figure 4-17. Binding of Ubc13 and Mms2 mutants *in vitro*. GST pull-downs were used to co-purify proteins that form stable interactions. (A) Purified wild-type (wt) or mutant GST-Ubc13 protein was immobilized as indicated. Non-fused Mms2 was then added and after washing, the eluted GST-Ubc13 was visualized by Coomassie Blue staining, and Mms2 was detected by Western blot with antibodies against Mms2. (B) as in (A) but with GST-Mms2 and cleaved Ubc13, and antibodies against Ubc13 were used for Western blot. The right-most lane in each figure contains purified proteins as control. Lines indicate that data taken from different parts of the same gel or blot.

4.5.6 Binding ability of interface mutants by surface plasmon resonance

Because *in vitro* pull-downs lack the quantitative capabilities for measuring binding strength, SPR was employed to more clearly show the effects of interface mutations on heterodimer formation. Immobilized anti-GST monoclonal antibodies were used to capture the GST fusion protein (ligand), and the non-fused soluble binding partner (analyte) was subsequently applied to generate the real-time binding curves.

Because binding constants for the human Ubc13-Mms2 pair have been previously estimated using sedimentation (Moraes et al., 2001) and isothermal titration calorimetry (McKenna et al., 2003b) analyses, I first sought to validate the SPR approach by determining the K_d for the wild-type Ubc13-Mms2 heterodimer. Using GST-Ubc13 fusions as the ligand, a series of curves over varied concentrations of native Mms2 as the analyte was generated (for example see Figure 2-2). These curves were used in BiaEvaluations curve-fitting software to determine the dissociation constant (K_d) for the interaction. The same data were also used to make double-reciprocal plots and dissociation constants were manually calculated (see Materials and Methods). The manually calculated K_d for GST-Ubc13 and Mms2 was found to be 1.07×10^{-7} M, which is in good agreement with the software-determined value of 1.87×10^{-7} M. To account for the possible effect that the N-terminal GST fusion might have on binding strength, a reciprocal approach using GST-Mms2 as the ligand and Ubc13 as the analyte was performed. As before, the dissociation constants were very similar between the manually determined and computer-generated methods which were 5.14×10^{-8} M and 6.22×10^{-8} M, respectively. Taken together, the dissociation constant for the human Ubc13-Mms2 heterodimer in these experiments was found to be nearly down to 5×10^{-8} M, which is

equal to the lowest value determined for Ubc13-Mms2 by isothermal titration calorimetry (McKenna et al., 2003a).

Perhaps not surprisingly, the calculation of meaningful binding constants for the Ubc13 and Mms2 mutant proteins was not possible. In all cases the binding was too weak to generate reliable data at the concentrations required for testing. Therefore, each of the mutations was tested against wild-type for a means of comparison. While using a constant concentration of analyte the peak response during binding at equilibrium (RU_{eq}) was recorded (Table 1). It is notable that in order to better visualize the relative binding of mutant proteins, the concentration of analyte that was required was well above that which gave a maximum response for the wild-type protein. The relative binding curves for the mutant proteins is shown in Figure 4-18. From Figure 4-18A and Table 4-1, it is seen that the Ubc13-F57E mutation results in barely detectable binding ($RU_{eq} = 6$) in the assay. On the other hand, the maximum response of the Ubc13-R70A mutation was almost 5-fold higher ($RU_{eq} = 27$).

It became apparent throughout these studies that the Mms2-Phe13 residue is a critical component to the interface. In order to better resolve the importance of Phe13, a third mutation at this position was made, Mms2-F13A. The F13A mutation corresponds to a yeast Mms2-F8A substitution that was created by another group (VanDemark et al., 2001), who suggested that it eliminates interaction and function with yeast Ubc13. Figure 4-18B shows that each of the mutations at Mms2-Phe13 results in considerably lower binding strength. Most strikingly, the introduction of a charged group into the core of the interface via Mms2-F13E had the greatest effect on binding (Table 4-1; Figure 4-18B). The Mms2-F13E mutation resulted in peak binding that was barely detectable

($RU_{eq} = 1$) whereas the interaction utilizing the F13A mutation was appreciably less affected ($RU_{eq} = 15$). The conservative introduction of small polar hydroxyl group by the Mms2-F13Y mutation caused a lesser disruption of the Ubc13 interaction and binds approximately two-fold stronger than F13A at equilibrium. Taken together, the SPR results for both the Mms2 and Ubc13 mutants are consistent with the initial observations for *in vivo* binding in the yeast two-hybrid assay.

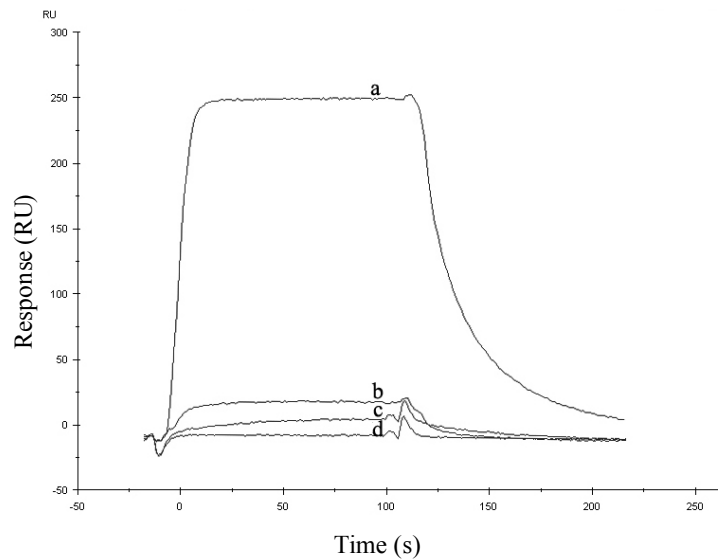
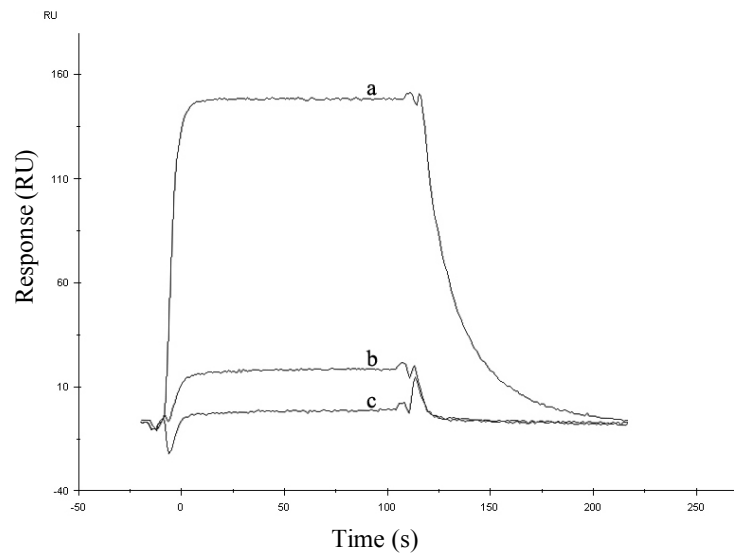


Figure 4-18. Relative *in vitro* binding of Ubc13 and Mms2 mutants measured by surface plasmon resonance. (A) Relative binding of Ubc13 mutants to GST-Mms2. a, wild-type Ubc13; b, R70A; c, F57E. (B) Relative binding of Mms2 mutants to GST-Ubc13. a, wild-type Mms2; b, F13Y; c, F13A; and d, F13E. Each experiment contains 1 μ M purified Ubc13 or Mms2 as the analyte. Note that the maximum response for the wild-type protein interactions was also achieved when using 0.5 μ M protein.

Table 4-1. SPR binding data of Ubc13-Mms2 and their mutants.

Ligand	Analyte	K_d (M)*	RU_{max}	Response (RU_{eq}) at 1 μM analyte
Ubc13	Mms2	1.87 X 10 ⁻⁷ (1.07 X 10 ⁻⁷)	262	262
Ubc13	Mms2-F13A	-	-	15
Ubc13	Mms2-F13E	-	-	1
Ubc13	Mms2-F13Y	-	-	28
Mms2	Ubc13	6.22 X 10 ⁻⁸ (5.14 X 10 ⁻⁸)	160	160
Mms2	Ubc13-F57E	-	-	6
Mms2	Ubc13-R70A	-	-	27

* Calculated from BiaEvaluations curve-fitting software. Brackets indicate manually calculated values.

4.5.7 Catalytic activity of interface mutants in ubiquitylation assays

Because Lys63-linked Ub chains synthesized by Ubc13-Mms2 are required for DNA repair function, the *in vivo* functional complementation tests in Figure 4-16 are a good indicator of Ub chain catalysis. However, it was wished to provide a more direct test of Ub chain formation by the mutant proteins. Therefore, the *in vitro* catalytic function of purified Ubc13 and Mms2 proteins was monitored in a di-Ub-formation assay. Using the purified proteins from this study, the experiment was performed by Trevor Moraes at the University of Alberta. Figure 4-19 shows that wild-type Ubc13 and Mms2 form a strong band representative of di-Ub. In contrast, each of the mutations had a severe effect on di-Ub formation. In fact, neither Mms2-F13A, -F13E, -F13Y nor Ubc13-F57E synthesized detectable Ub conjugates when paired with their wild-type partner. Only Ubc13-R70A led to observable di-Ub formation, which was much less than that observed for wild-type Ubc13. Taken together, the assay data help to show a correlation between a deficiency in *in vitro* Ub conjugation (Figure 4-19) and functional impairment *in vivo* (Figure 4-16). As previously reported (McKenna et al., 2001), human Ubc13 has self-Ub conjugation activity *in vitro* and it is noted that the interface mutations are not compromised in this regard.

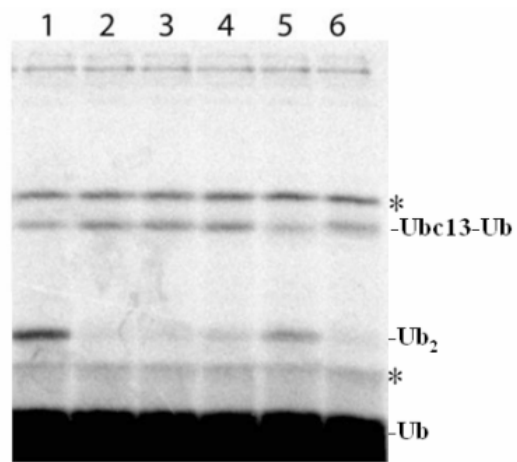


Figure 4-19. Catalytic activity of Ubc13 and Mms2 mutants *in vitro*. Ubiquitylation assays were performed by Trevor Moraes (University of Alberta) to monitor di-Ub formation by the Ubc13-Mms2 complex. The autoradiogram shows radiolabeled Ub alone or conjugated to Ub₂. The autocatalytic activity of Ubc13 is indicated and asterisks reveal artifacts of the ³⁵S-labeled Ub (McKenna et al., 2001). Ubc13 + Mms2 (Lane 1); Ubc13 + Mms2-F13A (Lane2); Ubc13 + Mms2-F13E (Lane 3); Ubc13 + Mms2-F13Y (Lane 4); Ubc13-R70A + Mms2 (Lane 5); Ubc13-F57E + Mms2 (Lane 6). The Ub₂ bands that appeared in Lanes 2, 3 and 6 are attributed to a background signal, since it was also seen in the absence of Mms2 (McKenna et al., 2001).

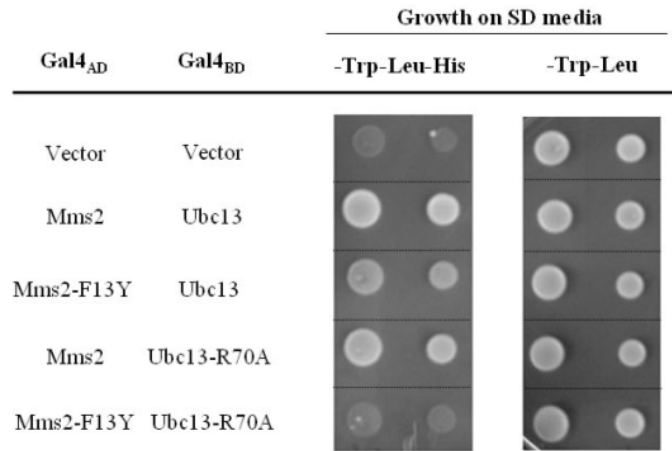
4.5.8 Interactions between Ubc13-Arg70 and Mms2-Phe13

As discussed earlier, it was originally suggested that the Ubc13-Arg70 residue has a dual purpose in mediating interactions at the interface. One is to share hydrophobic contacts with Mms2-Phe13 (Phe8 in yeast), while the other is to form polar contacts with the Mms2 backbone via its guanidinium group. To determine the validity of these proposals, the combinatorial effect of the Ubc13-R70A mutation with Mms2-F13Y was tested. Based on the crystal structures, it seemed that the Ubc13-R70A mutation would not hinder the hydrophobic contacts made with Mms2-Phe13; however, the H-bonds would be abolished. If the two mutations impinge on two different separate sites of the interface, it was felt that the combination of the two mutants would cause an additive effect on reducing Ubc13-Mms2 binding strength (and function). In support of this hypothesis, the pairing of the Ubc13-R70A and Mms2-F13Y mutations in the yeast two-hybrid assay did not result in a detectable interaction (Figure 4-20A). The additive effect was also observed in a functional complementation experiment. An *mms2 ubc13* double-deletion strain co-transformed with *UBC13-R70A* and *MMS2-F13Y* was severely sensitive to MMS treatment as compared with cells carrying only the single *UBC13-R70A* or *MMS2-F13Y* mutations (Figure 4-20B).

These results suggested that Ubc13-Arg70 was responsible for a second important interface contact point that is independent of the hydrophobic pocket. In order to better address this possibility, a Ubc13-R70L mutant was created that would also abrogate H-bonding. However, based on its size and shape, the R70L substitution would be a better candidate for retaining hydrophobic contacts with Mms2-Phe13 as compared to R70A. As is seen in Figure 4-20C, the combination of the Ubc13-R70A and Mms2-F13Y

mutations once again completely abolished the Ubc13-Mms2 interaction. In contrast, the Ubc13-R70L mutation did not demonstrate the same decrease in binding when coupled with Mms2-F13Y. In fact, the Ubc13-R70L mutation may have partially alleviated the effect of Mms2-F13Y. It is also noted that the Ubc13-R70L mutation was not sensitive to MMS treatment like Ubc13-R70A in functional complementation experiments (data not shown). Taken together, these results underscore the importance of Ubc13-Arg70 in helping to create a deep Ubc13 hydrophobic pocket for Mms2-Phe13.

A



B

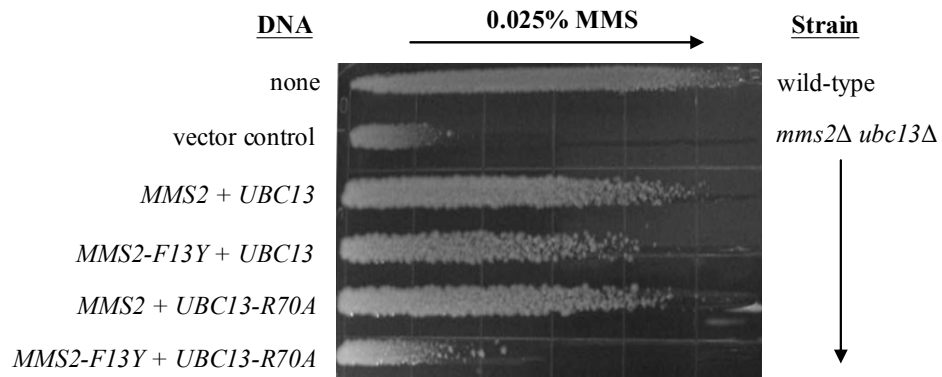


Figure 4-20. Physical and functional relationships between Ubc13-Arg70 and Mms2-Phe13. The Mms2-F13Y and Ubc13-R70A or Ubc13-R70L mutations were co-transformed into yeast cells and the double mutant was compared to wild type and single mutants. (A),(C) Yeast two-hybrid assay to assess the strength of interaction between Ubc13-R70A and Mms2-F13Y, and Ubc13-R70L and Mms2-F13Y, respectively. Association of the Gal4 fusion proteins turns on the *GAL1* promoter which transcribes the *HIS3* reporter gene. Positive interactions are observed by growth on media without His plus 1 mM 3-AT after incubation at 30°C for 60 hours in (A) and for 48 hours in (C). Plasmids were maintained in the cell by growth on media without Trp and Leu. At least four colonies from each combination were tested and two representative colonies are shown. (B) Gradient plate assay to evaluate the heterologous complementation of yeast *mms2 ubc13* double deletion strains. Cells were printed on YPD plates containing 0.025% MMS and cells with a greater ability to survive DNA damaging treatment grew further along the gradient. Incubation was carried out for 60 hours at 30°C. All cells grew equally well on YPD plates without MMS (data not shown). Test plasmids were pGBT-hUBC13 (and mutant derivatives) and pGAD-hMMS2 (and mutant derivatives).

C

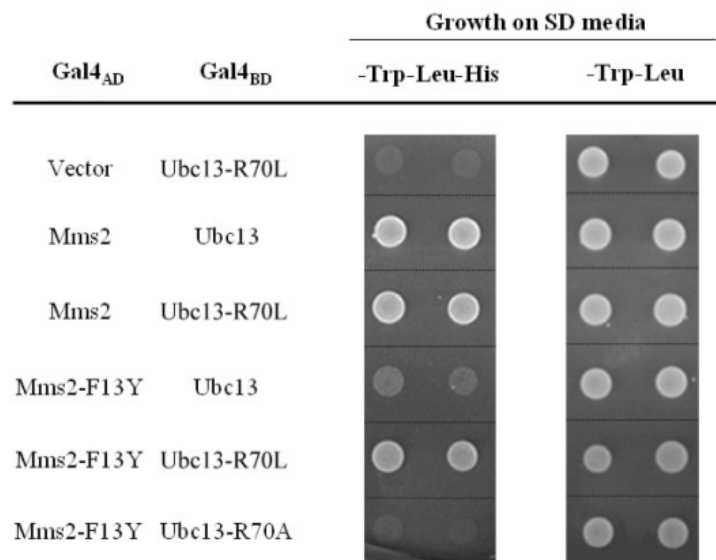


Figure 4-20. Physical and functional relationships between Ubc13-Arg70 and Mms2-Phe13. The Mms2-F13Y and Ubc13-R70A or Ubc13-R70L mutations were co-transformed into yeast cells and the double mutant was compared to wild type and single mutants. (A),(C) Yeast two-hybrid assay to assess the strength of interaction between Ubc13-R70A and Mms2-F13Y, and Ubc13-R70L and Mms2-F13Y, respectively. Association of the Gal4 fusion proteins turns on the *GAL1* promoter which transcribes the *HIS3* reporter gene. Positive interactions are observed by growth on media without His plus 1 mM 3-AT after incubation at 30°C for 60 hours in (A) and for 48 hours in (C). Test plasmids were pGBT-hUBC13 (and mutant derivatives) and pGAD-hMMS2 (and mutant derivatives).

4.5.9 Discussion of the Ubc13-Mms2 interface

The Ubc13-Mms2/Uev1 complex is the only E2 to be clearly shown to create atypical poly-Ub chains linked through Lys63 *in vivo*. The uniqueness of Ubc13 and Mms2 in Ub chain synthesis led to numerous detailed biochemical studies (McKenna et al., 2003a; McKenna et al., 2003b; McKenna et al., 2001) and the proposal of a model for the generation of Lys63-linked Ub chains. Although the mechanistic model has been widely accepted, it is contingent on a specific Ubc13-Mms2/Uev1 complex that had not been sufficiently experimentally addressed. The studies above were the first to systematically mutate Ubc13 and Mms2 in order to specifically address the specifics of Ubc13-Mms2 heterodimer formation and function. In this detailed analysis, several *in vivo* and *in vitro* methods were employed, including the yeast two-hybrid assay, GST pull-downs, and SPR in order to assess Ubc13-Mms2 binding strength. In addition, an *in vitro* ubiquitylation assay and a heterologous complementation approach were utilized to correlate binding ability with biochemical and biological activities. Overall, an excellent correlation between these experimental results was achieved.

The Ubc13-Mms2 interface is long and narrow, and buries a large solvent-accessible surface area of ~1500 Å². The studies above began with the systematic mutagenesis of a number of residues along the Loop 1, α1 helix, and the N-terminus of Mms2, all of which contain portions which visibly contact Ubc13 in the human (Figure 4-17, 4-18; Moraes et al., 2001) and yeast (VanDemark et al., 2001) crystal structures. The findings led to the identification of a rather unexpected pocket of interactions close to the α1 helix of Mms2 that appear to be critical for both complex formation and specificity. The pocket consists of Ubc13-Phe57, -Glu55, and -Arg70, which all reside in

close proximity to the N-terminal end of the Mms2 α 1 helix that is now believed to be the core of the Ubc13-Mms2 interface. Accordingly, the Ubc13-F57E and -E55Q mutations had extreme effects on disrupting the Ubc13-Mms2 interaction. Because it putatively contributes hydrophobic contacts to the α 1 helix of Mms2 (via Mms2-Phe13) and an H-bond with the Loop 1 backbone (via Mms2-Met41), Ubc13-Arg70 was originally believed to be a bridge between two separate Mms2 contact points. Through the testing of two Ubc13-Arg70 mutations (R70A and R70L), it was resolved that Ubc13-Arg70 makes its most significant contribution as a component of the hydrophobic pocket for Mms2-Phe13.

Focusing on the Mms2 complement of the core interface region, the Mms2-N12D and -N12A mutations were designed to disrupt H-bonding with Ubc13-Glu55. However, unlike Ubc13-E55Q, the Mms2-Asn12 mutations did not disrupt *in vivo* binding and function; arguing against a pair-wise relationship between Mms2-Asn12 and Ubc13-Glu55. On the other hand, the mutation of Mms2-Phe13 had profound effects on binding and function. Based on the Ubc13-Mms2 crystal structures, Mms2-Phe13 is seen to insert itself deep within a hydrophobic pocket formed by the Ubc13 backbone and several side-chain carbons (such as Ubc13-Glu55, -Phe57, -Arg70) in a manner that is similar to a key in a keyhole. To fully explore the significance of this critical interaction, three mutations at the Mms2-Phe13 residue were created in order to exploit the possibility that the hydrophobic pocket is critical to the Ubc13-Mms2 heterodimer interface. With Mms2-F13E, the aggressive introduction of a charged polar group in the region caused a complete loss in detectable binding in each of the *in vivo* and *in vitro* assays. Underscoring the importance of the deep hydrophobic contacts required for the Mms2

insertion of Phe13 into the Ubc13 pocket, the introduction of a small hydroxyl group (Mms2-F13Y) was sufficient to severely disrupt the Ubc13-Mms2 interface. In accordance, Ubc13-Mms2 heterodimer formation is impaired by an Mms2-F13A mutation that maintains hydrophobicity but cannot breach the Ubc13 surface in order to create the necessary hydrophobic contacts. These dramatic findings demonstrate that the key-like insertion of Phe13 into a Ubc13 hydrophobic pocket is a crucial determinant for the strong interaction strength of the Ubc13-Mms2 heterodimer (Figure 4-21).

Taken together, these studies have revealed several important Ubc13 interface residues; however, Mms2-Phe13 appears to be the only interface residue identified with a significant role in binding to Ubc13. A model based on visual inspection of the crystal structures and data found in this section suggests that Mms2-Phe13 is inserted between Ubc13-Glu55, -Phe57, and is flanked closely by -Arg70, which together form a critical hydrophobic interface pocket. This model is in agreement with the observations that the Ubc13-Mms2 heterodimer is stable in salt concentrations as high as 2.5 M (data not shown). It is thus possible that polar contacts, such as those observed in the crystal structures via the Ubc13-Arg70 and Ubc13-Glu55 residues do not significantly contribute to binding strength, and might instead play more subtle roles such as aiding Mms2-Ubc13 recognition.

Owing to their functional interchangeability, the human (Moraes et al., 2001) and yeast (VanDemark et al., 2001) crystal structures of the Ubc13-Mms2 heterodimers are very similar (Ashley et al., 2002; Xiao et al., 1998). In particular, the corresponding interface residues that were mutated in the human proteins are conserved and oriented identically in yeast. A slight exception is that the human Ubc13-Phe57 corresponds to

yeast Ubc13-Tyr57; however, the hydroxyl group of Tyr57 is pointed away from the critical hydrophobic pocket. Furthermore, a Ubc13-F57Y mutation behaved identically to wild-type Ubc13 in yeast-two hybrid and functional complementation assays (data not shown). The above information allows the use of sequence alignments to determine the residues in other yeast Ubc structures that correspond to human Ubc13-Glu55, -Phe57, and -Arg70 (Figure 4-22A). The positions of these corresponding residues for each of Ubc2/Rad6 (Worthylake et al., 1998), Ubc4 (Cook et al., 1993), and Ubc7 (Cook et al., 1997) are physically oriented such that the necessary hydrophobic pocket for Mms2-Phe13 is not permitted (Figure 4-22C, D, E). While it appears that Ubc1 could possibly allow an Mms2-Phe13 insertion from a spatial standpoint, the stoutness of its Asp and Gln residues corresponding to the Ubc13-Glu55 and -Arg70 positions, respectively, would not likely allow sufficient hydrophobic contacts from their side-chains. More significantly, Ubc1 contains a Glu residue that would correspond to the Ubc13-F57E substitution which caused a complete disruption in Ubc13-Mms2 binding and function. It would be of great interest in future studies to see whether these critical Ubc13 residues are not only required but also sufficient to interact with Mms2.

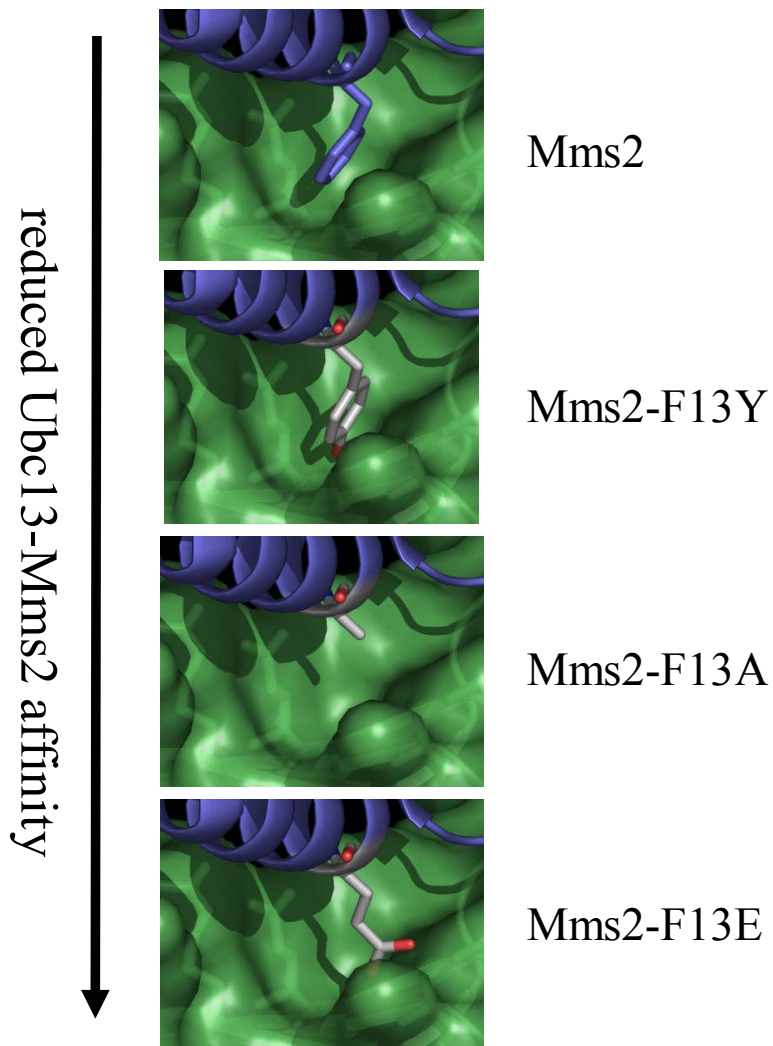


Figure 4-21. The Mms2-Phe insertion into a Ubc13 hydrophobic pocket is important for Ubc13-Mms2 affinity. Shown is a portion of the human Ubc13 (green)-Mms2 (blue) interface as resolved in the crystal structure (Morales et al., 2001). In the top-most panel, Mms2 is seen to insert a Phe (hMms2-Phe13) residue into a Ubc13 pocket and the consequences of the mutations created in this study at Mms2-Phe13 are depicted. The hypothetical orientation of each Phe13 mutation was computationally calculated using PyMOL version 0.96 by DeLano Scientific (<http://pymol.sourceforge.net/>) and the relative effect on binding to Ubc13 as determined in these studies is indicated by the arrow. This analysis is consistent with a model suggesting that the key-like insertion of Mms2-Phe into a Ubc13 pocket is mediated by hydrophobic interactions.

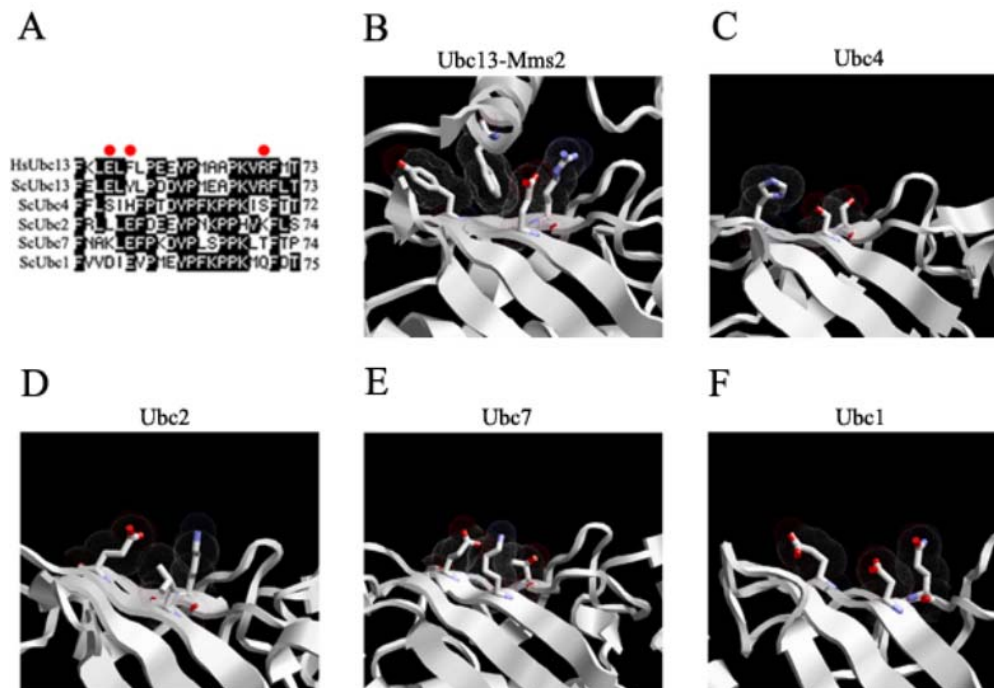


Figure 4-22. A hydrophobic pocket is conserved in Ubc13 but not other Ubcs. (A) Amino acid sequence alignment of human Ubc13 with the yeast E2s Ubc13, Ubc1, Ubc2/Rad6, Ubc4, and Ubc7. A red dot indicates the residues indicated in (B)-(F). (B)-(F) Crystal structure comparison of various Ubcs highlighting residues corresponding to hUbc13-Glu55, -Phe57 and -Arg70. (B) Interface of the yeast Ubc13-Mms2 crystal structure. (C)-(F) Other yeast Ubcs are presented in the same orientation as Ubc13 in (B). Visible residues are shown with Van der Waals forces and correspond to those found in this study to reside at critical positions in the human Ubc13-Mms2 complex. Images were generated using RasTop 2.0.3 by Philippe Valadon (<http://www.geneinfinity.org/rastop/>).

CHAPTER FIVE

A PHYSICAL RELATIONSHIP BETWEEN MMS2 AND RSP5

5.1 Rationale

As brought forth in the introduction, two of the most critical questions concerning Ubc13-Mms2 are the mechanism of Lys63-linked Ub conjugation and in what cellular roles these Lys63-Ub chains function. The largest body of work in this thesis was dedicated to the former, and the studies helped to identify several important structure-function relationships for Ubc13-Mms2. Regarding the latter, considerable effort was also spent to determine a novel involvement of Ubc13-Mms2 with other proteins. It was presumed that the identification of proteins interacting with Ubc13, Mms2, or both, would potentially reveal unidentified E3s or Lys63-linked polyubiquitylation targets. While the identification of DDT proteins was expected, the incidence of Lys63-conjugated Ub chains in other cellular roles suggested that novel physical affiliations between Ubc13-Mms2 and other proteins would also be encountered.

In order to screen for proteins that interact with human Ubc13 or Mms2, large amounts of GST-fused and native protein were purified. The GST fusion protein was used in GST pull-down assays in order to co-purify interacting proteins from human cell culture extracts. Using the native purified protein, I successfully generated specific polyclonal antibodies against human Ubc13 and Mms2. The antibody was then used in co-immunoprecipitation experiments that were done in parallel with the GST pull-downs.

Several possible co-purifying proteins were visible in silver-stained protein gels after much optimization and refinement. The protein bands in question were sent for analysis by mass spectroscopy but for various reasons, the unknowns were never identified with confidence. In case of some possible future importance I will report here that one of the putative interacting proteins has the National Center for Biotechnology Information accession number, AAC19150. AAC19150 is an uncharacterized human protein that is seen to contain a phosphotyrosine-binding domain when using the conserved domain architecture research tool (Geer et al., 2002). Around this same time, a large-scale screen to identify protein complexes in *S. cerevisiae* was published (Gavin et al., 2002). Among hundreds of other protein complexes, a novel physical interaction between Mms2 and Rsp5 was identified.

RSP5 is a multi-functional, essential gene in *S. cerevisiae* that encodes a protein shown to take part in very diverse cellular processes such as chromatin remodeling (Harkness et al., 2002), mitochondrial inheritance (Fisk and Yaffe, 1999), cytoskeleton dynamics (Kaminska et al., 2002), regulation of RNA transport (Gwizdek et al., 2005; Neumann et al., 2003), and membrane permease endocytosis (Horak, 2003; Rotin et al., 2000). The inviability of *rsp5* mutants is attributed to the transcriptional activation of the *OLE1* gene required for fatty-acid metabolism (Hoppe et al., 2000).

Adding merit to a physical relationship between Rsp5 and Mms2 is that Rsp5 is a *bona fide* E3 enzyme. Rsp5 contains an approximately 350 amino acid HECT domain that is situated at its C-terminus and is both necessary and sufficient for Ub thioester formation (Schwarz et al., 1998; Wang et al., 1999). Rsp5 is able to associate with various E2s such as Ubc1, Ubc4, Ubc5, and Ubc7 (Arnason et al., 2005; Dunn and Hicke,

2001b; Rotin et al., 2000) in order to carry out the ubiquitylation of various cellular targets. An association with Ubc13, however, has not been reported. Ubiquitylation via Rsp5 has been found to occur on the large subunit of RNA polymerase (Huibregtse et al., 1997), various plasma membrane proteins (Rotin et al., 2000), mitochondria (Fisk and Yaffe, 1999), and transcription factors (Hoppe et al., 2000). The list has been further expanded by a recent proteomic approach that identified many additional possible ubiquitylation targets of Rsp5 (Kus et al., 2005). An interesting feature of the ubiquitylation by Rsp5 is that its targets may be linked by mono- or poly-Ub. Furthermore, in at least a few cases, the poly-Ub chains generated via Rsp5 are not linked through Lys48. Given the ability of Rsp5 to associate with different E2s (and potentially with Ubc13-Mms2), it is suggested that the nature of the Ub linkage is attributed to a specific Rsp5-E2 interaction.

In addition to the HECT domain, Rsp5 contains two other characterized protein domain types (shown schematically in Figure 5-4B). A phosphoinositide-interacting C2 domain (Dunn et al., 2004) is situated at the N-terminus. The C2 domain is required to properly localize Rsp5 to cytosolic membranes *in vivo* and apparently facilitates the role of Rsp5 in endosomal sorting (Dunn et al., 2004; Morvan et al., 2004), but is dispensable for most other Rsp5 functions (Dunn and Hicke, 2001a; Wang et al., 1999). Three WW domains are centrally located within the Rsp5 protein sequence. WW domains are small (~40 amino acid) tryptophan-rich modules that mediate protein-protein interactions, with affinity for Pro-rich sequences such as the PY motif (Einbond and Sudol, 1996; Wang et al., 1999). They are implicated in binding to the target of ubiquitylation. The availability of three WW domains in Rsp5 permits a high degree of protein interaction variability,

since different combinations of the WW domains seem to be required for functioning in specific cellular pathways (Dunn and Hicke, 2001a; Gajewska et al., 2001). This is likely an important feature for enabling Rsp5 to take part in so many different cellular pathways. The arrangement of the C2, WW, and HECT domains of Rsp5 is representative of a large family of eukaryotic proteins with a common modular domain architecture (Ingham et al., 2004). The prevalence of these homologs throughout eukaryotes suggests that at least some of the functions of Rsp5 are conserved in nature. Indeed, like Rsp5, the mammalian homolog Nedd4 is involved in membrane permease turnover (Rotin et al., 2000; Staub et al., 2000). Furthermore, human *NEDD4* is able to complement some of the *rsp5* mutant phenotypes in *S. cerevisiae*, although it cannot restore the viability of *rsp5* Δ (Gajewska et al., 2003).

5.2 Results

5.2.1 Stable physical interactions are observed for Mms2 and Rsp5

The Mms2-Rsp5 physical interaction was identified in a proteomics-based screen for protein complexes in *S. cerevisiae* (Gavin et al., 2002). Such large-scale high-throughput studies are usually performed without sufficient attention to individual data points, and are therefore prone to false positives and false negatives. Furthermore, the proteomic study by Gavin *et al.* failed to follow-up on Mms2 and Rsp5 specifically. I thus sought to independently confirm the reported Mms2-Rsp5 physical interaction.

In the first approach, an anti-Myc antibody was used to precipitate Myc-Rsp5 protein from total yeast cell extracts. Western blots were then performed using anti-Mms2 polyclonal antibody to detect whether Mms2 had been co-immunoprecipitated.

However, the Co-IP of Myc-Rsp5 and Mms2 was not observed in these assays (data not shown). In order to enhance the possible Myc-Rsp5-Mms2 interaction, I performed subsequent Co-IP experiments by spiking the yeast cell extracts with purified Mms2 protein. In these assays, a physical interaction between Rsp5 and Mms2 was implicated because the detection of Mms2 in the Co-IP was dependent on cell extracts containing the Myc-Rsp5 protein (Figure 5-1A).

In another approach, the binding assays were not supplemented with purified protein. Yeast cells co-transformed with plasmids expressing Myc-Rsp5 and GST-Mms2 were used to make total cell extracts for use in GST pull-down experiments. After affinity purification of the GST-Mms2 fusion, an anti-Myc antibody was then used to determine whether Myc-Rsp5 had been co-purified. As seen in the lower panel of Figure 5-1B, Myc-Rsp5 was detected in the GST-Mms2 pull-down sample. On the other hand, Myc-Rsp5 was not detected in the same experiment using GST-Ubc13 in place of GST-Mms2 (Figure 5-1B, lower panel), despite the fact that a slightly greater amount of GST-Ubc13 was pulled from the extracts as compared with GST-Mms2 (Figure 5-1B, upper panel). The GST pull-down experiments were performed in *mms2* Δ and *ubc13* Δ yeast strains in order to eliminate competitive interference from endogenous Mms2 and Ubc13, respectively.

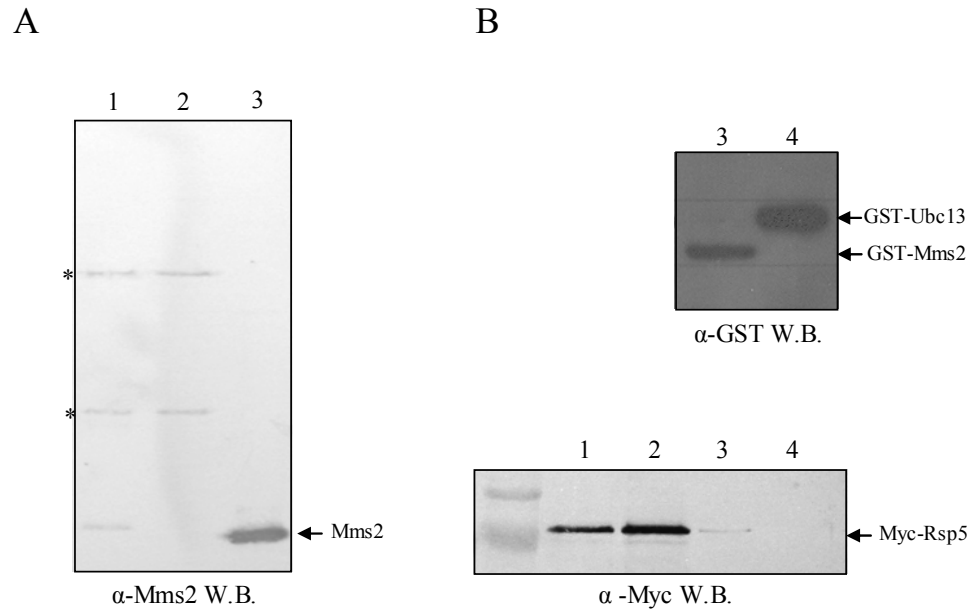


Figure 5-1. An Mms2-Rsp5 physical interaction is detected *in vitro*. Two separate methods were used to demonstrate a stable protein interaction between Mms2 and Rsp5. (A) Co-IP of Myc-Rsp5 and yeast Mms2. Anti-Myc antibody was immobilized onto Protein A Sepharose and cell lysates with (Lane1) or without (Lane2) Myc-Rsp5 were added for a 4 hour incubation at 4°C. 30 µg of purified yeast Mms2 protein was added in the last half of the incubation before the washing steps. Samples were analyzed via SDS-PAGE and the physical interaction is indicated by the presence of Mms2 in the Western Blot (W.B.) against Mms2. Lane 3, Mms2 protein alone. Asterisks indicate background bands from the antibody used in the Co-IP. (B) GST pull-down assay. Crude extracts containing Myc-Rsp5 and GST-Mms2 or GST-Ubc13 were incubated with Glutathione Sepharose 4B to immobilize GST. After the washing steps, samples were analyzed via SDS-PAGE and the physical interaction is indicated by the presence of Myc-Rsp5 in the Western Blot against Myc. Lanes 3 and 4, GST pull-down assays using GST-Mms2 and GST-Ubc13 respectively. Upper panel, Western Blot against GST. Lower panel, Western Blot against Myc. Lanes 1 and 2, samples of the extracts used in the GST-Mms2 and GST-Ubc13 pull-downs, respectively, to ensure the presence of Myc-Rsp5. The Myc-Rsp5 band was not seen in extracts that did not express Myc-Rsp5 (not depicted).

5.2.2 A physical interaction is observed for Mms2 and Rsp5 in the yeast two-hybrid assay

The *in vitro* binding studies above seemed to confirm the physical interaction between Mms2 and Rsp5, but it was felt that the interaction strength was probably weak because Western blots were required to detect the proteins of interest in each experiment. Weak or transient interactions involving E3 proteins are not surprising. For example, physical interactions between Ubc13-Rad5 and Ubc13-TRAF6 could only be detected in the yeast two-hybrid assay (Figure 4-6 and 4-7, respectively). Therefore, the yeast two-hybrid assay was used as a completely different and possibly more sensitive approach to detect the physical association between Mms2 and Rsp5.

RSP5 was cloned into two-hybrid vectors to create Gal4_{AD}- and Gal4_{BD}-Rsp5 fusion proteins. As seen in Figure 5-2, the Gal4_{BD}-Rsp5 and Gal4_{AD}-Mms2 pairing generated a clear protein interaction signal, whereas the Gal4_{BD}-Rsp5 negative control produced no positive signal whatsoever. It is noted that the Gal4_{AD}-Rsp5 hybrid protein itself generated a surprising false-positive result. It is perhaps possible that Rsp5 contains an unidentified cryptic DNA binding domain that is not normally realized due to Rsp5's exclusion from the nucleus. Further studies are needed to determine if this is truly the case. Nonetheless, the yeast two-hybrid results validated the Mms2-Rsp5 physical interaction as detected in the *in vitro* binding experiments.

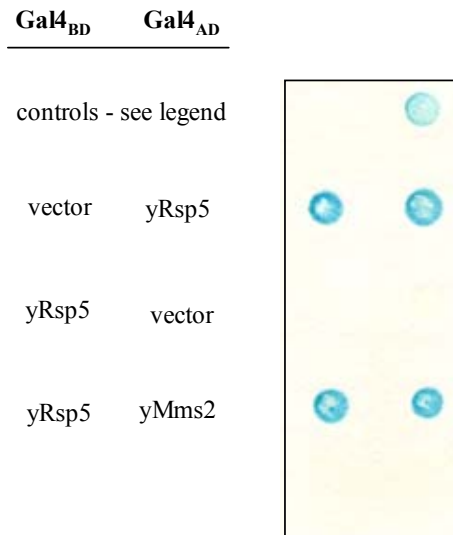


Figure 5-2. An Mms2-Rsp5 physical interaction is detected in the yeast two-hybrid assay. Yeast two-hybrid analysis of the Mms2-Rsp5 protein interaction using the β -galactosidase filter-lift detection method. Physical interaction of the Gal4 hybrid proteins leads to the expression of the β -galactosidase gene which causes blue colour development in the assay. Co-transformed plasmids were maintained with Trp and Leu markers and are indicated on the left. The picture was taken after 4 hours of colour development at 30°C. Two representative transformants from each combination is shown. Controls were cells co-transformed with Gal4_{AD} -yMMS2 + Gal4_{BD} (on left) and Gal4_{BD} -yMMS2 + Gal4_{AD} -yUBC13 (on right). Test plasmids were pGAD-yRSP5, pGBT-Rsp5, and pGAD-yMMS2.

5.2.3 A physical interaction between Ubc13 and Rsp5 is not observed

The GST pull-down results in Figure 5-2B suggested that Rsp5 does not physically interact with Ubc13 *in vitro*. However, given that the yeast two-hybrid approach was more successful in detecting the Mms2-Rsp5 interaction than the GST pull-downs, the testing of a possible Ubc13-Rsp5 physical interaction in the yeast two-hybrid assay was performed.

As seen in Figure 5-3, Ubc13 does not appear to physically interact with Rsp5 in the yeast two-hybrid assay. Despite using the same conditions and the equivalent constructs as for Rsp5-Mms2 in the filter-lift detection method, the Gal4_{BD}-Rsp5 and Gal4_{AD}-Ubc13 pairing did not generate a positive interaction signal. In an effort to provide a greater level of assay sensitivity, a second yeast two-hybrid assay making use of a *HIS3* reporter gene required for growth of a His auxotroph strain was tried. In personal observations, the yeast two-hybrid growth assay method is seen to be more sensitive than measuring colour development in the filter-lift assay. However, even using the most sensitive assay conditions possible with the *HIS3* reporter, a physical interaction between Rsp5 and Ubc13 was not detected (Figure 5-3).

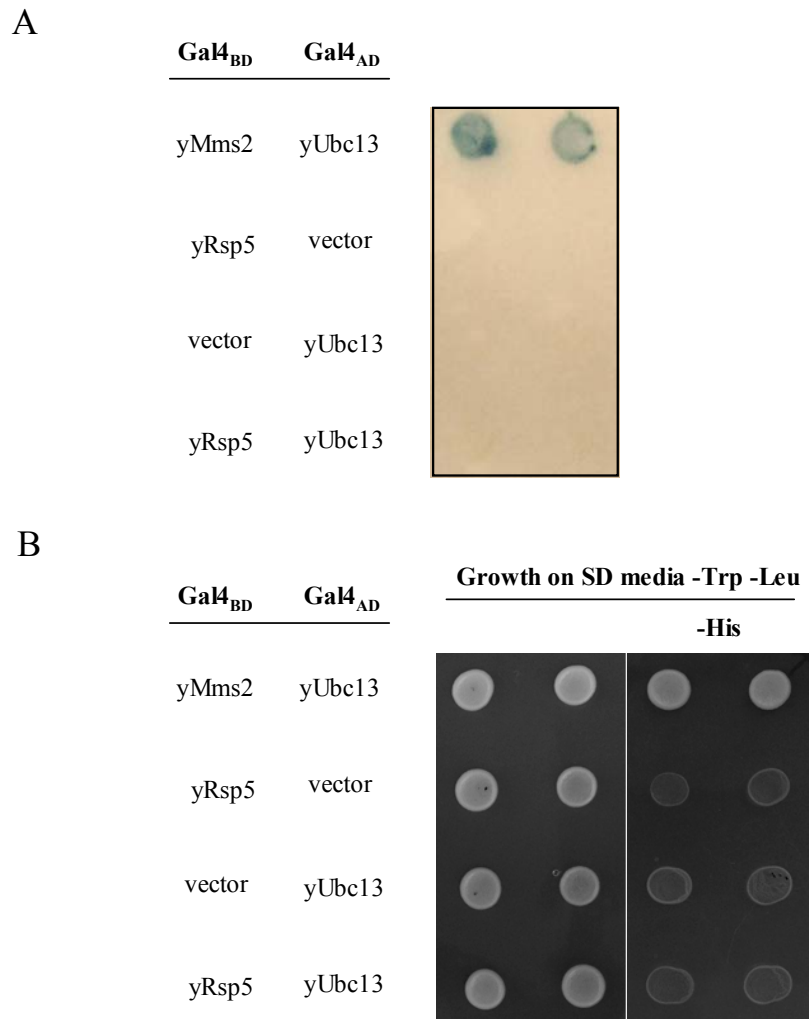


Figure 5-3. A Ubc13-Rsp5 physical interaction is not observed. Yeast two-hybrid analysis of Ubc13 and Rsp5. Co-transformed plasmids were maintained with Trp and Leu markers and are indicated on the left. (A) β -galactosidase filter-lift assay method. Physical interaction of the Gal4 hybrid proteins leads to the expression of the β -galactosidase gene which causes blue colour development in the assay. The picture was taken after 12 hours of colour development at 30°C. (B) Growth assay method. Physical interaction of the hybrid proteins causes the expression of the *HIS3* reporter which leads to growth on minimal medium lacking His. The plates were incubated for 72 hours before taking the photograph. Two representative transformants from each combination is shown. Test plasmids were pGBT-Rsp5, and pGBT-yMMS2, pGAD-yUBC13.

5.2.4 Deletion mapping of the Mms2-Rsp5 physical interaction

After demonstrating that Mms2 and Rsp5 do indeed physically interact, it became desirable to determine which protein regions or domains are required. Based on the high degree of similarity between Mms2 and E2s, it was expected that the HECT domain of Rsp5 would mediate its interaction with Mms2. E2-E3 interactions have been shown to typically occur via the HECT domain (Huang et al., 1999).

The yeast two-hybrid assay was used to map the Rsp5-Mms2 interaction because it had produced a strong positive signal with the full-length proteins. To provide the greatest insight into the interaction, deletions were created in Rsp5 because of its large size and multiple domains. Mms2 on the other hand has only a small single protein domain. The first series of Rsp5 deletions were generated as N-terminal truncations. They were designed to systematically remove the C2 and each of the three WW domains, leaving the shortest derivative to contain the HECT domain alone. As seen in Figure 5-4, the derivatives containing the HECT domain alone or the HECT domain plus the WW3 domain did not interact with Mms2 in the yeast two-hybrid assay. However, deletion of the C2 or the C2 and WW1 domains did not disrupt the Rsp5-Mms2 interaction. To ensure that the HECT domain was not required for the interaction with Mms2, another series of deletions was generated from the other end of Rsp5. The generation of C-terminal truncations would also help to address false negatives that may have arisen due to protein misfolding. As seen in Figure 5-4B, these C-terminal truncations were designed to remove the HECT domain itself, the HECT domain plus the WW1 and WW2 domains, or the HECT domain plus all of the WW domains. Of these Rsp5 C-terminal deletions, only the derivative that retained the WW2 and WW3 domains

was able to physically associate with Mms2. Taken together, the N-terminal and C-terminal truncations were in agreement with one another. The deletion mapping suggested that the C2, WW1, and HECT domains are not required for the Rsp5-Mms2 physical interaction. Put another way, it was deduced that the WW2 and WW3 domains were the important determinants for the interaction. To test whether the WW2 domain itself was sufficient for the interaction, a construct containing only the Rsp5 WW2 domain was generated. As seen in Figure 5-4, the Rsp5 WW2 domain alone did not interact with Mms2 in the yeast two-hybrid assay. However, a derivative containing only the WW2 and WW3 domains was able to restore the Mms2 interaction with Rsp5 (Figure 5-4).

A

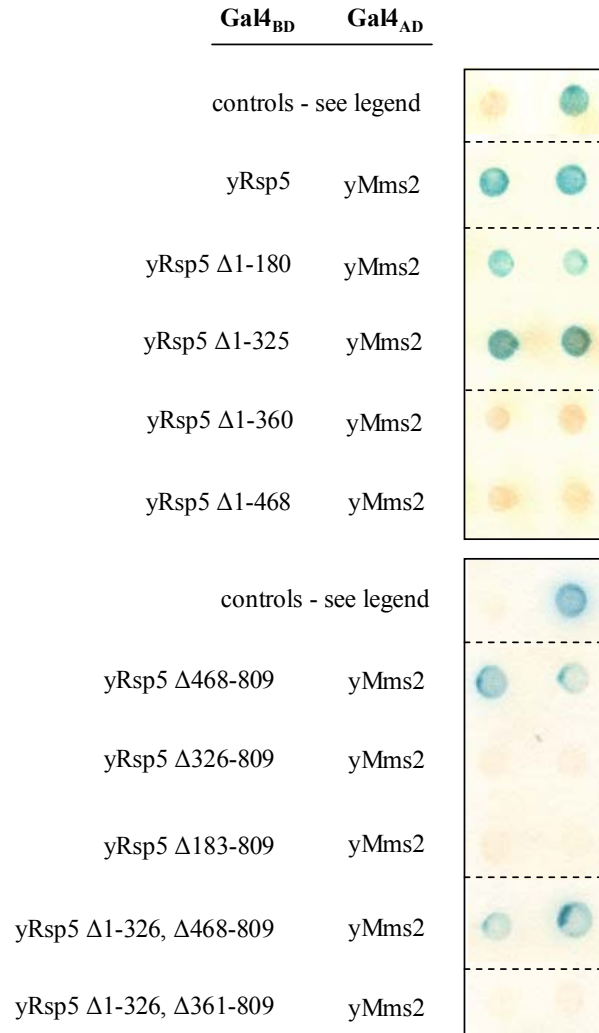


Figure 5-4. Mapping the Mms2-Rsp5 physical interaction. The yeast two-hybrid assay was used to test the ability of several Rsp5 deletions to physically interact with Mms2. (A) Data from the yeast two-hybrid assay filter-lift detection method. Physical interaction of the Gal4 hybrid proteins leads to the expression of the β -galactosidase gene which causes blue colour development in the assay. Co-transformed plasmids were maintained with Trp and Leu markers and are indicated on the left. The picture was taken after 4 hours of colour development at 30°C. Two representative transformants from each combination is shown. Controls were cells co-transformed with Gal4_{AD} + Gal4_{BD}-RSP5 (on left) and Gal4_{BD}-yMMS2 + Gal4_{AD}-yUBC13 (on right). Dotted line indicates data taken from a different region of the same assay filter. Test plasmids were pGBT-Rsp5 (and derivatives) and pGAD-yMMS2.

B

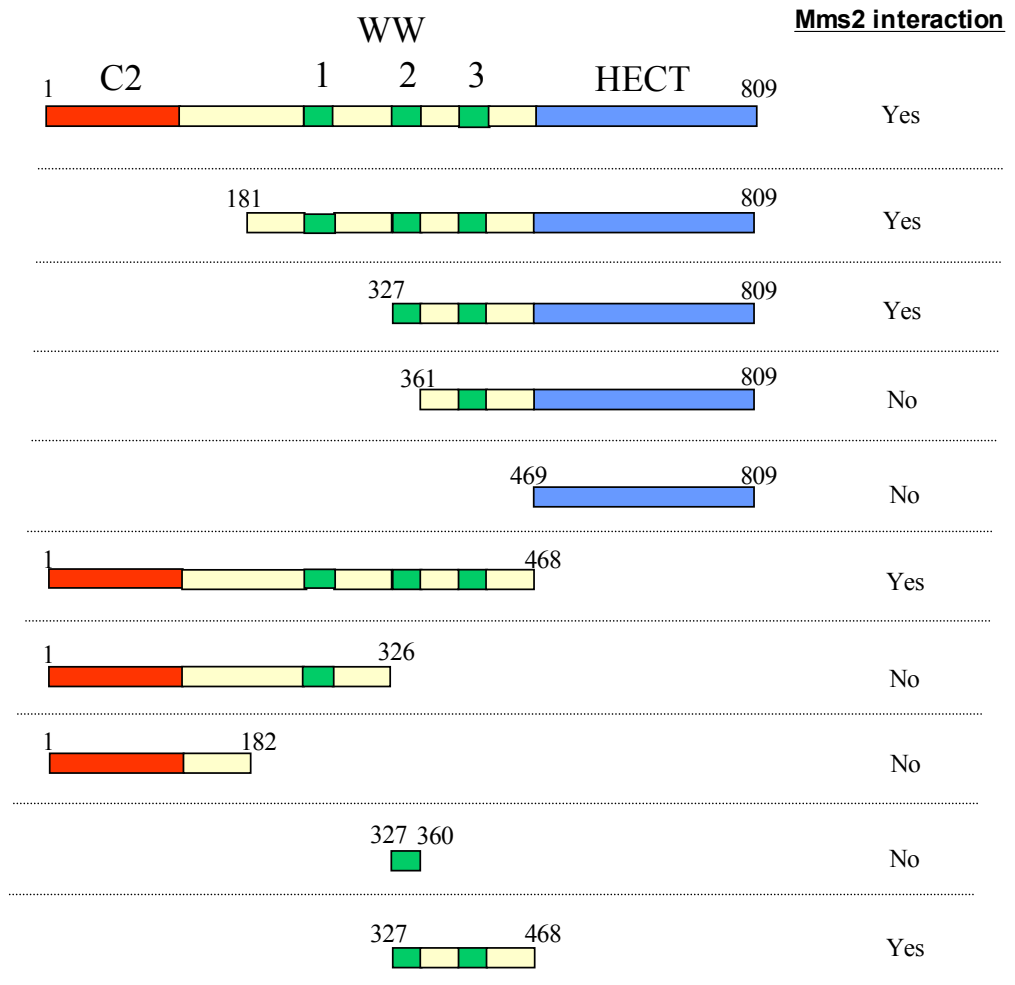


Figure 5-4. Mapping the Mms2-Rsp5 physical interaction. (B) A schematic of the various Rsp5 derivatives used in the yeast two-hybrid assay as performed in (A) is shown. The characterized protein domains are coloured for clarity: C2 (red); WW (green); HECT (blue). The ability of each derivative to physically interact with full-length Mms2 is indicated on the right.

5.2.5 Rsp5 does not likely function in error-free DDT

The considerable physical interaction data in this chapter made it apparent that Mms2 and Rsp5 are likely to function together in the cell. The notion that Rsp5 can function in error-free DDT seemed plausible given that it is an E3 involved in Ub-Lys63-mediated polyubiquitylation. Furthermore, a phenotypic connection between *RSP5* and error-free DDT was provided in an early *S. cerevisiae* screen that identified yeast strains with elevated spontaneous mutation rates (Gottlieb and von Borstel, 1976; Hastings et al., 1976). These so-called mutator strains have elevated mutagenesis rates because DNA lesions in these cases are channeled into mutagenic repair pathways (Hastings et al., 1976). One of the mutator strains in the screen contained an allele designated *mut2*, which was later mapped to the *RSP5* locus (M. Vandenbol, Gembloux Agricultural University, Belgium, personal communication). The mutator phenotype of *mut2* was thus reminiscent of the phenotype caused by the *mms2* mutation. Mutants of the error-free DDT genes are mutators because DNA lesions are channeled into the mutagenic translesion DNA synthesis pathway (Broomfield et al., 1998; Broomfield et al., 2001; Xiao et al., 1999). Adding yet another similarity between *mut2* and *mms2* was the observation that *mut2* is also sensitive to the DNA damaging agent MMS (Hastings et al., 1976 and personal observations).

A hypothesis to account for the possible role of Rsp5 in error-free DDT was made. Based on the phenotypic similarity of *mut2* and *mms2*, the physical interaction between Mms2 and Rsp5, and the reported exclusion of Rsp5 from the nucleus, it was felt that Rsp5 could regulate the function of Mms2 by sequestering it outside of the nucleus. Upon DNA damage, Mms2 would then dissociate from Rsp5 in order to enter

the nucleus and perform its function in error-free DDT. Indeed, the DNA damage dependent localization of Mms2 to the nucleus has been reported (Ulrich and Jentsch, 2000). Therefore, the *mut2* allele of *RSP5* could be envisioned to cause the constitutive binding to Mms2 in the cytosol, preventing its relocation to the nucleus. In this case, the polyubiquitylation of PCNA would not occur and an increased rate of mutagenesis and sensitivity to DNA damage would be observed. However, preliminary experimentation made it apparent that the hypothesis was not likely correct. When compared with their corresponding wild-type strains, it was found that *mut2* was less sensitive to MMS than *mms2* and more significantly, *mut2* was not sensitive to UV DNA damage whatsoever (data not shown). Mutants of the error-free DDT genes have the characteristic phenotype of being sensitive to a wide variety of DNA lesions, including those generated by UV irradiation (Broomfield et al., 2001). To definitively exclude the possibility that *RSP5* functions with *MMS2* in error-free DDT, it was desired to show a genetic relationship (or lack thereof) between *mms2* and *rsp5*. Unfortunately, epistatic analysis was not easily possible due to the lack of selectable markers in the *mut2* strain. Furthermore, genetic crosses using the *mut2* strain were not successful. This was not particularly surprising because sporulation deficiencies for *rsp5* mutant strains had been previously reported (Kanda, 1996).

5.2.6 Rsp5 is involved in the Lys63-dependent Ub conjugation of plasma membrane permeases

Since it seemed that Rsp5 does not function in error-free DDT, it was reasoned that the Mms2-Rsp5 physical interaction would be attributed to an unidentified cellular

role for each protein, a cellular role to which Rsp5 had already been described, or both. Regarding roles for which Rsp5 had already been described, several factors led to the hypothesis that the Mms2-Rsp5 interaction was a part of a plasma membrane protein endocytotic pathway.

One of the most clearly defined and experimentally studied roles for Rsp5 is in regulating the activity of plasma membrane proteins (Horak, 2003). The Rsp5-dependent conjugation of Ub to various permeases and transporters leads to their endocytosis. The physical removal of such proteins from their site of action (i.e. the plasma membrane) is a simple and direct method for negative regulation. The internalization step is followed by an endosomal sorting processes that also requires Ub and Rsp5 (Katzmann et al., 2004; Morvan et al., 2004; Urbe, 2005). The trafficking of such proteins through the multivesicular sorting pathways through this pathway normally leads to their proteasome-independent degradation in the vacuole or lysosome. With this general strategy, Rsp5 is implicated in down-regulating over a dozen plasma membrane proteins in yeast, such as amino acid permeases and mating-type receptors (Rotin et al., 2000). The importance of this cellular process is underscored by the apparent conservation throughout eukaryotes where at least 33 plasma membrane proteins have been identified to be modified in this manner (Dupre et al., 2004).

The greatest connection between Mms2 and Rsp5 with respect to plasma membrane protein endocytosis comes from the type of ubiquitylation that is sometimes performed. The predominant modification via Rsp5 is a single Ub moiety (mono-Ub). However, short poly-Ub chains linked through Lys63 have been experimentally demonstrated for two yeast membrane proteins. These proteins, Fur4 and Gap1, function

as the uracil and general amino acid permeases, respectively. Their Ub-Lys63-dependent ubiquitylation was revealed in yeast strains that produced lowered levels of wild-type Ub. When these cells were transformed with plasmids overexpressing a *ub-K63R* mutant (as compared to wild-type *UB*), the level of poly-ubiquitylated Fur4 or Gap1 was noticeably decreased (Galan and Haguenaer-Tsapis, 1997; Springael et al., 1999). These observations were supported by experiments using a yeast strain engineered to encode Ub-K63R as its sole source of Ub. In this strain, the Rsp5-dependent Lys63-linked ubiquitylation of Fur4 is completely abolished (Galan and Haguenaer-Tsapis, 1997; Galan et al., 1996). While modification by mono-Ub is sufficient for the internalization of Fur4 and Gap1, experimental data is consistent with a model whereby the rate of internalization is stimulated via Lys63-linked ubiquitylation. Interestingly, the E2 responsible for the Lys63-linked Ub conjugation of these membrane permeases was not identified (Galan and Haguenaer-Tsapis, 1997), therefore allowing the possibility that Mms2 (and Ubc13) may be responsible. The physical link between Mms2 and Rsp5 could be envisioned as a bridge between the Lys63-linked Ub conjugating complex (Ubc13-Mms2) and the plasma membrane proteins that are apparently modified by such poly-Ub chains.

5.2.7 MMS2 is not required for the Lys63-dependent Ub conjugation of the uracil permease

To address whether the *RSP5*-dependent Lys63-linked poly-ubiquitylation of membrane permeases is dependent on *MMS2*, Western blots were performed in order to directly visualize the ubiquitylation status of Fur4. However, two factors complicated the

initial analysis. First, typical soluble-phase yeast cell extracts could not be used to harvest the Fur4 protein due to its localization to plasma membranes and endosomes. Second, Fur4 is normally expressed at extremely low levels and is not normally detected in Western blots (Galan and Haguenaer-Tsapis, 1997). To overcome these limitations, a plasmid over-expressing *FUR4* was used in conjunction with an adapted procedure to prepare membrane-enriched fractions from yeast cells (Springael et al., 1999). A similar method had been used previously to show that yeast cells with Ub-K63R as their sole source of Ub are unable to poly-ubiquitylate Fur4 (Galan and Haguenaer-Tsapis, 1997).

As seen in Figure 5-5, a band of increasing molecular weight corresponding to the uracil permease is seen in the wild-type cell preparations (Lanes 1 and 3). These bands are completely absent in the *fur4* Δ strain (Lane 5). Similarly, the Fur4 bands were not detected in the yeast strain expressing *ub-K63R* as its sole source of Ub (Lane 2), indicating that the bands observed in Lane 1 correspond to various Lys63-dependent ubiquitylation states of the uracil permease. When the *mms2* Δ strain was tested (Lane 4), there was no apparent effect on the ubiquitylation of Fur4 as compared with the wild-type strain (Lane 3). It is noted that the smearing of bands is typical of proteins modified by Ub-chains *in vivo*, especially those isolated from membrane-enriched fractions (Galan and Haguenaer-Tsapis, 1997).

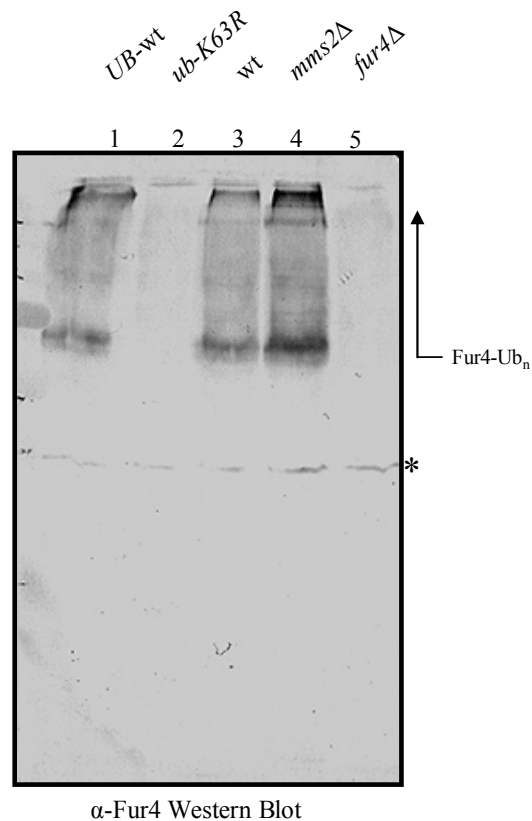


Figure 5-5. Mms2 is not required for the polyubiquitylation of the uracil permease.

The polyubiquitylation of Fur4 in various wild-type and mutant *S. cerevisiae* strains was monitored. Membrane-enriched samples were prepared for each strain and then run by SDS-PAGE. A Western blot of these samples using anti-Fur4 antibody is shown. Polyubiquitylated Fur4 is indicated (Fur4-Ub_n). Strains are: Lanes 1 and 2 represent engineered yeast strains expressing single copies of wild-type *UB* (SUB280) and *ub-K63R* (SUB413), respectively; wild-type (Lane 3); *mms2?* (Lane 4); *fur4?* (Lane 5). All strains except *fur4?* were transformed with a multi-copy plasmid (YEp352fF) expressing Fur4. A band cross-reacting with the Fur4 antibody is indicated with an asterisk and is used to ensure an approximately equal loading of samples. The smearing of *in vivo* polyubiquitylated proteins such as Fur4 is commonly seen (Galan and Haguenaer-Tsapis, 1997)

5.3 Discussion

A large portion of this thesis was dedicated to structure-function studies of Ubc13-Mms2, which provided substantial experimental evidence to support a model for the precise generation of Lys63-linked Ub chains. The Ubc13-Uev mechanism of Ub conjugation is unique in nature and to my knowledge there is no other reported explanation for how Ub can be specifically linked via Lys63. A paradox thus arises in yeast cells because Lys63-linked Ub chains have been identified in various cellular pathways but Ubc13 and Mms2 apparently function in error-free DDT only. The studies in this chapter sought to demonstrate novel physical interactions (and functions) for the Ubc13-Mms2 complex in order to address this disparity.

During my studies, a proteomic screen for protein complexes in yeast identified a novel physical interaction between Mms2 and Rsp5 (Gavin et al., 2002). In order to confirm the finding, two different affinity-based approaches were employed in this study. Indeed, a physical interaction between Mms2 and Rsp5 in Co-IP and GST pulldown experiments was observed. The Mms2-Rsp5 physical interaction was also detected in the yeast two-hybrid assay, which yielded a binding signal that was more readily detectable than in the affinity-based experiments. The clear demonstration of an Mms2-Rsp5 interaction is particularly significant because it is the first protein interaction found for the Mms2 family of Uevs that does not involve Ubc13 or Ub.

Given its large size, it was felt that Rsp5 could possibly bind to both Mms2 and Ubc13, perhaps leading to a higher-affinity association. However, a pull-down experiment suggested that this might not be the case (Figure 5-1). In accordance with this finding, a yeast two-hybrid assay was also not able to detect a physical interaction

between Ubc13 and Rsp5. It is noted that the N-terminal Ubc13 fusions may have obstructed a physical interaction with Rsp5. However, this possibility is felt to be unlikely because *GST* and *GAL4* fusions to yeast *UBC13* are fully proficient in functionally complementing *ubc13Δ* yeast strains (data not shown).

The three dimensional structure of the Uev domain is highly super-imposable with the Ubc domain and it was thus expected that Mms2 would bind to the HECT domain of Rsp5 in the conventional E2-E3 manner as discussed in Chapter 3 of this thesis. In accordance, crystal structure analysis reveals that the Mms2 surface corresponding to the E2 surface used to bind HECT domain E3s (Huang et al., 1999) is not obstructed by the Mms2-Ub or Mms2-Ubc13 physical interactions. In order to address the hypothesis experimentally, the yeast two-hybrid assay was used to test full-length Mms2 against a panel of Rsp5 deletions. Taken together, it was determined that the WW2 and WW3 domains are necessary for the Rsp5-Mms2 interaction. More specifically, the WW2 domain itself was found to be required but not sufficient for the interaction. It is noted that the WW2 fragment is small (33 amino acids) and could have been obstructed by the relatively large Gal4_{BD} fusion protein. Contrary to expectations, the Rsp5 HECT domain was not required for its interaction with Mms2.

The finding that the Rsp5-Mms2 interaction is mediated through WW domains was surprising but not without a good explanation. WW domains are *bona fide* protein-protein interaction modules with a binding preference for short Pro-containing sequences, such as the PY motif. Mms2 does not contain an authentic PY motif but was previously identified as a Pro-rich protein (Broomfield et al., 1998). Visual analysis of the Mms2 amino acid sequences reveals several short regions with multiple Pro residues.

The novel interaction discovered here between a Uev (Mms2) and a HECT domain E3 (Rsp5) presents an interesting possibility for coordinating multiple Ub conjugation activities. While binding to Mms2 through its WW domain(s), Rsp5 could simultaneously interact with an E2 via its HECT domain. In this way, Rsp5 could act as a physical bridge between Ubc13-Mms2 and another E2 with possibly distinct Ub conjugation activities. The bridging of two different E2s through a single E3 is reminiscent of the role for Rad5 in the yeast DDT pathway (Ulrich and Jentsch, 2000). Rad5 is proposed to simultaneously bind Rad6-Rad18 and Ubc13-Mms2 to allow the mono- and poly-ubiquitylation of PCNA, respectively (Hoege et al., 2002). This model is especially inviting in this case because Rsp5 is involved in the mono- and Lys63-linked poly-ubiquitylation of plasma membrane permeases, requiring E2s that have yet to be determined.

It was initially inviting to speculate that *RSP5* is a novel gene involved in error-free DDT because *mut2*, an allele of *RSP5*, was shown to exhibit mutator and MMS-sensitive phenotypes which are reminiscent of *mms2Δ*. However, further analysis of *mut2* suggested that this was not the case. It was also realized that the mutator and MMS-sensitive phenotypes of *mut2* may at least be partially explained by currently known roles for Rsp5. For example, Rsp5-dependent ubiquitylation is required for the turnover of at least 12 different plasma membrane proteins. A mutant disrupting this activity could lead to an over-abundance of permeases and possibly allow a greater amount of MMS into the cell. Also, an *rsp5* allele leads to various mitochondrial-associated phenotypes (Fisk and Yaffe, 1999) and a mitochondria-mediated nuclear mutator phenotype has been identified (Rasmussen et al., 2003). Nonetheless, it is felt

that future experimentation will be required to completely rule-out the possibility that *RSP5* is involved in error-free DDT.

Exploring another possibility, it was felt that the Mms2-Rsp5 physical interaction could be attributed to the role of Rsp5 in plasma membrane protein endocytosis. This was thought to be particularly likely because Rsp5 is required for the Lys63-linked Ub conjugation of the uracil and general amino acid permeases in a process requiring an unidentified E2(s). To test whether Ub conjugation via Mms2 is required in this role, the Lys63-dependent ubiquitylation of the uracil permease (Fur4) was monitored. When samples from the *mms2* Δ strain were analyzed, it was found that Fur4 was efficiently polyubiquitylated, with no discernable difference from the wild-type strain. It is concluded that *MMS2* is not required for the Lys63-dependent polyubiquitylation of Fur4. In support of this finding, the Lys63-dependent ubiquitylation of Fur4 was also unaffected in *ubc13* Δ yeast strains (R. Haguenaer-Tsapis, personal communication).

Based on the findings in this chapter, the following possibilities are noted:

- The Mms2-Rsp5 physical interaction is an experimental artifact.
- *RSP5* is involved in error-free DDT and the *mut2* allele will reveal novel error-free DDT phenotypes.
- *MMS2* is involved in the *RSP5*-mediated endocytosis of plasma membrane proteins (such as Fur4) but in a manner that is not directly related to their Lys63-dependent polyubiquitylation.
- The Mms2-Rsp5 physical interaction is attributed to a cellular role(s) that was not addressed in the experimentation above.

As a final note, the results concerning Fur4 in particular led me to reconsider the disparity between Lys63-linked Ub chains found *in vivo* and the lack of Ubc13-Mms2/Uev1 involvement. As will be discussed in chapter six, it is felt that a misinterpretation may be attributed to some of these cases.

CHAPTER SIX - CONCLUSIONS AND FUTURE DIRECTIONS

6.1 Conclusions

The implications and conclusions of the studies presented in this thesis have been discussed in detail in their respective chapters. For the sake of brevity and clarity, the major conclusions are summarized as follows:

6.1.1 Major conclusions from chapter three

- The human *UBC13* and *MMS2* genes can functionally complement their counterparts in *S. cerevisiae* DDT.
- Human *UEV1A* but not *UEV1B* is able to function in place of *MMS2* in *S. cerevisiae* DDT.
- There is a direct correlation between Ubc13-Uev complex formation and function in *S. cerevisiae* DDT.
- Heterologous (yeast-human) Ubc13-Uev pairs are functional in *S. cerevisiae* DDT.

6.1.2 Major conclusions from chapter four

- The functional analysis of site-directed point mutations in Ubc13 and Mms2 supports the prevailing *in vitro* mechanistic model of Lys63-linked Ub

conjugation; binding of donor and acceptor Ub by Ubc13 and Mms2, respectively, Ubc13-Mms2 heterodimer formation, and the binding of an E3 by Ubc13.

- Yeast Mms2-Ser27 (human Mms2-Ser32) is identified as a novel residue required for binding to Ub and suggests for the first time that polar contacts are important for the physical interaction.
- *MMS2-S27A/I57A* is severely sensitive to DNA damage and may be a potential dominant-negative regulator of *UBC13* activity.
- Human Ubc13 can physically interact with the RING finger E3s Rad5, TRAF6, and CHFR, but binding is lost in each case with the Ubc13-M64A mutation. The physical interaction with Rad5 is necessary for the function of human *UBC13* in yeast DDT.
- There is a direct correlation between the binding strength of Ubc13-Mms2 and their ability to alleviate the sensitivity of yeast cells to DNA damage.
- The binding and specificity of the Ubc13-Mms2 heterodimer relies on the insertion of an Mms2 Phe residue into a unique hydrophobic pocket formed by residues of Ubc13.

6.1.3 Major conclusions from chapter five

- Mms2 can make a direct physical interaction with Rsp5.
- The Mms2-Rsp5 physical interaction maps to the Rsp5 WW2 and WW3 domains.
- *MMS2* is not required for the Ub-Lys63-dependent ubiquitylation of the Fur4 plasma membrane permease.

6.2 Future directions

A number of future considerations and questions were brought up in previous chapters of this thesis. Three of these of immediate interest are discussed below.

6.2.1 Can an E2 be engineered to create a new physical interaction with Mms2?

With the detailed mutational analyses in chapter four, an explanation was provided for the specificity of Mms2 for Ubc13, but not other E2s. The model argues that the nature and spatial arrangement of residues comprising the necessary hydrophobic pocket for the hMms2-Phe13 (yMms2-Phe8) insertion is unique to Ubc13. However, it was noted in the visual comparison with Ubc13 that Ubc1 would be the most likely of the E2s to spatially accommodate a physical interaction with Mms2. In this context it is important to recall that the Phe→Glu mutation of the Ubc13-Phe57 residue caused a complete loss in binding to Mms2. Sequence alignments reveal that Ubc1 contains a Glu at this corresponding position (Figure 4-28). It is interesting to speculate that this Ubc1-Glu59 residue is under selective pressure because phylogenetic analysis reveals that Ubc1 is the closest evolutionary ancestor to Ubc13 (data not shown).

Future studies are proposed to first ensure that Mms2 does not physically interact with Ubc1 and then to systematically engineer the Ubc13 “pocket” onto Ubc1, beginning with a Ubc1-E59F mutation. The creation of a Ubc1-Mms2 physical interaction in this manner would be the best test of the Mms2-Ubc13 interaction model proposed in chapter four.

6.2.2 What is the mechanism of Lys63-linked Ub conjugation *in vivo*?

The functional data presented in this thesis has authenticated the prevailing mechanism of Lys63-linked Ub conjugation by Ubc13-Mms2. However, the model was created from *in vitro* observations and is not without its limitations. For instance, while the conjugation of Ub molecules through Lys63 is clear, a mechanism for how the di-Ub conjugate is delivered to the target (possibly via an E3) has not been explained. To accommodate this conceptual gap, I propose a simplified mechanism for Ubc13-Mms2 whereby the conjugation and target-delivery steps are performed concurrently *in vivo*.

A model for Lys63-linked Ub conjugation *in vivo* is diagrammed in Figure 6-1B. I propose that the Ub to be bound by Mms2 is not free, but already conjugated to the target (or E3 if applicable). In this case the Ubc13-Mms2 heterodimer containing a Ubc13-Ub thioester is directed at a pre-ubiquitylated target. The physical interaction between Mms2 and the Ub leads to the proper orientation to facilitate Lys63-linked Ub conjugation, and the Ubc13-Mms2 complex can be subsequently released. The simplicity of the model does not require a separate mechanism for the delivery of the Lys63-linked Ub conjugate.

At least two lines of evidence strongly support this proposed *in vivo* mechanism. First, the Lys63-linked ubiquitylation of PCNA by Ubc13-Mms2 is dependent on the mono-ubiquitylation of PCNA by Rad6-Rad18 at the same Lys residue (Hoegge et al., 2002). Second, Ub molecules are activated in a mechanism that involves the direct transfer of the Ub C-terminus from an E1 to an E2 thioester. The Ub bound by Mms2 in the mechanism shown in Figure 6-1A is therefore unlikely to be activated and would not be competent for conjugation to a target Lys. The pre-conjugation model shown in Figure 6-1B eliminates the problem of activation for the Mms2 acceptor Ub.

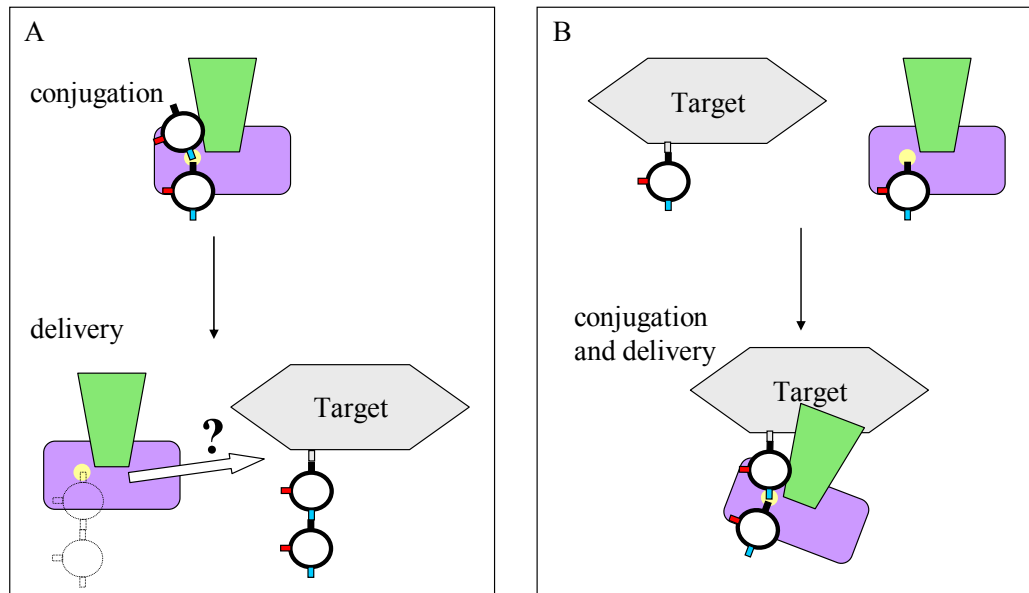


Figure 6-1. Proposed mechanisms for the Lys63-linked Ub conjugation of a target *in vivo*. (A) A two-step model showing the conjugation of di-Ub by Ubc13-Mms2 and the subsequent transfer of Ub₂ to the target by an unknown mechanism. (B) A single-step model showing that the conjugation of di-Ub by Ubc13-Mms2 occurs directly on a pre-ubiquitylated target. Coloured items in the figure correspond to Ubc13 (violet), Mms2 (green), Ub (white circles), Ub-C-terminus (black), Ub-Lys48 (red), Ub-Lys63 (blue), Ubc13 active-site (yellow).

6.2.3 Possible misinterpretation of Lys63-dependent Ub conjugation *in vivo*

Regarding Lys63-linked Ub chains, there appears to be a disparity between the enzyme shown to specifically generate them (i.e. Ubc13-Uev) and their apparent involvement in various cellular roles. For example, in *S. cerevisiae* there are several reported instances of Lys63-linked Ub chains *in vivo* that do not require Ubc13-Mms2 for their synthesis. This phenomenon was demonstrated in chapter five of this thesis with Mms2 and the Fur4 permease. The apparent paradox can be most easily explained by the existence of an additional undiscovered mechanism of Lys63-linked Ub conjugation that does not involve Ubc13-Uev. Another possibility may involve misinterpreted conclusions regarding Ub chain experimentation.

The experiments that clearly show the dependence of Ub-Lys63 *in vivo* make use of the *ub-K63R* mutation to demonstrate a certain phenotype. In many cases the apparent interpretation is that Lys63-linked Ub chains (linked via Lys63 only) are responsible for the observation. However, the conclusion may not be correct in all cases. An illustration of this point involving steric hindrance is shown in Figure 6-2. I propose that in some cases the first Ub molecule is linked to the target (or E3) in a manner that obstructs a particular Lys residue. In the hypothetical model in Figure 6-2A, the Ub-Lys48 residue is available for all conjugations. In another example, the Lys48 of the Ub conjugated to the target is physically obstructed (Figure 6-2B, upper panel). This latter case may lead to a chain that initially requires a Ub-Lys63 linkage but is otherwise linked via Ub-Lys48. In cells that express Ub-K63R alone, a target that would normally bear such chains would be indistinguishable from a target that was to be modified with Ub-Lys63 linkages only (Figure 6-2B, C, lower panel). Poly-ubiquitylation of the target would be prevented in

both cases, regardless of the particular chain that was to be made. Because of this ambiguity, I prefer the term “Lys63-dependent Ub chains” in place of “Lys63-linked Ub chains”, except when it is clear that all linkages are made via Ub-Lys63.

The use of Ub-Lys63 as the best initially-available Lys is particularly reasonable because it is situated approximately 180° from the Ub C-terminus, and is likely to be accessible to the conjugation machinery (shown schematically in Figure 6-2). On the other hand, the Ub-Lys48 residue is approximately 90° from the Ub C-terminus and can be envisioned to be more easily obstructed by steric hindrance. It is notable that this hypothetical scenario would likely argue against the “freeing” of Lys48 by Ub backbone rotation because the conjugating enzymes involved are likely to be conformationally restricted via physical interactions, such as between the E3 and target.

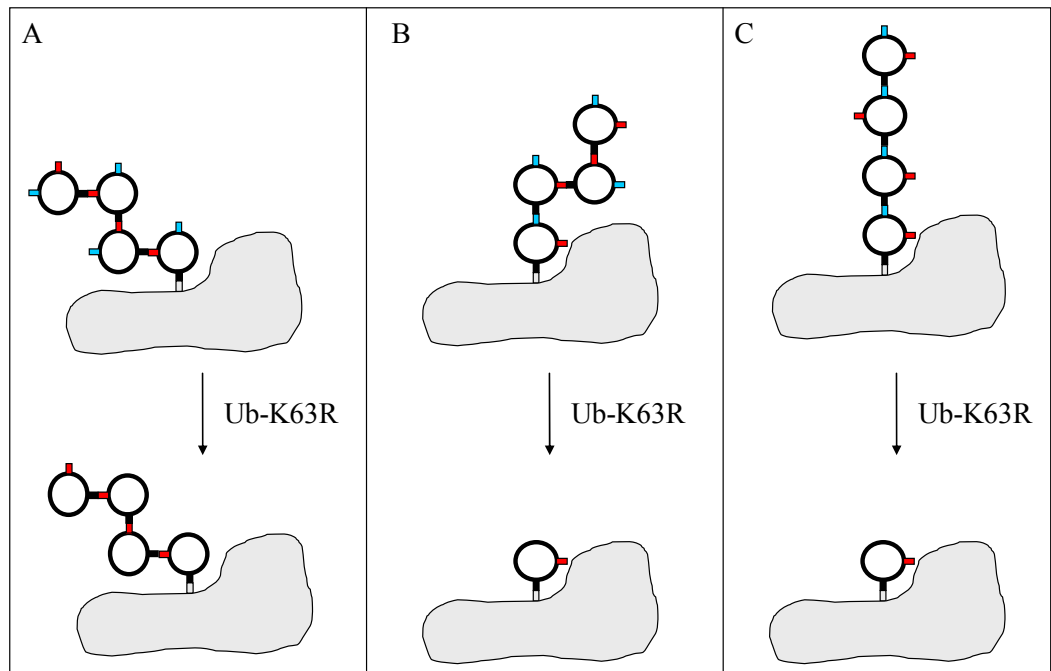


Figure 6-2. Possibilities for Ub_n chain formation involving Ub-Lys48 and -Lys63. A diagram showing the consequence that the Ub-K63R mutation would have on three different poly-Ub chains. (A) A poly-Ub chain with linkages via Ub-Lys48 (and the Ub-C-terminus) only. (B) A poly-Ub chain similar to (A) but using a single linkage via Ub-Lys63. (C) A poly-Ub chain with linkages via Ub-Lys63 (and the Ub C-terminus) only. Coloured items in the figure correspond to Ub (white circles), Ub-C-terminus (black), Ub-Lys48 (red), Ub-Lys63 (blue), target/E3 (gray).

REFERENCES

- Adames, A. G., D.E., Kaiser, C.A., Stearns, T. (1997). *Methods in yeast genetics*. (New York: Cold Spring Harbor laboratory press).
- Andersen, P. L., Zhou, H., Pastushok, L., Moraes, T., McKenna, S., Ziola, B., Ellison, M. J., Dixit, V. M., and Xiao, W. (2005). Distinct regulation of Ubc13 functions by the two ubiquitin-conjugating enzyme variants Mms2 and Uev1A. *J Cell Biol* *170*, 745-755.
- Aravind, L., and Koonin, E. V. (2000). The U box is a modified RING finger - a common domain in ubiquitination. *Curr Biol* *10*, R132-134.
- Arnason, T., and Ellison, M. J. (1994). Stress resistance in *Saccharomyces cerevisiae* is strongly correlated with assembly of a novel type of multiubiquitin chain. *Mol Cell Biol* *14*, 7876-7883.
- Arnason, T. G., Pisclevich, M. G., Dash, M. D., Davies, G. F., and Harkness, T. A. (2005). Novel interaction between Apc5p and Rsp5p in an intracellular signaling pathway in *Saccharomyces cerevisiae*. *Eukaryot Cell* *4*, 134-146.
- Ashley, C., Pastushok, L., McKenna, S., Ellison, M. J., and Xiao, W. (2002). Roles of mouse UBC13 in DNA postreplication repair and Lys63-linked ubiquitination. *Gene* *285*, 183-191.
- Ayyagari, R., Impellizzeri, K. J., Yoder, B. L., Gary, S. L., and Burgers, P. M. (1995). A mutational analysis of the yeast proliferating cell nuclear antigen indicates distinct roles in DNA replication and DNA repair. *Mol Cell Biol* *15*, 4420-4429.
- Baboshina, O. V., and Haas, A. L. (1996). Novel multiubiquitin chain linkages catalyzed by the conjugating enzymes E2EPF and RAD6 are recognized by 26 S proteasome subunit 5. *J Biol Chem* *271*, 2823-2831.
- Babu, J. R., Geetha, T., and Wooten, M. W. (2005). Sequestosome 1/p62 shuttles polyubiquitinated tau for proteasomal degradation. *J Neurochem* *94*, 192-203.
- Bachmair, A., Finley, D., and Varshavsky, A. (1986). In vivo half-life of a protein is a function of its amino-terminal residue. *Science* *234*, 179-186.

Bailly, V., Lamb, J., Sung, P., Prakash, S., and Prakash, L. (1994). Specific complex formation between yeast RAD6 and RAD18 proteins: a potential mechanism for targeting RAD6 ubiquitin-conjugating activity to DNA damage sites. *Genes Dev* 8, 811-820.

Bailly, V., Lauder, S., Prakash, S., and Prakash, L. (1997a). Yeast DNA repair proteins Rad6 and Rad18 form a heterodimer that has ubiquitin conjugating, DNA binding, and ATP hydrolytic activities. *J Biol Chem* 272, 23360-23365.

Bailly, V., Prakash, S., and Prakash, L. (1997b). Domains required for dimerization of yeast Rad6 ubiquitin-conjugating enzyme and Rad18 DNA binding protein. *Mol Cell Biol* 17, 4536-4543.

Baldwin, A. S., Jr. (1996). The NF-kappa B and I kappa B proteins: new discoveries and insights. *Annu Rev Immunol* 14, 649-683.

Ballinger, C. A., Connell, P., Wu, Y., Hu, Z., Thompson, L. J., Yin, L. Y., and Patterson, C. (1999). Identification of CHIP, a novel tetratricopeptide repeat-containing protein that interacts with heat shock proteins and negatively regulates chaperone functions. *Mol Cell Biol* 19, 4535-4545.

Barettino, D., Feigenbutz, M., Valcarcel, R., and Stunnenberg, H. G. (1994). Improved method for PCR-mediated site-directed mutagenesis. *Nucleic Acids Res* 22, 541-542.

Bartel, P. L., and Fields, S. (1995). Analyzing protein-protein interactions using two-hybrid system. *Methods Enzymol* 254, 241-263.

Bothos, J., Summers, M. K., Venere, M., Scolnick, D. M., and Halazonetis, T. D. (2003). The Chfr mitotic checkpoint protein functions with Ubc13-Mms2 to form Lys63-linked polyubiquitin chains. *Oncogene* 22, 7101-7107.

Broomfield, S., Chow, B. L., and Xiao, W. (1998). MMS2, encoding a ubiquitin-conjugating-enzyme-like protein, is a member of the yeast error-free postreplication repair pathway. *Proc Natl Acad Sci U S A* 95, 5678-5683.

Broomfield, S., Hryciw, T., and Xiao, W. (2001). DNA postreplication repair and mutagenesis in *Saccharomyces cerevisiae*. *Mutat Res* 486, 167-184.

Brown, M., Zhu, Y., Hemmingsen, S. M., and Xiao, W. (2002). Structural and functional conservation of error-free DNA postreplication repair in *Schizosaccharomyces pombe*. *DNA Repair (Amst) 1*, 869-880.

Brusky, J., Zhu, Y., and Xiao, W. (2000). UBC13, a DNA-damage-inducible gene, is a member of the error-free postreplication repair pathway in *Saccharomyces cerevisiae*. *Curr Genet 37*, 168-174.

Busch, H., and Goldknopf, I. L. (1981). Ubiquitin - protein conjugates. *Mol Cell Biochem 40*, 173-187.

Chen, F., Castranova, V., Shi, X., and Demers, L. M. (1999). New insights into the role of nuclear factor-kappaB, a ubiquitous transcription factor in the initiation of diseases. *Clin Chem 45*, 7-17.

Chen, Z., Hagler, J., Palombella, V. J., Melandri, F., Scherer, D., Ballard, D., and Maniatis, T. (1995). Signal-induced site-specific phosphorylation targets I kappa B alpha to the ubiquitin-proteasome pathway. *Genes Dev 9*, 1586-1597.

Chen, Z. J. (2005). Ubiquitin signalling in the NF-kappaB pathway. *Nat Cell Biol 7*, 758-765.

Cook, W. J., Jeffrey, L. C., Carson, M., Chen, Z., and Pickart, C. M. (1992). Structure of a diubiquitin conjugate and a model for interaction with ubiquitin conjugating enzyme (E2). *J Biol Chem 267*, 16467-16471.

Cook, W. J., Jeffrey, L. C., Kasperk, E., and Pickart, C. M. (1994). Structure of tetraubiquitin shows how multiubiquitin chains can be formed. *J Mol Biol 236*, 601-609.

Cook, W. J., Jeffrey, L. C., Xu, Y., and Chau, V. (1993). Tertiary structures of class I ubiquitin-conjugating enzymes are highly conserved: crystal structure of yeast Ubc4. *Biochemistry 32*, 13809-13817.

Cook, W. J., Martin, P. D., Edwards, B. F., Yamazaki, R. K., and Chau, V. (1997). Crystal structure of a class I ubiquitin conjugating enzyme (Ubc7) from *Saccharomyces cerevisiae* at 2.9 angstroms resolution. *Biochemistry 36*, 1621-1627.

Deng, L., Wang, C., Spencer, E., Yang, L., Braun, A., You, J., Slaughter, C., Pickart, C., and Chen, Z. J. (2000). Activation of the IkappaB kinase complex by TRAF6 requires a

dimeric ubiquitin-conjugating enzyme complex and a unique polyubiquitin chain. *Cell* 103, 351-361.

Devoy, A., Soane, T., Welchman, R., and Mayer, R. J. (2005). The ubiquitin-proteasome system and cancer. *Essays Biochem* 41, 187-203.

Didier, C., Broday, L., Bhoumik, A., Israeli, S., Takahashi, S., Nakayama, K., Thomas, S. M., Turner, C. E., Henderson, S., Sabe, H., and Ronai, Z. (2003). RNF5, a RING finger protein that regulates cell motility by targeting paxillin ubiquitination and altered localization. *Mol Cell Biol* 23, 5331-5345.

Dohmen, R. J., Madura, K., Bartel, B., and Varshavsky, A. (1991). The N-end rule is mediated by the UBC2(RAD6) ubiquitin-conjugating enzyme. *Proc Natl Acad Sci U S A* 88, 7351-7355.

Doss-Pepe, E. W., Chen, L., and Madura, K. (2005). Alpha-synuclein and parkin contribute to the assembly of ubiquitin lysine 63-linked multiubiquitin chains. *J Biol Chem* 280, 16619-16624.

Dunn, R., and Hicke, L. (2001a). Domains of the Rsp5 ubiquitin-protein ligase required for receptor-mediated and fluid-phase endocytosis. *Mol Biol Cell* 12, 421-435.

Dunn, R., and Hicke, L. (2001b). Multiple roles for Rsp5p-dependent ubiquitination at the internalization step of endocytosis. *J Biol Chem* 276, 25974-25981.

Dunn, R., Klos, D. A., Adler, A. S., and Hicke, L. (2004). The C2 domain of the Rsp5 ubiquitin ligase binds membrane phosphoinositides and directs ubiquitination of endosomal cargo. *J Cell Biol* 165, 135-144.

Dupre, S., Urban-Grimal, D., and Haguenauer-Tsapis, R. (2004). Ubiquitin and endocytic internalization in yeast and animal cells. *Biochim Biophys Acta* 1695, 89-111.

Einbond, A., and Sudol, M. (1996). Towards prediction of cognate complexes between the WW domain and proline-rich ligands. *FEBS Lett* 384, 1-8.

Fields, S., and Song, O. (1989). A novel genetic system to detect protein-protein interactions. *Nature* 340, 245-246.

Finley, D. (2001). Signal transduction. An alternative to destruction. *Nature* *412*, 283, 285-286.

Finley, D., Sadis, S., Monia, B. P., Boucher, P., Ecker, D. J., Crooke, S. T., and Chau, V. (1994). Inhibition of proteolysis and cell cycle progression in a multiubiquitination-deficient yeast mutant. *Mol Cell Biol* *14*, 5501-5509.

Fisk, H. A., and Yaffe, M. P. (1999). A role for ubiquitination in mitochondrial inheritance in *Saccharomyces cerevisiae*. *J Cell Biol* *145*, 1199-1208.

Freemont, P. S. (1993). The RING finger. A novel protein sequence motif related to the zinc finger. *Ann N Y Acad Sci* *684*, 174-192.

Freemont, P. S. (2000). RING for destruction? *Curr Biol* *10*, R84-87.

Freemont, P. S., Hanson, I. M., and Trowsdale, J. (1991). A novel cysteine-rich sequence motif. *Cell* *64*, 483-484.

Gajewska, B., Kaminska, J., Jesionowska, A., Martin, N. C., Hopper, A. K., and Zoladek, T. (2001). WW domains of Rsp5p define different functions: determination of roles in fluid phase and uracil permease endocytosis in *Saccharomyces cerevisiae*. *Genetics* *157*, 91-101.

Gajewska, B., Shcherbik, N., Oficjalska, D., Haines, D. S., and Zoladek, T. (2003). Functional analysis of the human orthologue of the RSP5-encoded ubiquitin protein ligase, hNedd4, in yeast. *Curr Genet* *43*, 1-10.

Galan, J. M., and Haguenaer-Tsapis, R. (1997). Ubiquitin lys63 is involved in ubiquitination of a yeast plasma membrane protein. *Embo J* *16*, 5847-5854.

Galan, J. M., Moreau, V., Andre, B., Volland, C., and Haguenaer-Tsapis, R. (1996). Ubiquitination mediated by the Npi1p/Rsp5p ubiquitin-protein ligase is required for endocytosis of the yeast uracil permease. *J Biol Chem* *271*, 10946-10952.

Gavin, A. C., Bosche, M., Krause, R., Grandi, P., Marzioch, M., Bauer, A., Schultz, J., Rick, J. M., Michon, A. M., Cruciat, C. M., *et al.* (2002). Functional organization of the yeast proteome by systematic analysis of protein complexes. *Nature* *415*, 141-147.

Geer, L. Y., Domrachev, M., Lipman, D. J., and Bryant, S. H. (2002). CDART: protein homology by domain architecture. *Genome Res* 12, 1619-1623.

Glotzer, M., Murray, A. W., and Kirschner, M. W. (1991). Cyclin is degraded by the ubiquitin pathway. *Nature* 349, 132-138.

Gottlieb, D. J., and von Borstel, R. C. (1976). Mutators in *Saccharomyces cerevisiae*: MUT1-1, MUT1-2 and MUT2-1. *Genetics* 83, 655-666.

Gwizdek, C., Hobeika, M., Kus, B., Ossareh-Nazari, B., Dargemont, C., and Rodriguez, M. S. (2005). The mRNA nuclear export factor Hpr1 is regulated by Rsp5-mediated ubiquitylation. *J Biol Chem* 280, 13401-13405.

Haas, A. L., Reback, P. B., and Chau, V. (1991). Ubiquitin conjugation by the yeast RAD6 and CDC34 gene products. Comparison to their putative rabbit homologs, E2(20K) AND E2(32K). *J Biol Chem* 266, 5104-5112.

Haas, A. L., and Rose, I. A. (1982). The mechanism of ubiquitin activating enzyme. A kinetic and equilibrium analysis. *J Biol Chem* 257, 10329-10337.

Hao, B., Zheng, N., Schulman, B. A., Wu, G., Miller, J. J., Pagano, M., and Pavletich, N. P. (2005). Structural basis of the Cks1-dependent recognition of p27(Kip1) by the SCF(Skp2) ubiquitin ligase. *Mol Cell* 20, 9-19.

Harkness, T. A., Davies, G. F., Ramaswamy, V., and Arnason, T. G. (2002). The ubiquitin-dependent targeting pathway in *Saccharomyces cerevisiae* plays a critical role in multiple chromatin assembly regulatory steps. *Genetics* 162, 615-632.

Hastings, P. J., Quah, S. K., and von Borstel, R. C. (1976). Spontaneous mutation by mutagenic repair of spontaneous lesions in DNA. *Nature* 264, 719-722.

Hatakeyama, S., and Nakayama, K. I. (2003). U-box proteins as a new family of ubiquitin ligases. *Biochem Biophys Res Commun* 302, 635-645.

Hatakeyama, S., Yada, M., Matsumoto, M., Ishida, N., and Nakayama, K. I. (2001). U box proteins as a new family of ubiquitin-protein ligases. *J Biol Chem* 276, 33111-33120.

Hershko, A., and Ciechanover, A. (1998). The ubiquitin system. *Annu Rev Biochem* 67, 425-479.

Hershko, A., Heller, H., Elias, S., and Ciechanover, A. (1983). Components of ubiquitin-protein ligase system. Resolution, affinity purification, and role in protein breakdown. *J Biol Chem* 258, 8206-8214.

Hicke, L., Schubert, H. L., and Hill, C. P. (2005). Ubiquitin-binding domains. *Nat Rev Mol Cell Biol* 6, 610-621.

Hill, J., Donald, K. A., and Griffiths, D. E. (1991). DMSO-enhanced whole cell yeast transformation. *Nucleic Acids Res* 19, 5791.

Hochstrasser, M. (1996). Ubiquitin-dependent protein degradation. *Annu Rev Genet* 30, 405-439.

Hochstrasser, M., Ellison, M. J., Chau, V., and Varshavsky, A. (1991). The short-lived MAT alpha 2 transcriptional regulator is ubiquitinated in vivo. *Proc Natl Acad Sci U S A* 88, 4606-4610.

Hoegel, C., Pfander, B., Moldovan, G. L., Pyrowolakis, G., and Jentsch, S. (2002). RAD6-dependent DNA repair is linked to modification of PCNA by ubiquitin and SUMO. *Nature* 419, 135-141.

Hofmann, R. M., and Pickart, C. M. (1999). Noncanonical MMS2-encoded ubiquitin-conjugating enzyme functions in assembly of novel polyubiquitin chains for DNA repair. *Cell* 96, 645-653.

Hofmann, R. M., and Pickart, C. M. (2001). In vitro assembly and recognition of Lys-63 polyubiquitin chains. *J Biol Chem* 276, 27936-27943.

Hoppe, T., Matuschewski, K., Rape, M., Schlenker, S., Ulrich, H. D., and Jentsch, S. (2000). Activation of a membrane-bound transcription factor by regulated ubiquitin/proteasome-dependent processing. *Cell* 102, 577-586.

Horak, J. (2003). The role of ubiquitin in down-regulation and intracellular sorting of membrane proteins: insights from yeast. *Biochim Biophys Acta* 1614, 139-155.

- Huang, J., Huang, Q., Zhou, X., Shen, M. M., Yen, A., Yu, S. X., Dong, G., Qu, K., Huang, P., Anderson, E. M., *et al.* (2004). The poxvirus p28 virulence factor is an E3 ubiquitin ligase. *J Biol Chem* *279*, 54110-54116.
- Huang, L., Kinnucan, E., Wang, G., Beaudenon, S., Howley, P. M., Huibregtse, J. M., and Pavletich, N. P. (1999). Structure of an E6AP-UbcH7 complex: insights into ubiquitination by the E2-E3 enzyme cascade. *Science* *286*, 1321-1326.
- Huibregtse, J. M., Yang, J. C., and Beaudenon, S. L. (1997). The large subunit of RNA polymerase II is a substrate of the Rsp5 ubiquitin-protein ligase. *Proc Natl Acad Sci U S A* *94*, 3656-3661.
- Hwang, W. W., Venkatasubrahmanyam, S., Ianculescu, A. G., Tong, A., Boone, C., and Madhani, H. D. (2003). A conserved RING finger protein required for histone H2B monoubiquitination and cell size control. *Mol Cell* *11*, 261-266.
- Imai, Y., Soda, M., Hatakeyama, S., Akagi, T., Hashikawa, T., Nakayama, K. I., and Takahashi, R. (2002). CHIP is associated with Parkin, a gene responsible for familial Parkinson's disease, and enhances its ubiquitin ligase activity. *Mol Cell* *10*, 55-67.
- Ingham, R. J., Gish, G., and Pawson, T. (2004). The Nedd4 family of E3 ubiquitin ligases: functional diversity within a common modular architecture. *Oncogene* *23*, 1972-1984.
- James, P., Halladay, J., and Craig, E. A. (1996). Genomic libraries and a host strain designed for highly efficient two-hybrid selection in yeast. *Genetics* *144*, 1425-1436.
- Jelinsky, S. A., Estep, P., Church, G. M., and Samson, L. D. (2000). Regulatory networks revealed by transcriptional profiling of damaged *Saccharomyces cerevisiae* cells: Rpn4 links base excision repair with proteasomes. *Mol Cell Biol* *20*, 8157-8167.
- Jelinsky, S. A., and Samson, L. D. (1999). Global response of *Saccharomyces cerevisiae* to an alkylating agent. *Proc Natl Acad Sci U S A* *96*, 1486-1491.
- Jentsch, S. (1992). The ubiquitin-conjugation system. *Annu Rev Genet* *26*, 179-207.
- Jentsch, S., McGrath, J. P., and Varshavsky, A. (1987). The yeast DNA repair gene RAD6 encodes a ubiquitin-conjugating enzyme. *Nature* *329*, 131-134.

Joazeiro, C. A., and Weissman, A. M. (2000). RING finger proteins: mediators of ubiquitin ligase activity. *Cell* *102*, 549-552.

Johnson, E. S., Bartel, B., Seufert, W., Varshavsky, A. (1992). Ubiquitin as a degradation signal. *Embo J*.

Johnson, E. S., Ma, P. C., Ota, I. M., and Varshavsky, A. (1995). A proteolytic pathway that recognizes ubiquitin as a degradation signal. *J Biol Chem* *270*, 17442-17456.

Johnson, R. E., Henderson, S. T., Petes, T. D., Prakash, S., Bankmann, M., and Prakash, L. (1992). *Saccharomyces cerevisiae* RAD5-encoded DNA repair protein contains DNA helicase and zinc-binding sequence motifs and affects the stability of simple repetitive sequences in the genome. *Mol Cell Biol* *12*, 3807-3818.

Kaminska, J., Gajewska, B., Hopper, A. K., and Zoladek, T. (2002). Rsp5p, a new link between the actin cytoskeleton and endocytosis in the yeast *Saccharomyces cerevisiae*. *Mol Cell Biol* *22*, 6946-6948.

Kanda, T. (1996). A ubiquitin-protein ligase (E3) mutation of *Saccharomyces cerevisiae* suppressed by co-overexpression of two ubiquitin-specific processing proteases. *Genes Genet Syst* *71*, 75-83.

Kannouche, P. L., Wing, J., and Lehmann, A. R. (2004). Interaction of human DNA polymerase eta with monoubiquitinated PCNA: a possible mechanism for the polymerase switch in response to DNA damage. *Mol Cell* *14*, 491-500.

Katzmann, D. J., Sarkar, S., Chu, T., Audhya, A., and Emr, S. D. (2004). Multivesicular body sorting: ubiquitin ligase Rsp5 is required for the modification and sorting of carboxypeptidase S. *Mol Biol Cell* *15*, 468-480.

Kelman, Z., and Hurwitz, J. (1998). Protein-PCNA interactions: a DNA-scanning mechanism? *Trends Biochem Sci* *23*, 236-238.

Koken, M. H., Reynolds, P., Jaspers-Dekker, I., Prakash, L., Prakash, S., Bootsma, D., and Hoeijmakers, J. H. (1991). Structural and functional conservation of two human homologs of the yeast DNA repair gene RAD6. *Proc Natl Acad Sci U S A* *88*, 8865-8869.

- Koonin, E. V., and Abagyan, R. A. (1997). TSG101 may be the prototype of a class of dominant negative ubiquitin regulators. *Nat Genet* *16*, 330-331.
- Krappmann, D., and Scheidereit, C. (2005). A pervasive role of ubiquitin conjugation in activation and termination of I κ B kinase pathways. *EMBO Rep* *6*, 321-326.
- Kus, B., Gajadhar, A., Stanger, K., Cho, R., Sun, W., Rouleau, N., Lee, T., Chan, D., Wolting, C., Edwards, A., *et al.* (2005). A high throughput screen to identify substrates for the ubiquitin ligase Rsp5. *J Biol Chem* *280*, 29470-29478.
- Landt, O., Grunert, H. P., and Hahn, U. (1990). A general method for rapid site-directed mutagenesis using the polymerase chain reaction. *Gene* *96*, 125-128.
- Lawrence, C. W. (1982). Mutagenesis in *Saccharomyces cerevisiae*. *Adv Genet* *21*, 173-254.
- Li, M., Brooks, C. L., Wu-Baer, F., Chen, D., Baer, R., and Gu, W. (2003). Mono- versus polyubiquitination: differential control of p53 fate by Mdm2. *Science* *302*, 1972-1975.
- Li, Z., Xiao, W., McCormick, J. J., and Maher, V. M. (2002). Identification of a protein essential for a major pathway used by human cells to avoid UV- induced DNA damage. *Proc Natl Acad Sci U S A* *99*, 4459-4464.
- Lim, K. L., Chew, K. C., Tan, J. M., Wang, C., Chung, K. K., Zhang, Y., Tanaka, Y., Smith, W., Engelender, S., Ross, C. A., *et al.* (2005a). Parkin mediates nonclassical, proteasomal-independent ubiquitination of synphilin-1: implications for Lewy body formation. *J Neurosci* *25*, 2002-2009.
- Lim, K. L., Dawson, V. L., and Dawson, T. M. (2005b). Parkin-mediated lysine 63-linked polyubiquitination: A link to protein inclusions formation in Parkinson's and other conformational diseases? *Neurobiol Aging*.
- Lovering, R., Hanson, I. M., Borden, K. L., Martin, S., O'Reilly, N. J., Evan, G. I., Rahman, D., Pappin, D. J., Trowsdale, J., and Freemont, P. S. (1993). Identification and preliminary characterization of a protein motif related to the zinc finger. *Proc Natl Acad Sci U S A* *90*, 2112-2116.
- Luftig, M., Prinarakis, E., Yasui, T., Tschritzis, T., Cahir-McFarland, E., Inoue, J., Nakano, H., Mak, T. W., Yeh, W. C., Li, X., *et al.* (2003). Epstein-Barr virus latent

membrane protein 1 activation of NF-kappaB through IRAK1 and TRAF6. *Proc Natl Acad Sci U S A* *100*, 15595-15600.

Ma, L., Broomfield, S., Lavery, C., Lin, S. L., Xiao, W., and Bacchetti, S. (1998). Up-regulation of CIR1/CROC1 expression upon cell immortalization and in tumor-derived human cell lines. *Oncogene* *17*, 1321-1326.

Maniatis, T., Fritsch, E. F., and Sambrook, J. (1982). *Molecular cloning: A laboratory manual*. (Cold Spring Harbor, NY: Cold Spring Harbor Laboratory).

McKenna, S., Hu, J., Moraes, T., Xiao, W., Ellison, M. J., and Spyropoulos, L. (2003a). Energetics and specificity of interactions within Ub.Uev.Ubc13 human ubiquitin conjugation complexes. *Biochemistry* *42*, 7922-7930.

McKenna, S., Moraes, T., Pastushok, L., Ptak, C., Xiao, W., Spyropoulos, L., and Ellison, M. J. (2003b). An NMR-based model of the ubiquitin-bound human ubiquitin conjugation complex Mms2.Ubc13. The structural basis for lysine 63 chain catalysis. *J Biol Chem* *278*, 13151-13158.

McKenna, S., Spyropoulos, L., Moraes, T., Pastushok, L., Ptak, C., Xiao, W., and Ellison, M. J. (2001). Noncovalent interaction between ubiquitin and the human DNA repair protein Mms2 is required for Ubc13-mediated polyubiquitination. *J Biol Chem* *276*, 40120-40126.

Moraes, T. F., Edwards, R. A., McKenna, S., Pastushok, L., Xiao, W., Glover, J. N., and Ellison, M. J. (2001). Crystal structure of the human ubiquitin conjugating enzyme complex, hMms2-hUbc13. *Nat Struct Biol* *8*, 669-673.

Morita, E., and Sundquist, W. I. (2004). Retrovirus budding. *Annu Rev Cell Dev Biol* *20*, 395-425.

Morvan, J., Froissard, M., Haguener-Tsapis, R., and Urban-Grimal, D. (2004). The ubiquitin ligase Rsp5p is required for modification and sorting of membrane proteins into multivesicular bodies. *Traffic* *5*, 383-392.

Murata, S., Minami, Y., Minami, M., Chiba, T., and Tanaka, K. (2001). CHIP is a chaperone-dependent E3 ligase that ubiquitylates unfolded protein. *EMBO Rep* *2*, 1133-1138.

Neumann, S., Petfalski, E., Brugger, B., Grosshans, H., Wieland, F., Tollervey, D., and Hurt, E. (2003). Formation and nuclear export of tRNA, rRNA and mRNA is regulated by the ubiquitin ligase Rsp5p. *EMBO Rep* 4, 1156-1162.

Nuber, U., and Scheffner, M. (1999). Identification of determinants in E2 ubiquitin-conjugating enzymes required for hect E3 ubiquitin-protein ligase interaction. *J Biol Chem* 274, 7576-7582.

Ohi, M. D., Vander Kooi, C. W., Rosenberg, J. A., Chazin, W. J., and Gould, K. L. (2003). Structural insights into the U-box, a domain associated with multi-ubiquitination. *Nat Struct Biol* 10, 250-255.

Ott, D. E., Coren, L. V., Copeland, T. D., Kane, B. P., Johnson, D. G., Sowder, R. C., 2nd, Yoshinaka, Y., Oroszlan, S., Arthur, L. O., and Henderson, L. E. (1998). Ubiquitin is covalently attached to the p6Gag proteins of human immunodeficiency virus type 1 and simian immunodeficiency virus and to the p12Gag protein of Moloney murine leukemia virus. *J Virol* 72, 2962-2968.

Pastushok, L., and Xiao, W. (2004). DNA postreplication repair modulated by ubiquitination and sumoylation. *Adv Protein Chem* 69, 279-306.

Patnaik, A., Chau, V., and Wills, J. W. (2000). Ubiquitin is part of the retrovirus budding machinery. *Proc Natl Acad Sci U S A* 97, 13069-13074.

Paunesku, T., Mittal, S., Protic, M., Oryhon, J., Korolev, S. V., Joachimiak, A., and Woloschak, G. E. (2001). Proliferating cell nuclear antigen (PCNA): ringmaster of the genome. *Int J Radiat Biol* 77, 1007-1021.

Peng, J., Schwartz, D., Elias, J. E., Thoreen, C. C., Cheng, D., Marsischky, G., Roelofs, J., Finley, D., and Gygi, S. P. (2003). A proteomics approach to understanding protein ubiquitination. *Nat Biotechnol* 21, 921-926.

Petrucelli, L., Dickson, D., Kehoe, K., Taylor, J., Snyder, H., Grover, A., De Lucia, M., McGowan, E., Lewis, J., Prihar, G., *et al.* (2004). CHIP and Hsp70 regulate tau ubiquitination, degradation and aggregation. *Hum Mol Genet* 13, 703-714.

Phillips, C. L., Thrower, J., Pickart, C. M., and Hill, C. P. (2001). Structure of a new crystal form of tetraubiquitin. *Acta Crystallogr D Biol Crystallogr* 57, 341-344.

- Pickart, C. M. (2001). Mechanisms underlying ubiquitination. *Annu Rev Biochem* 70, 503-533.
- Prakash, S., Johnson, R. E., and Prakash, L. (2005). Eukaryotic translesion synthesis DNA polymerases: specificity of structure and function. *Annu Rev Biochem* 74, 317-353.
- Prakash, S., Sung, P., and Prakash, L. (1993). DNA repair genes and proteins of *Saccharomyces cerevisiae*. *Annu Rev Genet* 27, 33-70.
- Rasmussen, A. K., Chatterjee, A., Rasmussen, L. J., and Singh, K. K. (2003). Mitochondria-mediated nuclear mutator phenotype in *Saccharomyces cerevisiae*. *Nucleic Acids Res* 31, 3909-3917.
- Richmond, E., and Peterson, C. L. (1996). Functional analysis of the DNA-stimulated ATPase domain of yeast SWI2/SNF2. *Nucleic Acids Res* 24, 3685-3692.
- Robzyk, K., Recht, J., and Osley, M. A. (2000). Rad6-dependent ubiquitination of histone H2B in yeast. *Science* 287, 501-504.
- Roche, H., Gietz, R. D., and Kunz, B. A. (1994). Specificity of the yeast rev3 delta antimutator and REV3 dependency of the mutator resulting from a defect (rad1 delta) in nucleotide excision repair. *Genetics* 137, 637-646.
- Roest, H. P., van Klaveren, J., de Wit, J., van Gurp, C. G., Koken, M. H., Vermey, M., van Roijen, J. H., Hoogerbrugge, J. W., Vreeburg, J. T., Baarends, W. M., *et al.* (1996). Inactivation of the HR6B ubiquitin-conjugating DNA repair enzyme in mice causes male sterility associated with chromatin modification. *Cell* 86, 799-810.
- Rothofsky, M. L., and Lin, S. L. (1997). CROC-1 encodes a protein which mediates transcriptional activation of the human FOS promoter. *Gene* 195, 141-149.
- Rothstein, R. J. (1983). One-step gene disruption in yeast. *Methods Enzymol* 101, 202-211.
- Rotin, D., Staub, O., and Haguenauer-Tsapis, R. (2000). Ubiquitination and endocytosis of plasma membrane proteins: role of Nedd4/Rsp5p family of ubiquitin-protein ligases. *J Membr Biol* 176, 1-17.

Salghetti, S. E., Caudy, A. A., Chenoweth, J. G., and Tansey, W. P. (2001). Regulation of transcriptional activation domain function by ubiquitin. *Science* 293, 1651-1653.

Sancho, E., Vila, M. R., Sanchez-Pulido, L., Lozano, J. J., Paciucci, R., Nadal, M., Fox, M., Harvey, C., Bercovich, B., Loukili, N., *et al.* (1998). Role of UEV-1, an inactive variant of the E2 ubiquitin-conjugating enzymes, in in vitro differentiation and cell cycle behavior of HT-29-M6 intestinal mucosecretory cells. *Mol Cell Biol* 18, 576-589.

Saurin, A. J., Borden, K. L., Boddy, M. N., and Freemont, P. S. (1996). Does this have a familiar RING? *Trends Biochem Sci* 21, 208-214.

Savelieva, E., Belair, C. D., Newton, M. A., DeVries, S., Gray, J. W., Waldman, F., and Reznikoff, C. A. (1997). 20q gain associates with immortalization: 20q13.2 amplification correlates with genome instability in human papillomavirus 16 E7 transformed human uroepithelial cells. *Oncogene* 14, 551-560.

Scheffner, M., Nuber, U., and Huibregtse, J. M. (1995). Protein ubiquitination involving an E1-E2-E3 enzyme ubiquitin thioester cascade. *Nature* 373, 81-83.

Scherer, D. C., Brockman, J. A., Chen, Z., Maniatis, T., and Ballard, D. W. (1995). Signal-induced degradation of I kappa B alpha requires site-specific ubiquitination. *Proc Natl Acad Sci U S A* 92, 11259-11263.

Schlesinger, D. H., Goldstein, G., and Niall, H. D. (1975). The complete amino acid sequence of ubiquitin, an adenylate cyclase stimulating polypeptide probably universal in living cells. *Biochemistry* 14, 2214-2218.

Schwarz, S. E., Rosa, J. L., and Scheffner, M. (1998). Characterization of human hect domain family members and their interaction with Ubch5 and Ubch7. *J Biol Chem* 273, 12148-12154.

Scolnick, D. M., and Halazonetis, T. D. (2000). Chfr defines a mitotic stress checkpoint that delays entry into metaphase. *Nature* 406, 430-435.

Seufert, W., and Jentsch, S. (1990). Ubiquitin-conjugating enzymes UBC4 and UBC5 mediate selective degradation of short-lived and abnormal proteins. *Embo J* 9, 543-550.

Shi, C. S., and Kehrl, J. H. (2003). Tumor necrosis factor (TNF)-induced germinal center kinase-related (GCKR) and stress-activated protein kinase (SAPK) activation depends

upon the E2/E3 complex Ubc13-Uev1A/TNF receptor-associated factor 2 (TRAF2). *J Biol Chem* 278, 15429-15434.

Shih, S. C., Prag, G., Francis, S. A., Sutanto, M. A., Hurley, J. H., and Hicke, L. (2003). A ubiquitin-binding motif required for intramolecular monoubiquitylation, the CUE domain. *Embo J* 22, 1273-1281.

Shimura, H., Schwartz, D., Gygi, S. P., and Kosik, K. S. (2004). CHIP-Hsc70 complex ubiquitinates phosphorylated tau and enhances cell survival. *J Biol Chem* 279, 4869-4876.

Smith, S. E., Koegl, M., and Jentsch, S. (1996). Role of the ubiquitin/proteasome system in regulated protein degradation in *Saccharomyces cerevisiae*. *Biol Chem* 377, 437-446.

Spence, J., Gali, R. R., Dittmar, G., Sherman, F., Karin, M., and Finley, D. (2000). Cell cycle-regulated modification of the ribosome by a variant multiubiquitin chain. *Cell* 102, 67-76.

Spence, J., Sadis, S., Haas, A. L., and Finley, D. (1995). A ubiquitin mutant with specific defects in DNA repair and multiubiquitination. *Mol Cell Biol* 15, 1265-1273.

Springael, J. Y., Galan, J. M., Haguenaer-Tsapis, R., and Andre, B. (1999). NH₄⁺-induced down-regulation of the *Saccharomyces cerevisiae* Gap1p permease involves its ubiquitination with lysine-63-linked chains. *J Cell Sci* 112 (Pt 9), 1375-1383.

Staub, O., Abriel, H., Plant, P., Ishikawa, T., Kanelis, V., Saleki, R., Horisberger, J. D., Schild, L., and Rotin, D. (2000). Regulation of the epithelial Na⁺ channel by Nedd4 and ubiquitination. *Kidney Int* 57, 809-815.

Stelter, P., and Ulrich, H. D. (2003). Control of spontaneous and damage-induced mutagenesis by SUMO and ubiquitin conjugation. *Nature* 425, 188-191.

Strack, B., Calistri, A., Accola, M. A., Palu, G., and Gottlinger, H. G. (2000). A role for ubiquitin ligase recruitment in retrovirus release. *Proc Natl Acad Sci U S A* 97, 13063-13068.

Sullivan, M. L., and Vierstra, R. D. (1993). Formation of a stable adduct between ubiquitin and the *Arabidopsis* ubiquitin-conjugating enzyme, AtUBC1+. *J Biol Chem* 268, 8777-8780.

Sun, L., Deng, L., Ea, C. K., Xia, Z. P., and Chen, Z. J. (2004). The TRAF6 ubiquitin ligase and TAK1 kinase mediate IKK activation by BCL10 and MALT1 in T lymphocytes. *Mol Cell* *14*, 289-301.

Sundquist, W. I., Schubert, H. L., Kelly, B. N., Hill, G. C., Holton, J. M., and Hill, C. P. (2004). Ubiquitin recognition by the human TSG101 protein. *Mol Cell* *13*, 783-789.

Sung, P., Berleth, E., Pickart, C., Prakash, S., and Prakash, L. (1991a). Yeast RAD6 encoded ubiquitin conjugating enzyme mediates protein degradation dependent on the N-end-recognizing E3 enzyme. *Embo J* *10*, 2187-2193.

Sung, P., Prakash, S., and Prakash, L. (1988). The RAD6 protein of *Saccharomyces cerevisiae* polyubiquitinates histones, and its acidic domain mediates this activity. *Genes Dev* *2*, 1476-1485.

Sung, P., Prakash, S., and Prakash, L. (1990). Mutation of cysteine-88 in the *Saccharomyces cerevisiae* RAD6 protein abolishes its ubiquitin-conjugating activity and its various biological functions. *Proc Natl Acad Sci U S A* *87*, 2695-2699.

Sung, P., Prakash, S., and Prakash, L. (1991b). Stable ester conjugate between the *Saccharomyces cerevisiae* RAD6 protein and ubiquitin has no biological activity. *J Mol Biol* *221*, 745-749.

Szabo, A., Stolz, L., and Granzow, R. (1995). Surface plasmon resonance and its use in biomolecular interaction analysis (BIA). *Curr Opin Struct Biol* *5*, 699-705.

Tanaka, K., Kawakami, T., Tateishi, K., Yashiroda, H., and Chiba, T. (2001). Control of IkappaBalpha proteolysis by the ubiquitin-proteasome pathway. *Biochimie* *83*, 351-356.

Tateishi, S., Sakuraba, Y., Masuyama, S., Inoue, H., and Yamaizumi, M. (2000). Dysfunction of human Rad18 results in defective postreplication repair and hypersensitivity to multiple mutagens. *Proc Natl Acad Sci U S A* *97*, 7927-7932.

Thrower, J. S., Hoffman, L., Rechsteiner, M., and Pickart, C. M. (2000). Recognition of the polyubiquitin proteolytic signal. *Embo J* *19*, 94-102.

Torres-Ramos, C. A., Yoder, B. L., Burgers, P. M., Prakash, S., and Prakash, L. (1996). Requirement of proliferating cell nuclear antigen in RAD6-dependent postreplicational DNA repair. *Proc Natl Acad Sci U S A* *93*, 9676-9681.

Tsirigotis, M., Zhang, M., Chiu, R. K., Wouters, B. G., and Gray, D. A. (2001). Sensitivity of mammalian cells expressing mutant ubiquitin to protein-damaging agents. *J Biol Chem* 276, 46073-46078.

Tsui, C., Raguraj, A., and Pickart, C. M. (2005). Ubiquitin binding site of the ubiquitin E2 variant (UEV) protein Mms2 is required for DNA damage tolerance in the yeast RAD6 pathway. *J Biol Chem* 280, 19829-19835.

Ulrich, H. D. (2002). Natural substrates of the proteasome and their recognition by the ubiquitin system. *Curr Top Microbiol Immunol* 268, 137-174.

Ulrich, H. D. (2003). Protein-protein interactions within an E2-RING finger complex. Implications for ubiquitin-dependent DNA damage repair. *J Biol Chem* 278, 7051-7058.

Ulrich, H. D., and Jentsch, S. (2000). Two RING finger proteins mediate cooperation between ubiquitin-conjugating enzymes in DNA repair. *Embo J* 19, 3388-3397.

Urbe, S. (2005). Ubiquitin and endocytic protein sorting. *Essays Biochem* 41, 81-98.

VanDemark, A. P., and Hill, C. P. (2002). Structural basis of ubiquitylation. *Curr Opin Struct Biol* 12, 822-830.

VanDemark, A. P., Hofmann, R. M., Tsui, C., Pickart, C. M., and Wolberger, C. (2001). Molecular insights into polyubiquitin chain assembly: crystal structure of the Mms2/Ubc13 heterodimer. *Cell* 105, 711-720.

Varadan, R., Assfalg, M., Haririnia, A., Raasi, S., Pickart, C., and Fushman, D. (2003). Solution conformation of Lys63-linked di-ubiquitin chain provides clues to functional diversity of polyubiquitin signaling. *J Biol Chem*.

Varadan, R., Assfalg, M., Haririnia, A., Raasi, S., Pickart, C., and Fushman, D. (2004). Solution conformation of Lys63-linked di-ubiquitin chain provides clues to functional diversity of polyubiquitin signaling. *J Biol Chem* 279, 7055-7063.

Varadan, R., Walker, O., Pickart, C., and Fushman, D. (2002). Structural properties of polyubiquitin chains in solution. *J Mol Biol* 324, 637-647.

- Verdecia, M. A., Joazeiro, C. A., Wells, N. J., Ferrer, J. L., Bowman, M. E., Hunter, T., and Noel, J. P. (2003). Conformational flexibility underlies ubiquitin ligation mediated by the WWP1 HECT domain E3 ligase. *Mol Cell* *11*, 249-259.
- Villalobo, E., Morin, L., Moch, C., Lescasse, R., Hanna, M., Xiao, W., and Baroin-Tourancheau, A. (2002). A homologue of CROC-1 in a ciliated protist (*Sterkiella histriomuscorum*) testifies to the ancient origin of the ubiquitin-conjugating enzyme variant family. *Mol Biol Evol* *19*, 39-48.
- Waga, S., and Stillman, B. (1998). The DNA replication fork in eukaryotic cells. *Annu Rev Biochem* *67*, 721-751.
- Wang, C., Deng, L., Hong, M., Akkaraju, G. R., Inoue, J., and Chen, Z. J. (2001). TAK1 is a ubiquitin-dependent kinase of MKK and IKK. *Nature* *412*, 346-351.
- Wang, G., Yang, J., and Huibregtse, J. M. (1999). Functional domains of the Rsp5 ubiquitin-protein ligase. *Mol Cell Biol* *19*, 342-352.
- Watanabe, K., Tateishi, S., Kawasuji, M., Tsurimoto, T., Inoue, H., and Yamaizumi, M. (2004). Rad18 guides poleta to replication stalling sites through physical interaction and PCNA monoubiquitination. *Embo J* *23*, 3886-3896.
- Waterman, H., Levkowitz, G., Alroy, I., and Yarden, Y. (1999). The RING finger of c-Cbl mediates desensitization of the epidermal growth factor receptor. *J Biol Chem* *274*, 22151-22154.
- Wood, A., Krogan, N. J., Dover, J., Schneider, J., Heidt, J., Boateng, M. A., Dean, K., Golshani, A., Zhang, Y., Greenblatt, J. F., *et al.* (2003). Bre1, an E3 ubiquitin ligase required for recruitment and substrate selection of Rad6 at a promoter. *Mol Cell* *11*, 267-274.
- Wooff, J., Pastushok, L., Hanna, M., Fu, Y., and Xiao, W. (2004). The TRAF6 RING finger domain mediates physical interaction with Ubc13. *FEBS Lett* *566*, 229-233.
- Worthylake, D. K., Prakash, S., Prakash, L., and Hill, C. P. (1998). Crystal structure of the *Saccharomyces cerevisiae* ubiquitin-conjugating enzyme Rad6 at 2.6 Å resolution. *J Biol Chem* *273*, 6271-6276.

Wu-Baer, F., Lagazon, K., Yuan, W., and Baer, R. (2003). The BRCA1/BARD1 heterodimer assembles polyubiquitin chains through an unconventional linkage involving lysine residue K6 of ubiquitin. *J Biol Chem* 278, 34743-34746.

Xiao, W., Chow, B. L., Broomfield, S., and Hanna, M. (2000). The *Saccharomyces cerevisiae* RAD6 group is composed of an error-prone and two error-free postreplication repair pathways. *Genetics* 155, 1633-1641.

Xiao, W., Chow, B. L., Fontanie, T., Ma, L., Bacchetti, S., Hryciw, T., and Broomfield, S. (1999). Genetic interactions between error-prone and error-free postreplication repair pathways in *Saccharomyces cerevisiae*. *Mutat Res* 435, 1-11.

Xiao, W., Lin, S. L., Broomfield, S., Chow, B. L., and Wei, Y. F. (1998). The products of the yeast MMS2 and two human homologs (hMMS2 and CROC-1) define a structurally and functionally conserved Ubc-like protein family. *Nucleic Acids Res* 26, 3908-3914.

Yanagawa, Y., Sullivan, J. A., Komatsu, S., Gusmaroli, G., Suzuki, G., Yin, J., Ishibashi, T., Saijo, Y., Rubio, V., Kimura, S., *et al.* (2004). Arabidopsis COP10 forms a complex with DDB1 and DET1 in vivo and enhances the activity of ubiquitin conjugating enzymes. *Genes Dev* 18, 2172-2181.

Zhang, M., Windheim, M., Roe, S. M., Peggie, M., Cohen, P., Prodromou, C., and Pearl, L. H. (2005). Chaperoned ubiquitylation--crystal structures of the CHIP U box E3 ubiquitin ligase and a CHIP-Ubc13-Uev1a complex. *Mol Cell* 20, 525-538.

Zhang, Z., Shibahara, K., and Stillman, B. (2000). PCNA connects DNA replication to epigenetic inheritance in yeast. *Nature* 408, 221-225.

Zheng, N., Schulman, B. A., Song, L., Miller, J. J., Jeffrey, P. D., Wang, P., Chu, C., Koepp, D. M., Elledge, S. J., Pagano, M., *et al.* (2002). Structure of the Cull1-Rbx1-Skp1-F boxSkp2 SCF ubiquitin ligase complex. *Nature* 416, 703-709.

Zheng, N., Wang, P., Jeffrey, P. D., and Pavletich, N. P. (2000). Structure of a c-Cbl-UbcH7 complex: RING domain function in ubiquitin-protein ligases. *Cell* 102, 533-539.

Zhou, H., Wertz, I., O'Rourke, K., Ultsch, M., Seshagiri, S., Eby, M., Xiao, W., and Dixit, V. M. (2004). Bcl10 activates the NF-kappaB pathway through ubiquitination of NEMO. *Nature* 427, 167-171.